Proteins at interfaces

Protein adsorption studied by X-ray and neutron reflectometry

Dissertation

vorgelegt von

Florian Evers

aus Steinfurt

Technische Universität Dortmund
Fakultät Physik
Experimentelle Physik I

November 2010

Contents

1 Introduction

The general objective of this thesis is to further the understanding of protein adsorption phenomena. To this end, a lot of simple or sophisticated model systems have been developed, and their interfacial structures are analyzed by X-ray and neutron scattering techniques. These model systems serve as a basis from which the mechanisms of protein adsorption are explored and means for controlling protein interfacial behavior are concluded.

Proteins are complex biological macromolecules composed of about 20 different amino acids [8, 24, 50]; and thus, protein adsorption is governed by protein-surface, protein-protein, and protein-solvent interactions [50, 163], exploiting a complex interplay of various driving forces, such as Coulomb and van der Waals forces, the hydrophobic effect, and adsorption-induced conformational changes [19, 50].

Since the fundamental process of protein adsorption exerts severe implications in the fields of biomaterials as well as bio- and nanotechnology, understanding the mechanisms and controlling the degree of protein adsorption at surfaces have become intriguing and interdisciplinary research topics [39, 50, 86, 93, 94, 100, 133, 134, 163, 177, 207, 277]. Moreover, proteins tend to adsorb spontaneously at almost any surface [12, 19, 30, 50, 109, 163]. Hence, protein adsorption is an ubiquitous phenomenon, which deserves special attention.

Examples of biomaterials are medical implants [39, 134, 207], like artificial joints, dental implants, stents used as vascular grafts, and artificial organs. Such devices are intended to substitute missing or impaired biological structures in the human body. Upon implantation of biomaterials into the human body, non-specific protein adsorption at biomaterials occurs, which is absent in the normal wound healing process under physiological conditions [207]. Hence, non-specific protein adsorption on biomaterials might instigate and govern the next steps of the foreign body reaction [207]. Thus, protein adsorption is related to the bio- and hemocompatibility of implants, and therefore, a lot of studies are focused on the mechanisms of non-specific protein adsorption [50, 86, 94, 163, 277] and on the design of protein-resistant surfaces [18, 75, 91, 98, 139, 271, 293]. With regard to nanotechnology, the specific adsorption of proteins at biosensors represents a prominent example. Examples of biosensors are protein-biochips in proteomics and solid-phase immunoassays in medical diagnostics [130, 180, 181, 283, 288]. For example, enzyme immunoassays (ELISA) are applied to detect the presence of antibodies or antigens, as used in pregnancy tests [50, 51].

In this work, protein adsorption is studied by applying a physicochemical approach. Therefore, model systems with well-defined and reproducible properties are employed, and thus, the

complexity of protein adsorption under natural and physiological conditions is reduced. To do so, model systems are chosen, which are composed of (i) specific proteins, (ii) substrates of specially designed surface chemistry, as well as (iii) selected subphase composition and solvent properties. In this way, the complex interplay of proteins at interfaces can be further elucidated. The studies presented in this thesis extend the knowledge in the field of protein adsorption with respect to all of the three above mentioned components of common model systems.

The major achievements in the field of protein adsorption are summarized as follows: So far, strategies to prevent protein adsorption have mainly focused on the role of surface chemistry and protein structure, whereas the influence of solvent composition on protein adsorption and, in particular, the effect of adding cosolvents to protein solutions have often been neglected. In this work, comprehensive studies on the effects of nonionic cosolvents on protein adsorption are reported [80, 113]. The results of these studies have implications for the design of protein-resistant surfaces. Moreover, the influence of salts on protein adsorption is investigated. Interestingly, non-specific ionic interactions can lead to increased adsorption [78]. On the contrary, kosmotropic and chaotropic salts selected from the Hofmeister series can lower the degree of protein adsorption at hydrophobic surfaces [79]. This is – to our knowledge – the first thorough investigation of Hofmeister effects on protein adsorption. Furthermore, a comprehensive study on the influence of surface chemistry and substrate composition on protein adsorption [89, 90] reveals that van der Waals forces can affect the interfacial structure and the degree of protein adsorption. In addition, the extent of protein denaturation is deduced from the interfacial structure of proteins adsorbed at hydrophobic surfaces. This study demonstrates that the hydrophobic effect acts as dominating driving force at silane-based hydrophobic surfaces. In another study, the interaction of insulin with polyelectrolyte brushes is investigated [75]. In contrast to the other model proteins used, insulin is an aggregation-prone peptide and can form amyloid fibrils. However, the results of this study show that the amyloidogenic nature of insulin is suppressed by a poly(acrylic acid) brush, qualifying poly(acrylic acid) brushes as a potent biocompatible coating for insulin.

X-ray and neutron reflectometry are the main techniques applied to study protein adsorption in this work. While optical methods are able to characterize adsorbed protein films only in terms of surface excess, spectroscopic techniques yield information on both surface excess and protein conformation in terms of secondary and tertiary structure [50]. Notably, from X-ray and neutron scattering measurements, not only the degree of protein adsorption, but also the interfacial structure of adsorbed protein films can be determined, which is described in terms of film thickness and protein packing density of the adsorb layer [76]. Moreover, the layer thickness provides a parameter that is related to the conformation of adsorbed proteins. Altogether, X-ray and neutron reflectometry serve as powerful tools for the analysis of adsorbed protein films.

The organization of this thesis is outlined as follows: In the first part (Chapters $2-4$), basic principles of protein adsorption, X-ray and neutron reflectometry, as well as experimental protocols are described, while the results of different studies performed in this work are presented and discussed in the second part (Chapters $5-8$).

- **Chapter 2** contains an introduction to protein biochemistry, to the interaction of proteins with surfaces and the driving forces for protein adsorption, as well as a description of the model proteins used in this work. The theory of X-ray and neutron reflectometry is presented in **Chapter 3**, emphasizing aspects which are relevant for the characterization of adsorbed protein films. Details of the experimental set-ups used for the study of protein adsorption at solid-liquid and air-water interfaces as well as methods of surface functionalization are described in **Chapter 4**.

- The main focus of this work is on the effects of ionic and nonionic cosolvents on protein adsorption. The results presented in **Chapter 5** show that nonionic cosolvents are able to alter and control the adsorption behavior of ribonuclease A (RNase) and bovine serum albumin (BSA). All nonionic cosolvents studied – whether kosmotropic or not – lower the interfacial affinity of RNase, thus providing a novel means to render surfaces protein-resistant. The decreased surface excess in the presence of nonionic cosolvents is ascribed to a reduced protein packing density in the adsorbed layer. Moreover, ionic cosolvents (as presented in **Chapter 6**) might enhance or reduce the degree of protein adsorption. Again, both kosmotropic and chaotropic ions are found to reduce the packing density of adsorbed protein films.

- In another study (**Chapter 7**), polyelectrolyte brushes formed at planar surfaces are used as a model system for insulin adsorption. At first, the typical properties of poly(acrylic acid) brushes are analyzed in the case of insulin adsorption; that is, PAA brushes are either protein-repellent or provide a mild environment for adsorbed proteins depending on the ionic strengths of the subphase. Then, the effect of glycerol on insulin adsorption at PAA brushes highlights that these brushes can provide a mild, biocompatible environment even for aggregation-prone proteins.

- **Chapter 8** provides a comprehensive study on the effect of short- and long-range forces on protein adsorption. Silicon wafers with native and thermally grown oxide layer exert different long-range forces on adsorbing proteins. Coating these wafers with self-assembled monolayers yields a variation in hydrophobicity of the substrates. For the adsorption of lysozyme, BSA, and α-amylase at these surfaces, a clear tendency is revealed: while wafers with a native oxide layer show maximum adsorption in the case of hydrophobic substrates, a reversed order (maximum adsorption at wafers with a thermally grown oxide layer) is found in the case of hydrophilic substrates. Moreover, protein films adsorbed at hydrophobic surfaces form extremely thin layers with an enhanced packing density, indicating adsorption-induced conformational changes. On the other hand, proteins might adsorb in near-native conditions at hydrophilic substrates.

- **Chapter 9** summarizes the results of this thesis and gives an outlook on potential future research in the field of protein adsorption.

2 Proteins at interfaces

Proteins are biological macromolecules found in all living organisms, like polysaccharides and nucleic acids, and are involved in virtually all cellular processes. Protein molecules show a high surface activity and tend to adsorb spontaneously at almost any interface. The process of protein adsorption has implications in such diverse fields as biomaterials, drug delivery, biocompatibility of implants, biofouling, food chemistry, contact lenses, and immunoassays [39, 50, 60, 94, 134, 163, 177]. In nature, protein-membrane interactions are extremely relevant, as, for example, biological energy conversion processes, like photosynthesis and oxidative phosphorylation, take place at membranes [24]. Moreover, blood comprises various proteins, such as fibrinogen, that take a role in blood clotting. The adsorption of blood proteins affects the bio- and hemocompatibility of implants, such as stents [39, 134]. At contact lenses, the formation of biofilms comprising lysozyme can lead to immunological reactions and infections of the eye [122]. Furthermore, proteins adsorbing at ship hulls or underwater structures can cause biofouling, leading to increased fuel consumption of ships. Protein-biochips sense the specific adsorption of proteins, which is, for example, used in pregnancy tests [181, 288].

In this Chapter, (i) the biochemistry of proteins and the protein structure, (ii) the interaction of proteins with solid and liquid surfaces, (iii) driving forces for protein adsorption, and (iv) characteristics of proteins used in this work are introduced.

2.1 Proteins and protein structure

Proteins are among the most fundamental constituents of all living organisms and take thus part in almost any biological process [8, 225, 275, 289]. Hence, proteins accomplish a number of different functions: Examples of structural proteins are actin and tubulin in the cytoskeleton, collagen and elastin in connective tissue, and keratin in hair or nails. These proteins confer mechanical rigidity and stability of cells. Enzymes are proteins that catalyze chemical reactions in organisms, in particular processes involved in metabolism and DNA manipulation. Moreover, many proteins, e. g., peptide hormones, are engaged with signal transduction and cell signalling; for example, some proteins can transmit a signal from one cell to another, while membrane proteins can provide a binding site for signalling molecules, inducing chemical responses of the cell. Ligand transport proteins are able to bind specific small molecules, conveying them to their destiny in the organism. The typical example of ligand-binding proteins is hemoglobin, which transports oxygen from the lungs to organs and tissues in all vertebrates. Furthermore,

antibodies are proteins used by the immune system in order to identify and bind antigens and foreign body substances.

With respect to chemistry, proteins are copolymers generally composed of a sequence of the 20 different L-α-amino acids which are arranged in a linear polypeptide chain and folded into a globular conformation (cf. Figure 2.1) [8, 24, 225]. The amino acids in the polypeptide chain are connected via peptide bonds between the carboxyl and amino groups of neighboring amino acid residues. As most amino acid residues have a zwitterionic character, proteins are polyampholytes. Besides, amino acid residues differ widely in their polarity and hydrophobicity, thus rendering proteins amphiphilic.

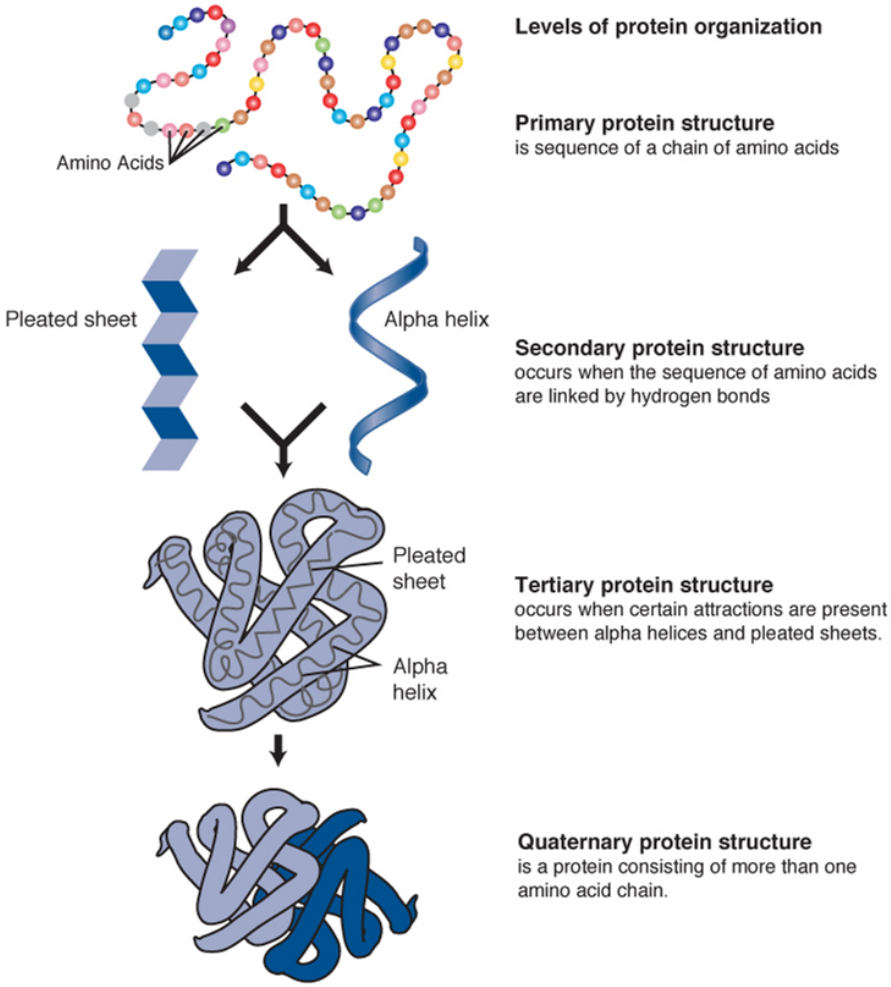

Figure 2.1: Proteins and protein structure [2]. Different levels of structural organization of protein can be identified: primary, secondary, tertiary, and quaternary structure.

Proteins are able to perform their biological function adequately, contingent upon proper pro-

tein folding [8, 24]. Naturally, proteins are folded into their native conformation. However, proteins are not rigid molecules, but are able to undergo transitions between various conformations (conformational changes) each relevant for different biological functions. Protein folding is driven by non-covalent interactions, like the hydrophobic effect, hydrogen bonding, and Coulomb as well as van der Waals forces. Moreover, covalent disulfide bonds can contribute significantly to the stability of globular proteins. Structural biology is devoted to analyze the biological functions of proteins at a molecular scale. To this end, methods, like X-ray crystallography, nuclear magnetic resonance (NMR) spectroscopy, and dual polarization interferometry, are used for the structure determination of proteins.

Occasionally, proteins are classified according to their three-dimensional (tertiary) structure and functional role into three main categories: globular, fibrous, and membrane proteins. Globular proteins are known for their high solubility in aqueous solution and their "globe"-like shape, which is achieved by exposing polar residues to the protein surface and burying hydrophobic residues in the protein interior. Fibrous proteins form long protein filaments and often have a structural role, for example, in forming connective tissue and muscle fibre. Membrane proteins are attached to or associated with cell membranes and provide simple binding sites or channels for molecules passing through the membrane. This work is mainly focused on globular proteins.

Given physiological conditions, standard Gibbs energies of unfolding, ΔG_0, of proteins are on the order of $20 - 60$ kJ/mol [50, 220]. Hence, proteins are only marginally stable against unfolding. Thus, proteins gain a high conformational flexibility, and changes of the protein environment can be directly adopted to. Upon protein denaturation, globular proteins can adopt a random coil configuration, and upon protein aggregation, proteins can even form fibrous or amyloidal structures, which play a crucial role in the pathogenesis in many neurodegenerative diseases, e.g., in Alzheimer's disease or Type 2 diabetes mellitus.

With regard to protein structure, different levels of the organization of proteins can be identified, as illustrated in Figure 2.1 [2, 8, 24, 275, 289]. The term "primary structure" refers to the sequence of amino acids of a protein. Secondary structure elements are units of regularly repeating local structures, for example, α-helices as well as β-sheets and turns. Secondary structure elements are often stabilized by hydrogen bonds. The tertiary structure of a protein explains how secondary structure elements are folded into a compact conformation. Hence, the tertiary structure describes the overall three-dimensional shape of proteins, which is relevant for their biological function. The tertiary structure is stabilized by hydrophobic interactions, salt bridges, hydrogen bonds, and disulfide bonds. Proteins consisting of more than one polypeptide chain form a quaternary structure, which describes the spatial organization of the protein subunits.

2.2 Interactions of proteins with surfaces

Whenever an aqueous protein solution is exposed to a solid surface, protein molecules will generally tend to adsorb spontaneously at the solid-liquid interface [12, 19, 30, 50, 51, 163, 177]. The

different steps of protein adsorption are illustrated in Figure 2.2. Initially, proteins dissolved in aqueous solution tend to have native-state conformation. Some proteins are transported to the interfacial region by diffusion. Then, proteins interact with and attach to the surface. In the next step, adsorbed protein molecules can undergo structural rearrangements in order to optimize their conformation and packing inside the adsorbed layer. Eventually, the adsorbed layer becomes saturated and adsorbed proteins might cluster, forming networks of adsorbed proteins. Surface-induced conformational changes of proteins often lead to irreversibly adsorbed protein layers, as evidenced by many studies [17, 36, 50, 232, 285]. The inset in Figure 2.2 shows the common time-evolution of the surface excess of proteins, Γ. At solid-liquid interfaces, adsorption reaches a steady state after an equilibration time of about an hour.

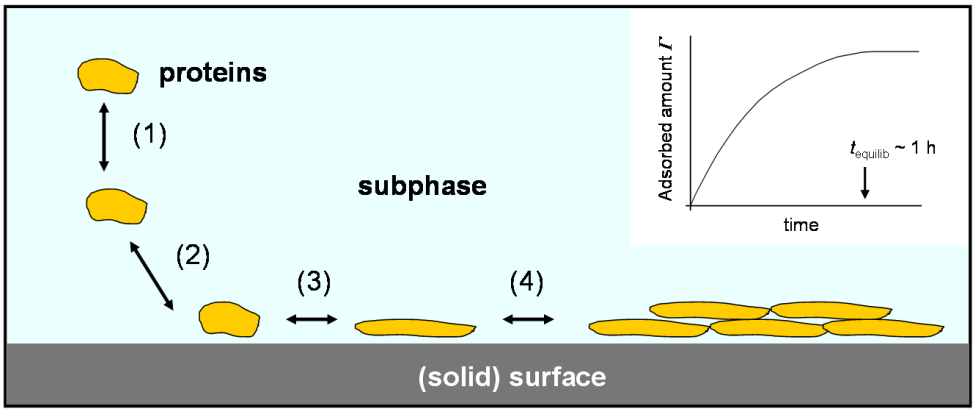

Figure 2.2: Different steps of the protein adsorption process [148, 183, 184, 186]: (1) diffusional transport, (2) adsorption and desorption at the surface, (3) surface-induced conformational changes of protein molecules, (4) saturation of the adsorbed layer and network formation. (Inset) Adsorbed amount as a function of time showing the different steps of the adsorption process. At solid-liquid interfaces, adsorption equilibrium is usually reached after about an hour.

Both protein-surface interactions and protein-protein interactions inside the absorbed layer influence the extent and shape of the adsorbed protein layer [19, 50]. In order to control the process of protein adsorption, parameter of three different ranges can be tuned or varied: (i) the surface chemistry of the substrate, (ii) the environment provided by the aqueous phase, and (iii) the specific structure of the protein.

The degree of protein adsorption at interfaces can be strongly modulated by the physicochemical properties of the interface, as for example, surface charge, surface hydrophobicity, and surface roughness. Proteins adsorbing at hydrophobic surfaces tend to expose their hydrophobic patches to the surface, due to the hydrophobic effect, resulting in pronounced conformational changes and irreversible adsorption. Hydrophilic surfaces interact with charged and polar residues of the protein surface, leading to reorientation processes of the adsorbed proteins. Therefore, proteins

have, in general, a higher tendency to spread and denature at hydrophobic surfaces than at hydrophilic ones [148, 284].

In this work, the surface chemistry of substrates for protein adsorption has been manipulated by various surface modifications, as illustrated in Figure 2.3. Polymer brushes are covalently linked to a solid substrate and provide either a mild, biocompatible environment for proteins or a protein-resistant coating, depending on the salt concentration of the subphase [75, 102, 103, 105, 214, 215, 294]. Thin polymer films can be prepared by spin-coating, yielding, for instance, non-polar, hydrophobic surfaces when poly(styrene) is used as a polymer [78–80]. Moreover, polyelectrolyte multilayers can be prepared by dip-coating via layer-by-layer assembly [57, 116, 127, 231]. Self-assembled monolayers (SAMs) represent another approach to provide substrates for protein adsorption with well-defined properties [175, 235], which can be functionalized by many chemical groups R (cf. Figure 2.3). The two most prominent examples of SAMs are alkanethiols covalently bound to gold and chlorosilanes covalently bound to silica. Here, we use octadecyltrichlorosilane (OTS) on silica, in order to prepare extremely hydrophobic surfaces (cf. Chapter 8) [89, 90].

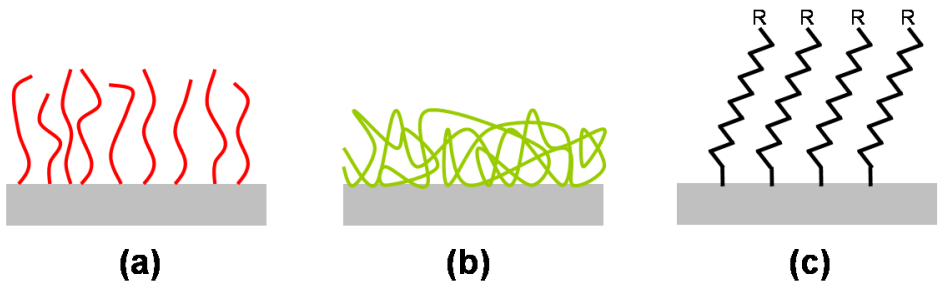

Figure 2.3: Surface functionalization used in this work: (a) polymer brushes, (b) thin polymer films, and (c) self-assembled monolayers [50]. These surface modifications can be used to control protein adsorption.

Solvent properties affect the degree of protein adsorption significantly. The pH value of the subphase determines the net charge of protein molecules. When the pH value of the subphase equals the isoelectric point of the proteins, maximum adsorption is found in general [185]. Moreover, temperature and pressure of the subphase can alter the degree of protein adsorption as well [117]. The ionic strength of the subphase affects electrostatic protein-surface and protein-protein interactions. Recently, it has been found that the addition of ionic or nonionic cosolvents to a protein solution can drastically reduce the interfacial affinity of protein [72, 75, 78–80, 113, 114, 143].

Since the structure of proteins can vary remarkably from each other (cf. Section 2.1), proteins with different masses, isoelectric points, different distribution of charged and non-charged, hydrophilic and hydrophobic residues, different conformational stability etc. show different adsorption behavior.

Diverse techniques exist to probe the interfacial structure of proteins adsorbed at planar sur-

faces [50, 163, 177]. The surface excess can be determined, e. g., by ellipsometry, surface plasmon resonance (SPR) spectroscopy, the quartz crystal microbalance (QCM) technique and by optical reflectometry. X-ray and neutron reflectometry not only yield information on the surface excess, but also reveal the vertical density profile along the surface normal. Thus, the thickness of adsorbed films and the packing density of protein molecules inside the adsorbate can be assessed. In order to characterize of the conformational state of adsorbed proteins in terms of secondary and tertiary structure, attenuated total reflection Fourier transform infrared (ATR-FTIR) spectroscopy and total internal reflection fluorescence (TIRF) spectroscopy can be applied. Moreover, computational studies of protein adsorption become more and more important, although such studies are rather challenging due to the complexity of the systems.

2.3 Driving forces for protein adsorption

Independent of the actual driving force, protein adsorption occurs spontaneously – at a constant temperature, T, and a constant pressure, p – if the Gibbs energy of adsorption, ΔG, is negative:

$$\Delta G = \Delta H - T\Delta S < 0. \tag{2.1}$$

Here, ΔH und ΔS denote the change in enthalpy and the entropy during adsorption. The more negative the value of ΔG is, the more increases the affinity to adsorption [183]. Equation (2.1) shows that driving forces for protein adsorption have either entropic or enthalpic character. Typical driving forces for protein adsorption are illustrated in Figure 2.4: electrostatic and van der Waals forces as well as hydrophobic interactions between proteins and surfaces, and adsorption-induced conformational changes. A detailed description of the driving forces for protein adsorption can be found in the literature [50, 51, 71, 183].

Describing Coulomb interactions between protein molecules and charged surfaces is complicated by the fact that the specific charge distribution of the protein surface crucially depends on the pH value and the ionic strength of the protein solution. As a general rule, maximum adsorption of proteins occurs at the isoelectric point when the protein has a zero net charge and repulsive electrostatic forces are diminished.

Moreover, hydrophobic interactions between proteins and surfaces represent another important – maybe the most important – driving force for protein adsorption [50]. In general, the hydrophobic effect relates to the fact that polar water molecules tend to exclude non-polar molecules, leading to the segregation of water and nonpolar substances [115]. When proteins adsorb at hydrophobic surfaces, the dehydration of nonpolar amino acids contributes to the Gibbs energy of adsorption.

Many experimental studies [50, 69, 182] suggest that conformational changes can lead to alterations of the protein structure, resulting in a gain of conformational entropy. Thus, conformational changes represent another driving force for protein adsorption.

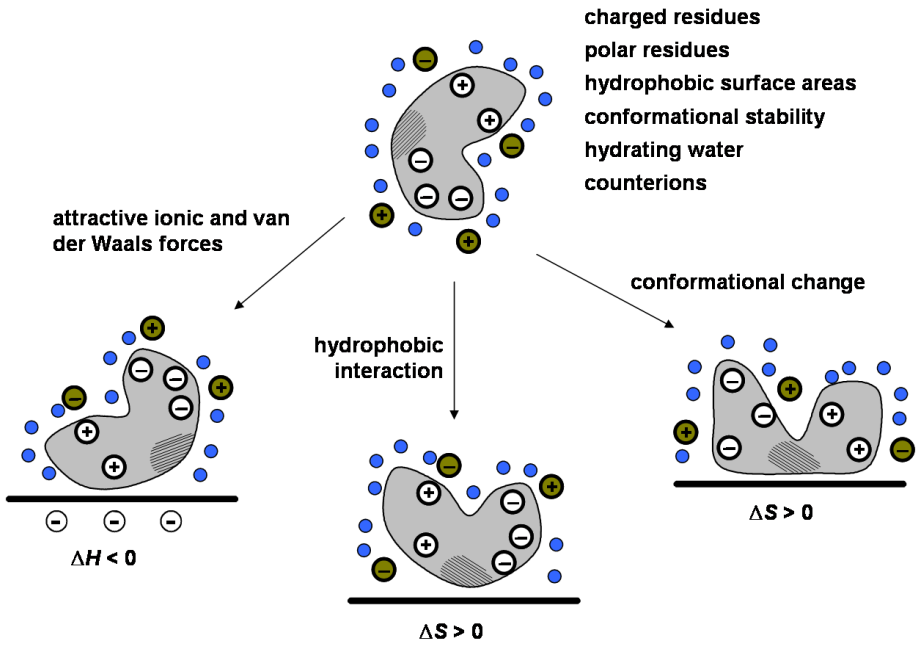

Figure 2.4: Driving forces for protein adsorption [50, 182, 184]. In general, a protein molecule (grey area) is composed of charged and polar residues (white circles) as well as hydrophobic surface areas (shaded) and surrounded by hydating water (blue) and counterions (darkgreen circles). Driving forces for protein adsorption have either enthalpic ($\Delta H < 0$) or entropic character ($\Delta S < 0$).

2.4 Model proteins

In this section, basic properties of the different model proteins are discussed. An overview of important properties is given in Table 2.1, and ribbon models of the proteins are shown in Figure 2.5.

Ribonuclease A (RNase)

Bovine Ribonuclease A (RNase) is a pancreatic enzyme that catalyzes the cleavage of single-stranded RNA. It has 124 amino acids, a molecular mass of 13.7 kDa, and an isoelectric point of 9.3 [206]. The crystal [295] and solution structure [229] of RNase are well-known. The shape of RNase resembles that of a kidney; the molecular dimensions are $22 \times 28 \times 38$ Å^3. RNase comprises three α-helices, a four-stranded antiparallel β-sheet and four disulfide bonds responsible for its high internal stability. Due to its high conformational stability, RNase is often referred to as a "hard protein" [93, 163, 206]. Moreover, RNase serves as a model protein in many

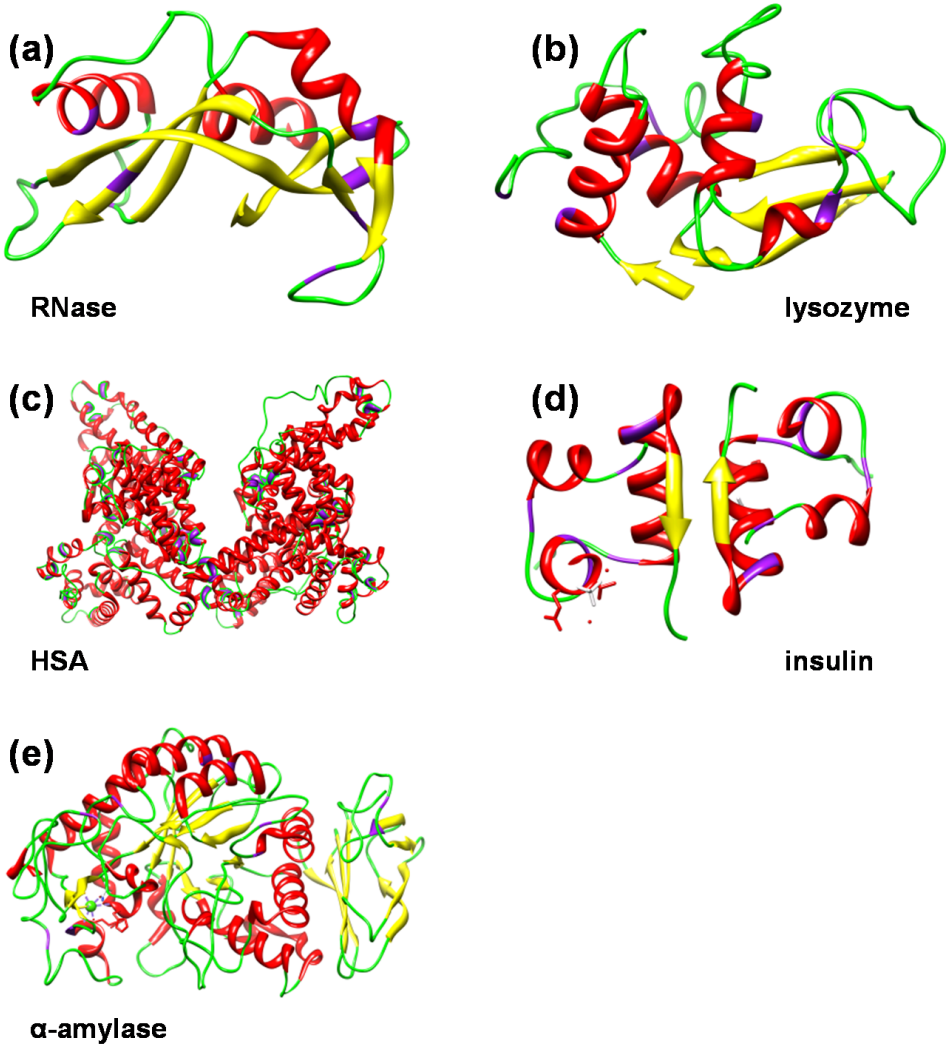

Figure 2.5: Ribbon model of the model proteins studied drawn by Chimera [5]: (a) ribonuclease A (RNase A), PDB-file 1C9X [4, 192]; (b) lysozyme, PDB-file 1LYZ [4, 58]; human serum albumin (HSA), PDB-file 1AO6 [4, 257]; (d) insulin dimer at acidic conditions (pH = 2), PDB-file 1GUJ [4, 287]; (e) α-amylase, PDB-file 1C8Q [4]. α-helices, β-strands, disulfides, and disordered structures and turns are shown in red, yellow, purple, and green, respectively.

Table 2.1: Structural and physicochemical properties of the proteins studied: RNase, lysozyme, BSA, insulin, α-amylase.[a]

protein	M [kg mol^{-1}]	pI [pH value]	net charge [b] at pH = 7	ΔG_0 [kJ mol^{-1}]	PDB-file	references
RNase	13.7	9.3	+ 4	45	1C9X	[48, 192, 203, 206]
lysozyme	14.6	11	+ 7	63	1LYZ	[48, 58, 203, 258]
BSA	68	5.3	− 15	18		[38, 103, 131, 221]
insulin	5.8	5.3	− 2	19	1GUJ	[31, 248, 250, 287, 290]
α-amylase	5.6	6.5			1C8Q	

[a] M, pI, and ΔG_0 indicate the molecular weigth, the isoelectric point and the Gibbs energy of unfolding.
[b] Data taken from [143, 214].

studies on protein folding, on protein adsorption, and in particular, on the effect of cosolvents on proteins in solution [23, 79, 80, 143, 150, 206, 222, 239, 292].

Lysozyme

Lysozyme is an enzyme, which can be found in saliva, in tear fluid and other excrements of humans. Lysozyme acts as a natural antibiotic, catalyzing the hydrolytic cleavage of polysaccharides in the membranes of certain bacteria [8]. Lysozyme is a small, globular protein. Hen egg-white lysozyme, which was used in this work, has an ellipsoidal shape ($30 \times 30 \times 45$ Å^3), a molecular weight of 14 kDa, and an isoelectric point of 11 [48, 93, 163]. Lysozyme has four disulfide bonds and is famous for its high conformational stability (a "hard" protein) [93, 163]. Hence, it serves as a model protein with a well-known structure [27, 199, 252]. As a result, its adsorption onto solid or liquid surfaces is an area of current research [76, 254, 300].

Serum Albumin

Serum albumins are the most abundant blood proteins in humans and other mammals [275]. Bovine serum albumin (BSA) is a large, globular protein mainly composed of helical structures. Its dimensions are given as 80 Å for the sides and 30 Å for the thickness [38]. It has a molecular weight of 66 kDa and an isoelectric point of 5.3 [131]. Depending on the pH value, BSA can adopt different conformations. Moreover, the conformational stability of BSA is much less than that of lysozyme or RNase [221], and therefore, BSA is called a "soft" protein [163]. BSA has well-characterized physical properties [21, 38] and thus often serves as a model protein for adsorption studies [78, 103, 255, 256].

Insulin

Insulin, a 5.7 kDa peptide hormone, is produced in the β-cells of the pancreatic islets of Langerhans [8, 48]. Its natural function is to lower the level of glucose in the blood. A lack of insulin due to a degradation of β-cells can cause diabetes mellitus type 1, which is usually treated by a lifelong medication with insulin injections. On the other hand, insulin is often used as a model protein to study the misfolding of proteins and the formation of amyloid fibrils [123]. There is a series of diseases which are associated with the formation of amyloid fibrils, such as diabetes mellitus type 2, Creutzfeldt-Jakob and Alzheimer's disease [62, 286]. Therefore, bovine insulin serves as an interesting model peptide to study the aggregation and adsorption of proteins.

α-amylase

α-amylase is a large protein composed of 496 amino acids, its molecular dimensions are $53 \times 75 \times 137$ Å^3, and its isoelectric point is at a pH-value of 6.5. α-amylase is an enzyme able to split starch into maltose and is also known as a primary colonizer for bacteria in the human oral cavity leading to the formation of plaque. Therefore, α-amylase represents an interesting model system.

3 X-ray and neutron reflectometry as methods for studying protein adsorption

In this Chapter, basic concepts of X-ray and neutron reflectometry are presented, which are relevant for the study of protein adsorption phenomena. For an in-depth treatment of surface-sensitive X-ray and neutron scattering, the reader is referred to the literature [9, 10, 55, 119, 125, 224, 267].

3.1 X-rays versus neutrons

X-ray and neutron scattering are two of the most powerful techniques suitable for providing information on the structure and dynamics of macromolecules. In this Section, the basic physical properties of neutrons and X-rays are introduced, and the production of photon and neutron beams dedicated to scattering experiments is described [135].

The neutron was discovered by James Chadwick in 1932. Neutrons are electrically neutral fundamental particles, having a mass slightly larger than a proton, a nuclear spin of $\frac{1}{2}$, and a magnetic moment. Neutrons bound to atomic nuclei are stable, while free neutrons have a lifetime of approximately 900 s.

The interaction of neutrons with atomic nuclei is weak, and the neutron scattering cross section of an atom is not related to its atomic number. The scattering cross sections of neighboring elements in the periodic table can differ remarkably from each other, because neutron scattering lengths depend on the neutron-nucleus interactions in a complex way, varying randomly with atomic and isotopic number. The variation of X-ray and neutron scattering cross sections in the periodic table is illustrated in Figure 3.1. The most prominent example of this is the isotopic substitution of light (^{1}H) for heavy hydrogen (^{2}H, D, or deuterium), which is frequently used in the study of polymeric or biological materials. Thus, the contrast of a macromolecule can be tuned selectively; and moreover, neutrons are able to locate light among heavier atoms, which are almost invisible to X-rays. Due to the weak interactions of neutrons with matter, neutrons have a high penetration power, thus being a suitable, non-destructive probe for the study of bulk processes. Furthermore, as neutrons possess a magnetic moment, spin-polarized neutron beams are apt to study magnetic structures. Interestingly, magnetic contrast has recently been used to facilitate revealing the structure of soft matter and biological materials [106].

Neutron beams with neutron fluxes suitable for scattering experiments can be produced by

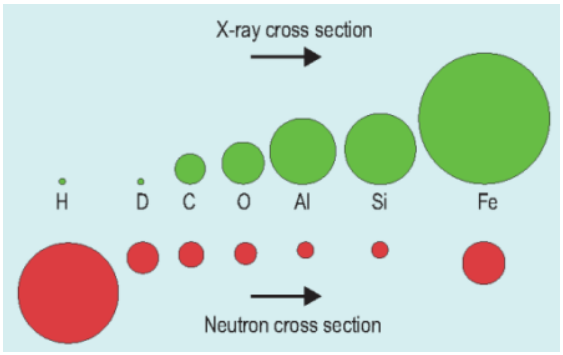

Figure 3.1: Comparision of X-ray and neutron scattering cross sections [3]. For neutrons, the scattering cross section varies erratically from one element to another, whereas, for X-rays, the scattering amplitude increases systematically with the atomic number.

nuclear reactors or by spallation sources. In a nuclear reactor (e.g., at the Institut Laue-Langevin ILL, Grenoble, France, or at the Helmholtz-Zentrum Berlin HZB, Berlin, Germany), neutron beams are produced by the fission of uranium nuclei, whereas, in a spallation source (e.g., at the Spallation Neutron Source SNS, Oak Ridge, USA, or at the Forschungsneutronenquelle Heinz Maier-Leibnitz FRM II, Garching, Germany), neutrons are expelled from a target nuclei, which is composed of a heavy metal (e.g., Hg, Ta) and is hit by charged particles.

X-rays are electromagnetic waves with wavelengths on the order of angstroms. When Wilhelm Conrad Röntgen performed experiments on discharging electrical currents in evacuated glass tubes (Crookes tube), he discovered X-rays in 1895. While neutrons are primarily scattered by atomic nuclei, X-rays show an intense interaction with the electron clouds of atoms. The scattering strength of an element is quantified by the atomic form factor, which is – for very small scattering angles – proportional to Z, the number of electrons in the element, and also the atomic number. As the volume and shape of atoms is largely built up by electron clouds, the X-ray form factor is strongly dependent on the photon scattering angle. On the contrary, the nucleus can be described as a point source in neutron-nucleus interactions.

In a laboratory, X-rays can be produced by X-ray tubes, in which electrons from the cathode collide with the anode material (e.g., Cu, Mo). X-ray beams with higher intensities are produced by synchrotron radiation sources, where electrons or positrons are accelerated by bending magnets, wigglers, or undulators, thus emitting synchrotron radiation. The flux of third-generation synchrotrons (e.g., at the European Synchrotron Radiation Facility ESRF, Grenoble, France) is 10^{13} times higher than the flux of the most brilliant neutron sources. However, biological samples often suffer from radiation damage due to the high brilliance of X-ray beams.

3.2 Surface-sensitive scattering – basic principles and scattering geometry

It is well known that visible light is reflected and transmitted at an interface between two media of different optical properties [28, 154]. Likewise, X-rays and neutrons undergo reflection and refraction at an interface if the refractive indices of the two media are different [121, 154]. For X-rays and neutrons of wave vector k (or wavelength λ), the refractive index, n, of a specimen is given, to a good approximation [224], by

$$n = 1 - \delta + i\beta. \tag{3.1}$$

The real and imaginary components of the refractive index are called dispersion, δ, and absorption, β, respectively. As δ is typically on the order of 10^{-6}, the real part of n is on the order of unity. The dispersion and absorption of a specimen are given by

$$\delta = \frac{\lambda^2}{2\pi} r_e \rho, \tag{3.2}$$

$$\beta = \frac{\lambda}{4\pi} \mu_X, \tag{3.3}$$

for X-rays, and by

$$\delta = \frac{\lambda^2}{2\pi} N b, \tag{3.4}$$

$$\beta = \frac{\lambda}{4\pi} \mu_N, \tag{3.5}$$

for neutrons, where λ is the wavelength of the incident radiation, r_e the classical electron radius, ρ the electron density in the sample, N the number density of scattering centres, b the scattering length, and μ_X and μ_N are the X-ray and neutron linear attenuation coefficients, respectively. In the following, ρ is referred to as electron density (ED) in an X-ray scattering experiment, and $\rho = Nb$ is referred to as scattering length density (SLD) in a neutron scattering experiment.

Table 3.1: Electron densities and scattering length densities of some typical substances used in this work [1, 3].

material	electron density (ED) [e Å^{-3}]	scattering length density (SLD) [10^{-6} Å^{-2}]
H_2O	0.334	-0.56
D_2O		6.36
Si	0.708	2.07
SiO_2	0.618	3.48
poly(styrene) (PS)	0.339	1.41
deuterated poly(styrene) (dPS)		6.42

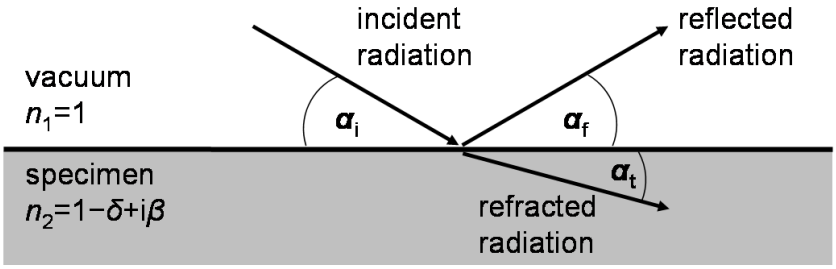

Figure 3.2: A neutron or X-ray beam is incident on a surface at an angle α_i. Portions of the beam are reflected at an angle $\alpha_f = \alpha_i$ and are refracted at an angle α_t, respectively.

Table 3.1 lists values of some typical substances studied in this work [1, 3]. It is important to note that H_2O and D_2O have quite different scattering length densities; therefore, it is possible to tune the scattering contrast over a broad range by mixing H_2O and D_2O. This unique advantage of neutron scattering is known as "contrast matching" [81]. However, when increasing the content of H-atoms, the background signal from incoherent scattering is increased as well. In this work, contrast matching is used to study protein adsorption as discussed in Section 3.9.1. A detailed description of contrast matching can be found in the literature [81]. At an interface separating two media with refractive indices, n_1 and n_2 (Figure 3.2), Snell's law

$$n_1 \cos(\alpha_i) = n_2 \cos(\alpha_t) \tag{3.6}$$

determines the angle, α_t, at which radiation is refracted as a function of the grazing angle of incidence, α_i. For a single vacuum-medium interface ($n_1 = 1$, $n_2 = n < 1$), total external reflection ($\alpha_t = 0$) occurs below a critical angle of incidence, α_c:

$$\cos(\alpha_c) = n. \tag{3.7}$$

For $\alpha_i < \alpha_c$, only an evanescent wave penetrates into the medium. Since δ is very small, Equation (3.7) yields

$$\alpha_c \approx \sqrt{2\delta} \propto \lambda\sqrt{\rho}. \tag{3.8}$$

It is common to express the scattered intensity, I, as a function of the scattering vector, $\vec{Q}$, which is also known as wave vector or momentum transfer (cf. Figure 3.3):

$$\vec{Q} = \vec{k}_f - \vec{k}_i \tag{3.9}$$

with $|\vec{k}_i| = |\vec{k}_f| = k$ for elastic scattering.

In the case of specular reflection ($\alpha_i = \alpha_f$), the wave vectors $\vec{k}_i$ and $\vec{k}_f$ are confined to the

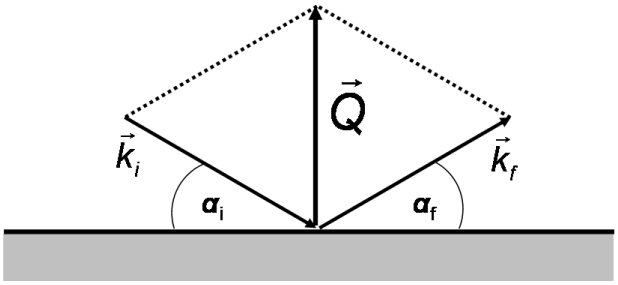

Figure 3.3: Illustration of the definition of momentum transfer, $\vec{Q}$, according to Equation (3.9).

xz-plane and are equal in magnitude. Hence, the scattering vector has only a z component, Q:

$$Q = |\vec{Q}| = 2k \sin(\alpha_\mathrm{i}) = \frac{4\pi}{\lambda} \sin(\alpha_\mathrm{i}). \tag{3.10}$$

In the literature, the z component of $\vec{Q}$ is also termed as Q_z or q_z or q. Accordingly, the critical wave vector, Q_c, is given by

$$Q_c = \frac{4\pi}{\lambda} \sin(\alpha_\mathrm{c}) \approx 4\sqrt{\pi r_\mathrm{e} \rho}. \tag{3.11}$$

3.3 Scattering from smooth surfaces

In this Section, the Fresnel reflectivity is introduced, which describes scattering from smooth surfaces. We consider a plane wave hitting an ideally flat, sharp interface between vacuum ($n = 1$) and a medium ($n = 1 - \delta + i\beta$). According to the optical treatment described in Section 3.2, the reflectivity of an ideally smooth interface can be described in terms of classical Fresnel coefficients. The reflected and transmitted amplitude (r and t) are derived from the continuity relation at the interface derived from Maxwell's equations. Hence, the Fresnel formulas can be written as

$$\begin{aligned} r &= \frac{k_{i,z} - k_{t,z}}{k_{i,z} + k_{t,z}}, \\ \text{and} \qquad t &= \frac{2k_{i,z}}{k_{i,z} + k_{t,z}}, \end{aligned} \tag{3.12}$$

where $k_{i,z} = k \sin\alpha_\mathrm{i}$ and $k_{t,z} = nk \sin\alpha_\mathrm{t} = k(n^2 - \cos^2\alpha_\mathrm{i})^{1/2}$ are the z components of the incident and transmitted wave vectors, respectively.[1]

[1] Here, the Fresnel formulas are given for s-polarized light. However, the differences between the Fresnel formulas for s- and p-polarized light can be neglected in the case of X-rays [267].

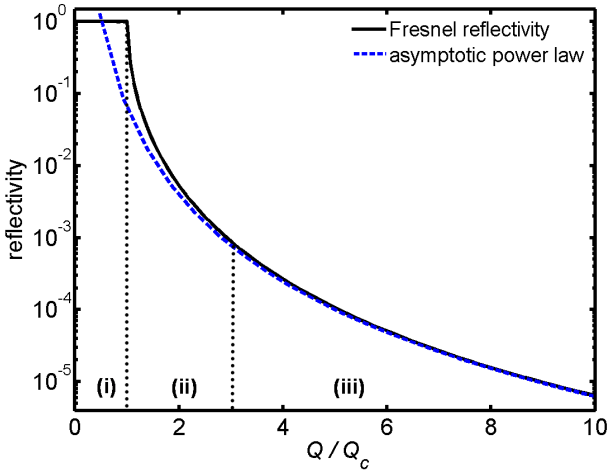

Figure 3.4: Calculated Fresnel reflectivity of an ideally flat air-water interface (solid line) and asymptotic Q^{-4} power law behavior (dashed line). Three different regions can be identified: (i) a plateau of total external reflection ($R_\mathrm{F} = 1$) when $Q < Q_c$, (ii) a steep decrease when $Q = Q_c$, and (iii) an asymptotic Q^{-4} power law behavior when $Q > 3Q_c$.

Hence, the Fresnel reflectivity, $R_\mathrm{F} = |r|^2$, of a sharp interface is given as

$$R_\mathrm{F}(Q) = \left| \frac{Q - \sqrt{Q^2 - Q_c^2}}{Q + \sqrt{Q^2 - Q_c^2}} \right|^2 = \left| \frac{1 - \sqrt{1 - \left(\frac{Q_c}{Q}\right)^2}}{1 + \sqrt{1 - \left(\frac{Q_c}{Q}\right)^2}} \right|^2 . \tag{3.13}$$

Equation (3.13) describes the specularly scattered intensity from an ideally smooth surface neglecting absorption. As can be seen in Figure 3.4, the reflectivity curve of an ideally flat surface consists of three different regimes: (i) a plateau of total external reflection ($R_\mathrm{F} = 1$) when $Q < Q_c$, (ii) a steep decrease when $Q = Q_c$, and (iii) an asymptotic Q^{-4} power law behavior when $Q > 3Q_c$.

3.4 Scattering from multiple interfaces

Figure 3.5 illustrates a system of $N + 1$ smooth, independent layers with different refractive indices. These layers are separated by N sharply defined interfaces. In layer j, the amplitudes of the transmitted and reflected wave and the layer thickness are denominated by T_j, R_j, and d_j, respectively. The amplitude of the impinging wave, hitting the surface ($z_1 = 0$) at an incident angle, α_i, is normalized ($T_1 = 1$). Both vacuum ($n_1 = 1$) and substrate are considered to be semi-infinite. Hence, no X-rays are reflected off the substrate ($R_{N+1} = 0$).

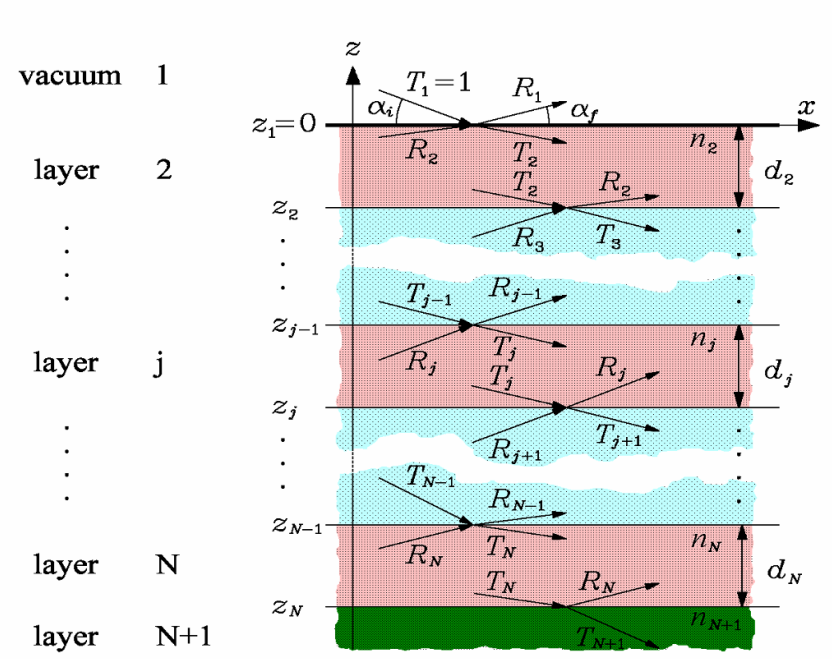

Figure 3.5: Scattering from multiple interfaces [267]. The Figure shows a system of $N+1$ ideally flat, independent layers. With respect to Parratt's recursive method, the reflectivity of this multilayer system can be calculated by computing the ratio of the reflected and transmitted amplitude for each layer, starting at the bottom of the stack.

In an optical treatment, specular scattering from a multilayer system can be calculated according to Maxwell's equations. This means summing up the reflected intensities from all interfaces with the correct phase. To tackle this problem, Abelès has proposed the transfer matrix formalism in 1950 [6]. Four years later, Parratt published an equivalent, recursive method commonly known as Parratt's algorithm [193].

In the framework of Parratt's algorithm, X_j denotes the ratio of reflected and transmitted amplitudes (R_j, T_j) of layer j. If X_{j+1} is known, then X_j for the layer above can be retrieved from Parratt's recursion formula:

$$X_j = \frac{R_j}{T_j} = \exp\left(-2ik_{z,j}z_j\right)\frac{r_{j,j+1} + X_{j+1}\exp\left(2ik_{z,j+1}z_j\right)}{1 + r_{j,j+1}X_{j+1}\exp\left(2ik_{z,j+1}z_j\right)}, \tag{3.14}$$

where

$$r_{j,j+1} = \frac{k_{z,j} - k_{z,j+1}}{k_{z,j} + k_{z,j+1}}$$

is the Fresnel coefficient of layer j with $k_{z,j} = k\left(n_j^2 - \cos^2\left(\alpha_\mathrm{i}\right)\right)^{1/2}$. Using $R_{N+1} = X_{N+1} = 0$ as a starting condition, the reflected intensity R can be calculated after N iterations of Parratt's

recursion formula (3.14), starting at interface N:

$$R = |X_1|^2 = |R_1|^2 . \tag{3.15}$$

As a simple example, scattering from a one-layer system (as shown in Figure 3.6) is illustrated in Figure 3.7. In Figure 3.7, the reflectivity and the scattering length density profile of a film (with a thickness of $d = 250$ Å) adsorbed at a silicon wafer are shown.

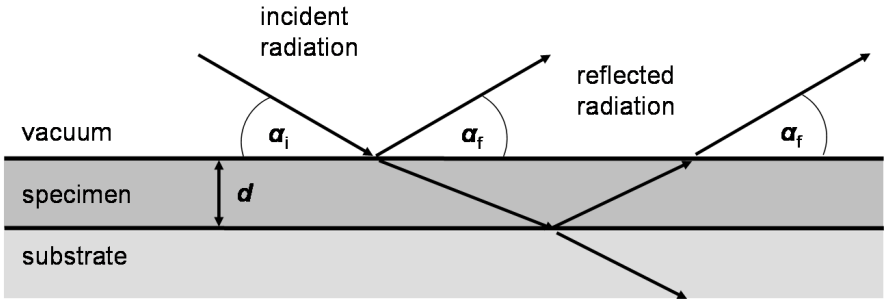

Figure 3.6: Scattering from a one-layer system. Since waves, which are reflected from the different interfaces of the system, interfere with each other, the reflected intensity of this system oscillates (cf. Figure 3.7).

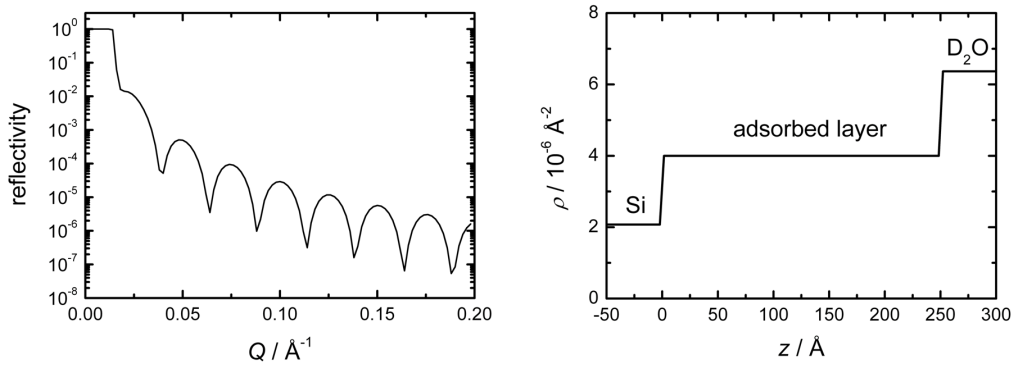

Figure 3.7: (Left) Calculated reflectivity curve and (Right) scattering length density profile of a one-layer system. The oscillations in the reflectivity curve are known as "Kiessig fringes"; and their period in Q is related to the thickness of the adsorbed film.

The reflection coefficient, r, and reflected intensity, R, of such a one-layer system are given by

$$r = \frac{r_{0,1} + r_{1,2} \exp\left(-2ik_{z,1}d\right)}{1 + r_{0,1}r_{1,2} \exp\left(-2ik_{z,1}d\right)} \tag{3.16}$$

and

$$R = \frac{r_{0,1}^2 + r_{1,2}^2 + 2r_{0,1}r_{1,2} \cos\left(2ik_{z,1}d\right)}{1 + r_{0,1}^2 r_{1,2}^2 + 2r_{0,1}r_{1,2} \cos\left(2ik_{z,1}d\right)}. \tag{3.17}$$

The presence of the cosine terms in the last equation indicates the oscillatory behavior of the reflectivity curve in reciprocal space, as shown in Figure 3.7. These oscillations are also referred to as "Kiessig fringes" [137]. The oscillation period, ΔQ, can be related to the layer thickness: $d = \frac{2\pi}{\Delta Q}$.

3.5 Scattering from rough interfaces

Up to this point, the reflectivity of infinitely sharp interfaces has been discussed, only. However, surfaces and interfaces are always rough in practice; thus, surfaces do not exhibit a stepwise, but rather a gradual change in density in going, for example, from the air into the specimen.

Figure 3.8 shows an interface whose deviations from the mean height of the interface can be described by Gaussian statistics. In an equivalent approach, the profile of an infinitely sharp profile can be convoluted with a Gaussian smoothing function, as given in Equation (3.18).

$$G(z) = \frac{1}{\sqrt{2\pi}\sigma} \exp\left(-\frac{z^2}{2\sigma^2}\right). \tag{3.18}$$

Here, the roughness, σ, is the standard deviation from the mean height of the interface. In this case, the density profile of the interface can be described by an erf-function [7].

According to the Born approximation, the reflectivity, $R(Q)$, is given by

$$R(Q) = R_{\mathrm{F}}(Q) \left| \frac{1}{\rho_{\mathrm{sub}}} \int \left(\frac{\mathrm{d}\rho(z)}{\mathrm{d}z}\right) e^{iQz} \mathrm{d}z \right|^2, \tag{3.19}$$

where R_{F}, ρ_{sub}, and $\rho(z)$ denote the Fresnel reflectivity, the electron or scattering length density of the subphase and the vertical electron or scattering length density profile, respectively. According to this equation, the reflectivity is directly related to the one-dimensional Fourier transform of the electron density or scattering length density profile. Since $G(z)$ is the derivate of $\rho(z)$, we obtain

$$R(Q) = R_{\mathrm{F}}(Q) e^{-Q^2\sigma^2}. \tag{3.20}$$

Equation (3.20) demonstrates the effect of increased roughness on reflectivity curves, which is illustrated in Figure 3.9. Local variations of the incident angle due to interfacial roughness lead to diffuse scattering, lowering the reflectivity of a system. Describing interfacial roughness by Gaussian statistics is also referred to as Nevot-Croce model [55].

Using the optical treatment of reflectivity analysis, the Fresnel coefficients of Equation (3.14) have to be modified [267], including interfacial roughness:

$$\tilde{r}_{j,j+1} = r_{j,j+1} \exp\left(-2k_{z,j}k_{z,j+1}\sigma_j^2\right). \tag{3.21}$$

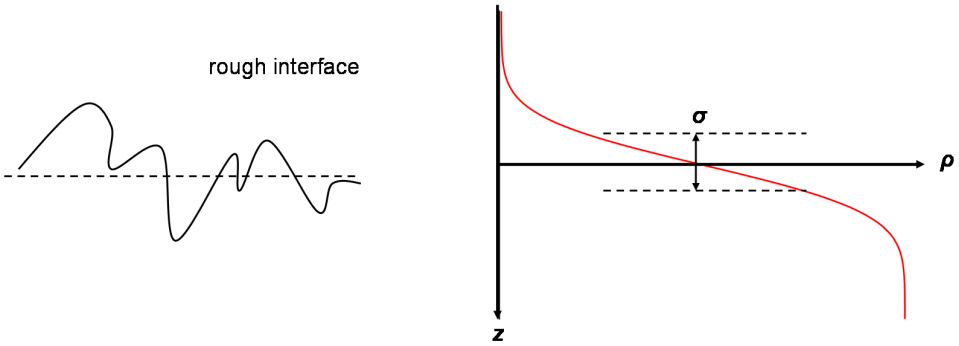

Figure 3.8: (Left) Rough interface (solid line) whose deviations from the mean height of the surface (dotted line) can be described by Gaussian statistics. (Right) Analogously, the density profile of an ideally flat interface can be convoluted by a Gaussian smoothing function, accounting for interfacial roughness.

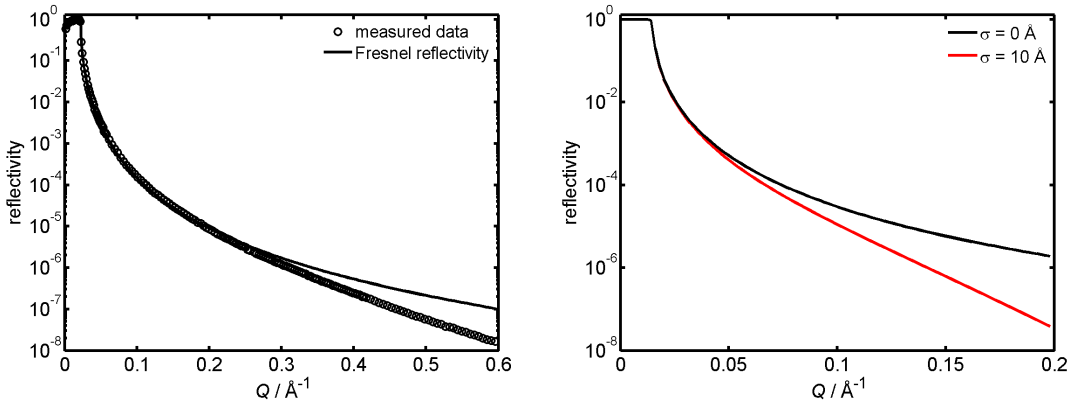

Figure 3.9: (Left) X-ray reflectivity data of an air-water interface (symbols) and the calculated Fresnel reflectivity (solid line). Due to interfacial roughness, the measured reflectivity is reduced as compared to the Fresnel reflectivity. (Right) Calculated neutron reflectivity curves of a smooth ($\sigma = 0$ Å, black line) and a rough silica-water interface ($\sigma = 10$ Å, red line). Obviously, an increased roughness leads to a reduction of the reflectivity.

3.6 Arbitrary density profiles

So far, the reflectivity of multilayer systems and the reflectivity from rough interfaces has been discussed. However, this treatment will yield relevant information only if the roughness of the interfaces is significantly smaller than the thickness of the layers. If this condition is violated, and the interfacial roughness is indeed on the order of the film thickness or even larger, then the different layers cannot be considered as independent. In this case, the nominal values of the

refractive indices (or of the scattering length density or the electron density) are not reached within the layers, and the density profile becomes discontinuous. In order to overcome this problem, the effective density model has been introduced [267], which is especially relevant for molecularly thin films.

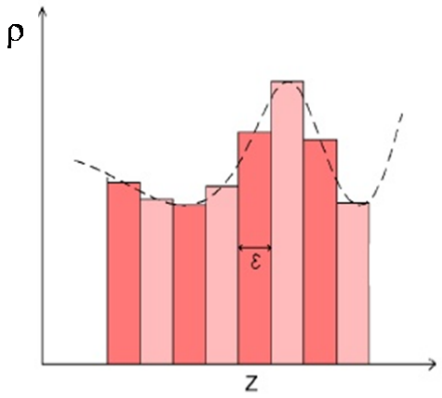

Figure 3.10: The density profile in the effective density model [267], assuring for a continuous density profile (even in the case of large interfacial roughness). Here, the initially guessed density profile is chopped into small, ideally flat layer (of thickness, ε) with uniform density.

According to the effective density model, the whole density profile, $\rho(z)$, has to be guessed at first. In the next step, the profile of this "initial guess" is subdivided into very thin discrete layers (with a thickness, ε, of approximately 1 Å) with uniform density and sharp interfaces, representing the profile histogramatically, as illustrated in Figure 3.10. Eventually, the reflectivity of this system is calculated by Parratt's recursive method [193]. It is important to note that the mathematical formulation of this model ensures for the continuity of the profile. Mathematical details of the effective density model are described in the literature [243, 267].

However, the interpretation of the model parameters is complicated in the effective density model. In particular, the density of a distinct layer can be much less than its nominal value, ρ_j; in the framework of the effective density model, the density profile at a certain depth z is to be understood as "effective density at depth z".

3.7 Measuring the reflectivity curve

The definition of the wavevector transfer, Q, in a reflectivity experiment in Equation (3.10) shows that Q can be altered either by varying the incident angle at a fixed wavelength or by varying the wavelength at a fixed incident angle [224]. Hence, in a scattering experiment, the reflectivity,

R, is usually given by

$$R(\alpha_\mathrm{i}) = \frac{I(\alpha_\mathrm{i})}{I_0}, \tag{3.22}$$

$$\text{or} \qquad R(Q) = \frac{I(Q)}{I_0}, \tag{3.23}$$

where $I(\alpha_\mathrm{i})$ or $I(Q)$ are the reflected intensity for an angle of incidence α_i (or wave-vector transfer Q), and I_0 is the intensity of the incident beam.

Owing to these two ways of variation in Q, two different types of reflectometers have been developed. Given a fixed, monochromatic wavelength of the incoming beam, the reflectivity is collected by varying the angle of incidence and measuring the specularly scattered intensity, as shown in Figure 3.11. On the contrary, it is also possible to collect reflectivity curves at a fixed incident angle. To do so, one can use a polychromatic neutron or photon beam with a defined spectrum of wavelengths (time-of-flight neutron reflectometer, TOF, or energy-dispersive X-ray reflectometer) [54]. Both types of reflectometers (fixed λ or fixed α_i) can be found throughout the world. For example, neutron and X-ray reflectometers with a fixed wavelength are available at the HZB, at the ESRF, at the synchrotron light source DELTA, Dortmund, Germany, or at the Deutsches Elektronensynchrotron DESY, Hamburg, Germany, whereas TOF reflectometers can be found at the SNS and FRM II.

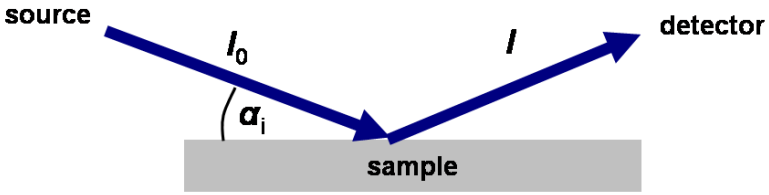

Figure 3.11: Measuring the reflectivity. Using a monochromatic reflectometer, one can measure the reflectivity of a system by collecting the intensity of the incident beam, I_0, and the specularly scattered intensity $I(\alpha_\mathrm{i})$ in a broad range of incident angles α_i.

3.8 Data reduction and analysis of reflectivity curves

Data reduction usually comprises background correction and normalization of the raw data, and scaling them as a function of Q. Reflectivity data are often normalized to the Fresnel reflectivity, R_F, in order to highlight features stemming from thin layers of the system in the case of low density contrast.

To obtain the electron or scattering length density profile from reflectivity data, a model of

the vertical structure of the studied system is proposed from which a reflectivity is calculated by Parratt's recursive method [193]. The proposed density profile is varied in such a way that the mean square variation, χ^2, of the difference between calculated, R_{theo}, and observed reflectivity curve, R_{exp}, is minimized:

$$\chi^2 = \frac{1}{N}\sum_{i=1}^{N}\left(\log R_{\mathrm{exp}}(Q,i) - \log R_{\mathrm{theo}}(Q,i)\right)^2, \tag{3.24}$$

where i stands for the measuring point and N is the sum of all measuring points. In this work, X-ray reflectivity data were fitted by the program LSFIT [236], using the effective density model; on the contrary, neutron reflectivity data were fitted by the program Parratt32, using the Nevot-Croce model.[2]

In general, the density profile is given as a stack of homogeneous layers each with a distinct electron density, ρ, layer thickness, d, and interfacial roughness, σ, between adjacent layers. In most cases, several strategies minimizing the number of fitting parameters were undertaken. To this end, it is beneficial, for example, to characterize the interfacial structure of the substrate without adsorbed proteins prior to the adsorption experiment, keeping the parameters of the substrate constant when fitting the measurements with protein. It is common to estimate the errors of the fitting parameters by allowing a variation of 5 % from the χ^2 of the best fit [113].

3.9 Protein adsorption studied by X-ray and neutron reflectometry

In this Section, peculiarities of X-ray and neutron reflectometry with respect to the study of adsorbed protein films are presented. In the first part, the high adsorption sensitivity of neutron reflectometry is related to the possibility of contrast matching. In the second part, the calculation of the volume fraction and surface excess of adsorbed protein films is explained. Using X-ray reflectometry, even volume fraction profiles can be computed, due to the large Q range covered by X-ray measurements.

3.9.1 Contrast matching and adsorbate sensitivity in neutron reflectometry

Hydrogen atoms are ubiquitous in nature and play a crucial role in the stability of biomolecular structures. While the scattering contribution of hydrogen atoms is almost invisible to X-rays, even the isotopes of hydrogen have different neutron scattering properties. Owing to these differences, the scattering density, and thus, the scattering contrast of a macromolecule or a solvent can be changed dramatically by manipulating the ratio of ^{1}H and ^{2}H in those systems, as illustrated in Figure 3.12. Three examples applying the contrast variation technique are (i) the

[2] Techniques for the analysis of X-ray and neutron reflectivity data are reviewed in [228, 273].

deuteration of biological macromolecules using bacterial expression systems, (ii) the synthesis of deuterated polymers, and (iii) the systematic variation of deuterium content in the solvent of biological systems.

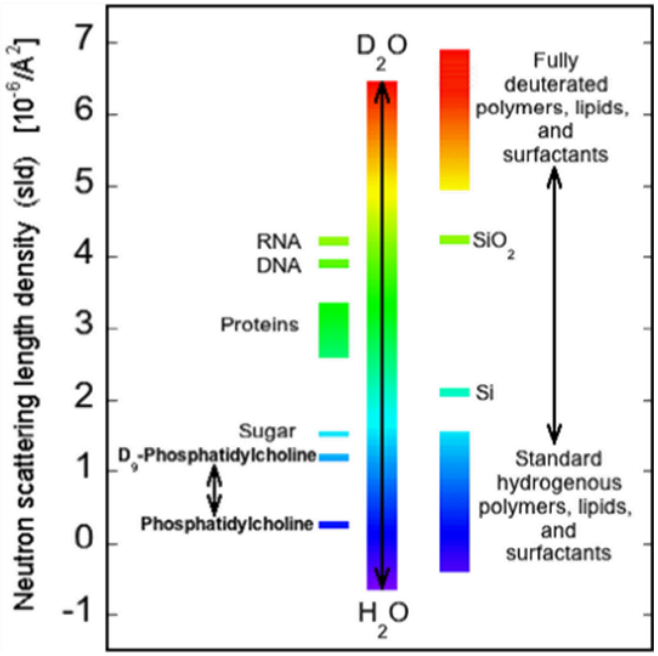

Figure 3.12: Contrast variation [120]. By manipulating the ratio of ^{1}H and ^{2}H, structural features in organic and biological systems can be selectively highlighted.

Figure 3.13 shows how hydrogeneous and perdeuterated polymer films can be used to enhance scattering contrast. Part (a) shows a hydrogeneous poly(styrene) film (PS) attached to a silicon wafer in an aqueous (D_2O) environment. As the scattering length densities of PS and D_2O differ remarkably from each other, the reflectivity curve shows clear Kiessig fringes. On the contrary, no Kiessig oscillations can be observed in part (b), as perdeuterated poly(styrene) (poly(styrene-d_8), dPS) and D_2O environment have almost the same scattering length density. In this sense, dPS layer and D_2O subphase are "contrast matched". Introducing proteins into the D_2O solution and subsequent spontaneous formation of an adsorbed protein film, changes this situation dramatically, as shown in part (c). The presence of the protein adsorbate which has a lower scattering length density than dPS or D_2O increases the scattering contrast and thus induces pronounced Kiessig oscillations in the reflectivity curve, highlighting features of both the dPS and the adsorbate film. This methodology has been used to characterize adsorbed protein films in this work, as discussed in Sections 5.1 [80] and 6.2 [79]. However, the dPS film has been characterized in a mixture of light and heavy water at first, improving the scattering contrast as compared to part (b).

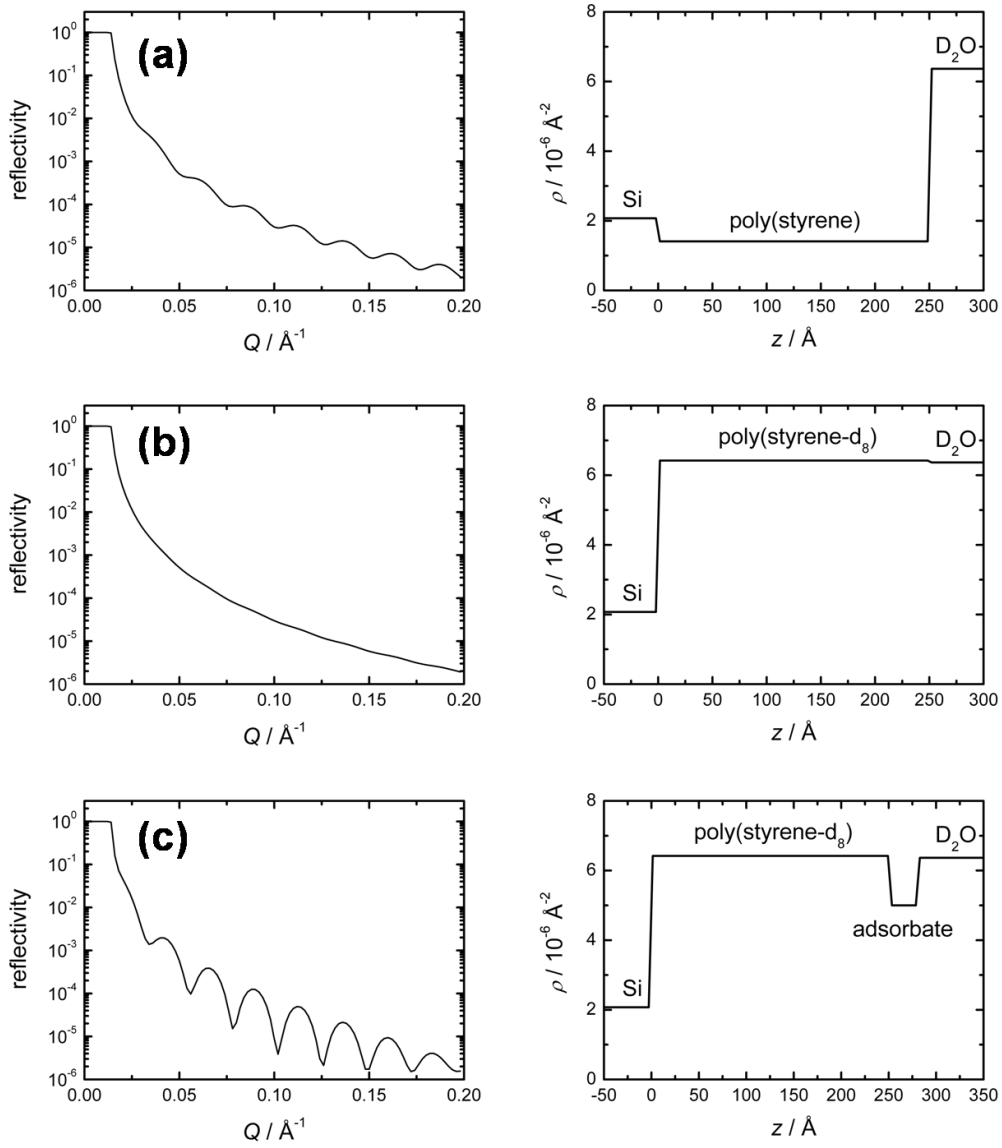

Figure 3.13: Contrast matching and adsorbate sensitivity in neutron reflectometry using polymer films. (Left) Reflectivity curves and (Right) scattering length density profiles of hydrogeneous and perdeuterated polymer films in an aqueous (D_2O) environment in parts (a) and (b), respectively. Part (c) illustrates how the presence of an adsorbed protein film affects the reflectivity curve of the contrast matched system in part (b).

3.9.2 Volume fraction and surface excess of adsorbed protein films

Methods for studying protein adsorption usually access the amount of adsorbed proteins or surface excess, Γ. However, from neutron or X-ray reflectivity data, not only the adsorbed amount, Γ, but also the volume fraction profile, $\phi(z)$, along the surface normal can be obtained [78, 105].

In an electron or scattering length density profile, adsorbed protein films are characterized by a layer thickness, d, and by an electron density or scattering length density, $\rho_{\mathrm{adsorbate}}$. These parameters can be used to calculate the packing density of the protein molecules inside the adsorbed layer, ϕ, and the mass of adsorbed proteins, Γ. To do so, $\rho_{\mathrm{adsorbate}}$ can be decomposed in contributions from the pure protein and from the buffer, according to Equation (3.25) [76, 117, 129].

$$\rho_{\mathrm{adsorbate}} = \phi\rho_{\mathrm{protein}} + (1-\phi)\rho_{\mathrm{subphase}} \tag{3.25}$$

$$\Rightarrow \qquad \phi = \frac{\rho_{\mathrm{adsorbate}} - \rho_{\mathrm{subphase}}}{\rho_{\mathrm{protein}} - \rho_{\mathrm{subphase}}} \tag{3.26}$$

Here, $\rho_{\mathrm{adsorbate}}$ and ρ_{subphase} are the electron density or scattering length density of the pure protein and the subphase, respectively, which are weighted by their volume fractions ϕ and $(1-\phi)$ within the adsorbate. While $\rho_{\mathrm{adsorbate}}$ and ρ_{subphase} are given from the electron density or scattering length density profile, ρ_{protein} must be calculated. This has been done by summing up the electrons or scattering lengths of all atoms of a protein molecule and dividing through the molecular volume. To this end, the scattering lengths published by NIST [3] and primary sequences published in the Protein Data Bank [4] were used. Values of ρ_{protein} in water or D_2O-solution are listed in Table 3.2.

Table 3.2: Electron densities (ρ_X), neutron scattering length densities (ρ_n, when dissolved in D_2O) and specific volume (v) of typical proteins used in this work [1, 3].

protein	ρ_X [e Å^{-3}]	ρ_n [10^{-6} Å^{-2}]	v [cm^3 g^{-1}]	PDB-file / references
RNase	0.4561	3.553	0.703	1C9X [48, 192]
lysozyme	0.4558	3.632	1.425	1LYZ [48, 58]
BSA	0.4387	3.187	1.364	[103, 131]
insulin	0.4471	3.273	0.717	[248, 250]
α-amylase	0.4713		0.533	1C8Q

In Equation (3.26) a mean volume fraction, ϕ, inside adsorbed protein films is defined. In a more generalized approach, even the volume fraction profile, $\phi(z)$, can be calculated from the density profile in the presence of the adsorbed film, $\rho(z)$, and the reference profile in the absence of proteins, $\rho_{\mathrm{ref}}(z)$.

$$\phi(z) = \frac{\rho(z) - \rho_{\mathrm{ref}}(z)}{\rho_{\mathrm{protein}} - \rho_{\mathrm{ref}}(z)} \tag{3.27}$$

Using $\phi(z)$ of Equation (3.27), the adsorbed amount is given by

$$\Gamma = \frac{1}{v} \int \phi(z) \mathrm{d}z; \tag{3.28}$$

using the mean volume fraction, ϕ, defined by Equation (3.26), the calculation of Γ is simplified:

$$\Gamma = \frac{\phi d}{v}. \tag{3.29}$$

The values of the specific volume, v, for various protein used in this work are listed in Table 3.2.

4 Experimental section

In this Chapter, the set-up used in X-ray and neutron scattering experiments as well as experimental details of the different sample environments are presented. In the first Section, the set-up for measurements at solid-liquid interfaces and, in particular, methods of surface functionalization are introduced. After this, the experimental set-up for measurements at the air-water interface is described.

4.1 Experiments at solid-liquid interfaces

Originally, neutron reflectometry was the leading technique for the characterization of buried interfaces, because neutrons can penetrate matter over macroscopic distances, and X-ray reflectometry was limited to the study of air-solid and air-liquid interfaces. However, during the last ten years, X-ray reflectivity studies at the solid-liquid interface have become feasible using high-energy synchrotron radiation [70, 211, 218, 219]. Recently, this technique has been applied to biological and soft matter thin films [170, 210] and to adsorbed protein films [76–78, 194]. As outlined in Section 3, neutron reflectometry provides the advantages of contrast variation and little beam damage, while suffering from a limited Q range, a restricted real-space resolution as well as long data acquisition times. On the other hand, X-ray reflectometry using high-energy photons offers the advantages of increased resolution, faster measurements, and smaller sample amounts without the need for deuteration [170, 194]. However, possible beam damage caused by the high photon flux represents a severe drawback of this technique.

In the following, the different experimental layouts of the reflectometers used in this work to access solid-liquid interfaces are introduced: the V6 reflectometer at the HZB and the high-energy surface diffractometer of beamline BL9 at DELTA.

4.1.1 Neutron reflectivity measurements: the V6 reflectometer at the HZB

Neutron reflectivity measurements were carried out at the HZB using the instrument V6 [167]. The neutron beam was produced in the light-water reactor BER II at the Berlin Neutron Scattering Center (BENSC), generating a neutron flux density of 1×10^{14} n·cm^{-2}·s^{-1} at a thermal power of 10 MW. Thermal neutrons were decelerated in a cold source, and after this, cold neutrons were conveyed to the experimental stations via neutron guides. The experimental set-up of the V6 reflectometer is sketched schematically in Figure 4.1. The neutron wavelength ($\lambda = 4.66$ Å) was

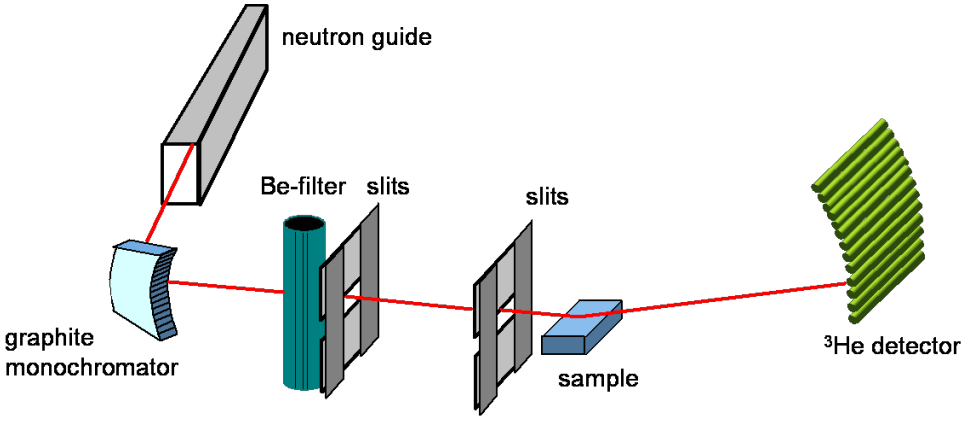

Figure 4.1: Experimental set-up of the neutron reflectometer V6. A beam of cold neutrons (red line) was monochromated by graphite crystals and collimated by a slit system before impinging on the sample. Scattered neutrons were monitored by an array of ^{3}He detectors. As the position of the incident beam was fixed, reflectivity measurements were performed by simultaneously rotating sample stage and detector system in $\theta - 2\theta$ geometry.

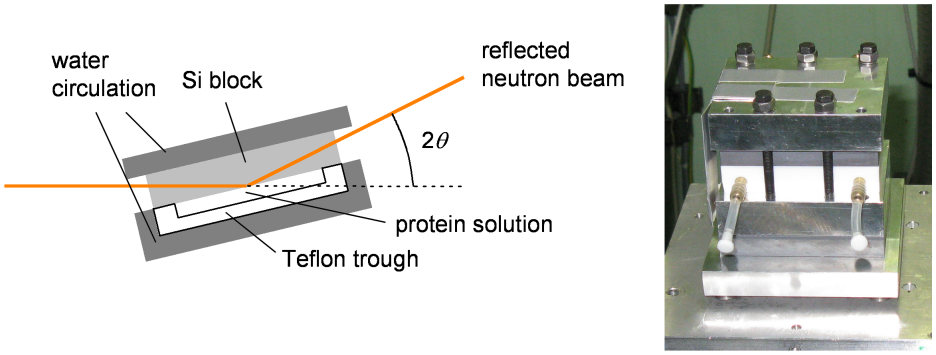

Figure 4.2: (Left) Sketch and (Right) photo of the sample cell, which was constructed during this work for neutron reflectivity measurements at solid-liquid interfaces [110]. A silicon wafer was fixed between two frame blocks consisting of aluminum. A Teflon trough, into which the sample solution was injected, was placed into a cavity underneath the wafer. If necessary, temperature-control was achieved via thermostated water flowing through the frame blocks. The neutron beam (orange line) entered and left the wafer through one of the small sides.

selected by a monochromator composed of pyrolytic graphite crystals, and higher-order wavelengths were suppressed by a beryllium filter cooled with liquid nitrogen. The monochromatic neutron beam was collimated by a system of cadmium slits. In the sample cell [110], a Teflon trough was mounted underneath a silicon wafer ($8 \times 5 \times 1.5$ cm^3) and was filled with approximately 10 mL of the sample solution, as illustrated in Figure 4.2. The neutrons entered the silicon block through one of the small sides (5×1.5 cm^2), were reflected off the silicon-solution interface, and left the silicon block through the other small side. The cross section of the neutron beam was confined to 0.5×40 mm^2 for $Q \leq 0.052$ Å^{-1} and to 1×40 mm^2 for $Q > 0.052$ Å^{-1}. Based on this, the instrument resolution was calculated to $\Delta Q/Q = 0.001$ Å^{-1} and 0.002 Å^{-1}, respectively. Neutron reflectivity measurements were performed with a fixed incident neutron beam in $\theta - 2\theta$ geometry by simultaneously rotating the sample cell (θ) and the detector system (2θ) and recording the specularly scattered intensity. The detector system consisted of an array of ^{3}He gas detectors. The angle of incidence, θ, usually ranged from 0.1° to 2.55°, yielding a Q-range of $0.005 - 0.12$ Å^{-1}. Raw data were normalized to the number of incoming neutrons hitting the silica-solution interface. Prior to each run, the sample cell was rinsed with copious amounts of ultrapure water, filled with freshly prepared sample solution, and was equilibrated for at least 1 h. All measurements were performed at room temperature.

4.1.2 X-ray reflectivity measurements from buried interfaces: the high-energy X-ray scattering set-up of beamline BL9 at DELTA

X-ray reflectivity measurements at solid-liquid interfaces were conducted at the surface diffractometer of beamline BL9 at the synchrotron light source DELTA (Dortmund, Germany) [144, 194]. The electron storage ring at DELTA was operated with a maximum electron energy of 1.5 GeV at an maximum electrical current of 130 mA with lifetimes of 10 h. Photons used at beamline BL9 were produced in a superconducting, asymmetric wiggler with a critical energy of 7.9 keV. The photon beam was monochromatized by a silicon (311) double-crystal with an energy resolution of $\Delta E/E = 10^{-4}$. In order to access buried solid-liquid interfaces, a photon energy of 27 keV ($\lambda = 0.459$ Å) was chosen, as explained below, yielding a photon flux density of 7×10^8 photons mm^{-2}·s^{-1} at 100 mA. The photon beam was focused horizontally by sagittal bending of the second monochromator crystal. The experimental set-up of beamline BL9 used for studying solid-liquid interfaces and the sample cell in this set-up are shown in Figures 4.3 and 4.4, respectively. Incoming and scattered photon beam (large red arrows) were collimated and defined by slit systems (indicated by facing arrows). At the sample position, the beam had a cross section of 1×0.2 mm^2. Moreover, an auto-absorber system (grey box in the beam path) was installed for beam attenuation, limiting the photon flux incident on the sample. In order to monitor the incoming photon beam before and after the attenuator and to measure the specularly scattered intensity, NaI detectors (small grey boxes along and at the end of the beam path) were used. The typical angular resolution was 0.015°.

The sample cell (Figure 4.4), which was mounted on the diffractometer, consisted of a hollow

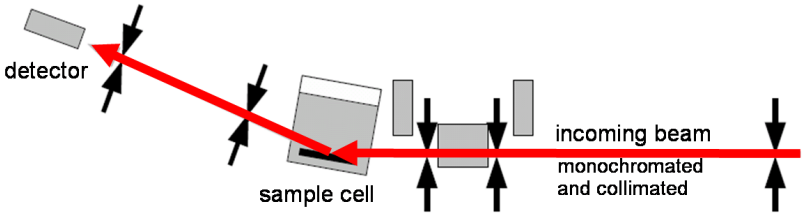

Figure 4.3: Layout of the set-up of beamline BL9 at DELTA using a high photon energy of 27 keV to access buried solid-liquid interfaces [76, 194]. The intensity of the incident photon beam (red arrow) was monitored before and after the attenuator (grey box in the beam path). For this purpose and for measuring the scattered intensity, NaI detectors (small grey boxes along and at the end of the beam path) were used. Slit systems (facing arrows) were used to confine the beam. Reflectivity measurements were performed in $\theta - 2\theta$ geometry.

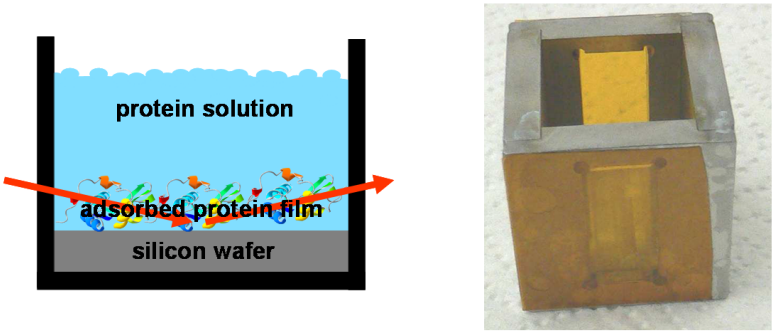

Figure 4.4: (Left) Sketch and (Right) photo of the common sample cell for the study of solid-liquid interfaces at beamline BL9 (DELTA). The volume of the sample cell is about 10 mL, the path of the X-ray beam through the cell is approximately 30 mm.

steel cube with Kapton windows for beam entrance and beam exit. For each measurement, the sample cell was cleaned thoroughly and a new silicon wafer (18×18.8 mm^2) was put into a sample carrier (20×20 mm^2), which was fixed at the bottom of the sample cell. All measurements were performed at room temperature. Specular reflectivity scans were performed in $\theta - 2\theta$ geometry by simultaneously rotating the sample stage (θ) and the detector (2θ), so that the angle of incidence, θ, equalled the exit angle of the radiation relative to the sample surface. In order to obtain the "true" specular reflectivity, diffuse scattering was measured by longitudinal-diffuse scans with a constant angular detector offset of 0.1°. A typical X-ray reflectivity measurement with a measuring time of 20 min covered a dynamic range of about seven orders of magnitude and an angular range of $0.02° - 1.0°$ (corresponding Q-range $0.001 - 0.5$ Å^{-1}).

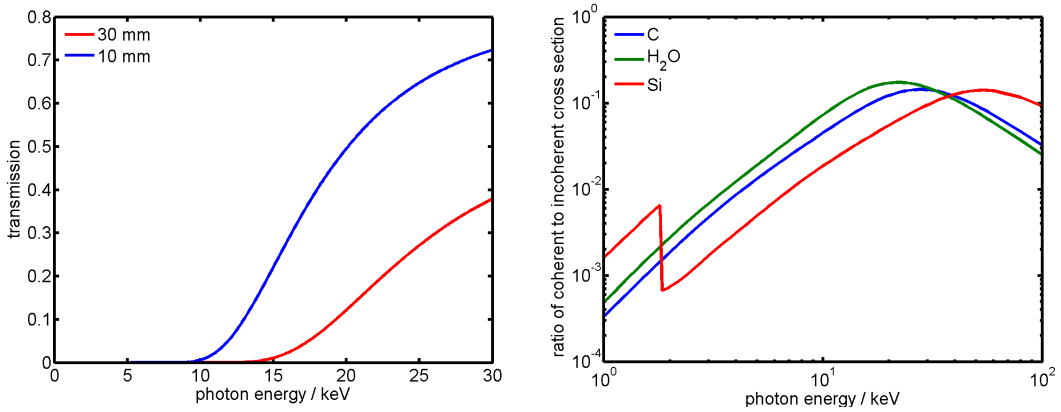

Figure 4.5: (Left) Transmission of X-rays through 10 mm and 30 mm of H_2O, which is the typical X-ray path length in the two different sample cells available, yielding a transmission of 32 % and 68 %, respectively [77]. (Right) Ratio of coherent to incoherent X-ray scattering cross section for H_2O (maximum at 26 keV), C (maximum at 22 keV) and Si (maximum at 52 keV) [25, 209]. Both figures indicate that an X-ray energy range between 20 and 30 keV is optimal for the study of biological and soft matter materials [77, 210].

At beamline BL9, a photon energy of 27 keV was chosen to study solid-liquid interfaces, because of several reasons [170, 210]: First of all, the transmission through the water filled sample cell should be high (cf. Figure 4.5). Second, incoherent scattering processes can cause radiation damage to biological or soft matter samples. This is a serious issue in the context of biomolecules, and, hence, beam damage should be minimal. Third, the diffraction signal from the interface which is given by the coherent cross section should be high. In this context, Figure 4.5 illustrates that the investigation of organic materials is favored by X-ray energies in the regime between 20 and 30 keV.

4.1.3 Surface functionalization

In this Subsection, the preparation of substrates for studies at solid-liquid interfaces [50] is described. Clean surfaces with well-defined and reproducible properties are a prerequisite for the study of interfacial phenomena [82]. To this end, silicon or quartz wafers serve as appropriate sample materials. In the first step of surface functionalization, wafers are cleaned and become hydrophilic. After this, various, functionally different surface architectures can be designed, as illustrated, for example, in Figure 4.6.

For neutron reflectivity measurements, silicon wafers with a size of $8 \times 5 \times 1.5$ cm^3 (CrysTec, Berlin, Germany) were cleaned in a $1:1:4$ mixture of NH_3 (30 %), H_2O_2 (30 %), and H_2O at 70 °C for 15 min, followed by intensive rinsing with copious amounts of ultrapure water. For X-ray reflectivity measurements, silicon wafers (provided by Wacker Siltronic, Burghausen,

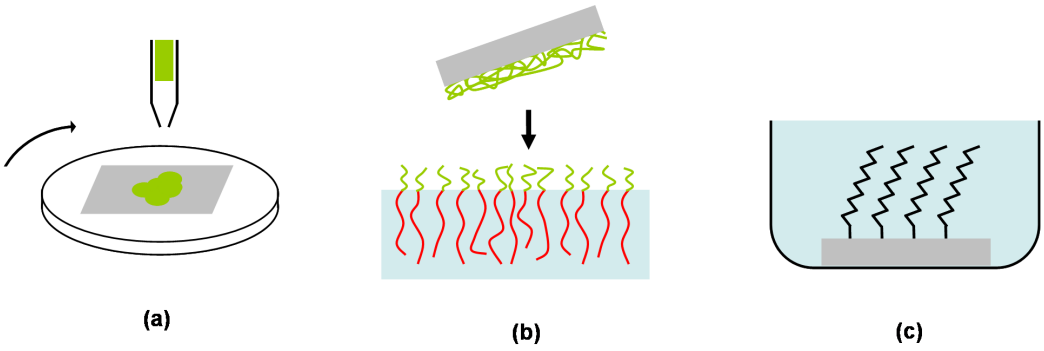

Figure 4.6: Different methods of surface functionalization applied in this work (cf. Figure 2.3): (a) preparation of thin polymer films by spin-coating, (b) preparation of polyelectrolyte brushes on a wafer previously covered with a polymer film by the Langmuir-Schaeffer technique, and (c) preparation of self-assembled monolayers by immersion coating.

Germany) were cut into pieces of 18×18.8 mm^2 and cleaned with piranha solution for about 15 min at 90 °C. Piranha solution is a 1 : 1 mixture of H_2SO_4 (96 %) and H_2O_2 (30 %). Cleaned wafers were stored under ultrapure water until use. Due to the cleaning process, a native, amorphous silica (SiO_2) layer with a thickness of $10 - 30$ Å was formed at the surface of the silicon wafer [71, 82, 136, 200], decorating the surface with OH-groups.

Thin polymer films on cleaned wafers were prepared by spin-coating (Figure 4.6 a). For this purpose, poly(styrene) (PS, obtained from Aldrich, Taufkirchen, Germany) or perdeuterated poly(styrene) (dPS, purchased from Polymer Standards Service, Mainz, Germany) was dissolved in toluene (5 mg/mL). Then, the PS or dPS solution was deposited on one of the large, polished sides of a silicon wafer. In the end, the silicon wafer was spun at 3700 rpm for 1 min (spincoater KW-4A from Chemat Technology, Northridge, CA). In this way, hydrophobic, nonpolar PS films with a layer thickness ranging from 150 to 300 Å were obtained. Thin polymer films are well-characterized model systems [142, 158, 236, 253, 268, 279].

Using wafers covered with a PS or dPS film, polyelectrolyte brushes were formed at this surface (Figure 4.6 b) by the Langmuir-Schaeffer technique, which is described in detail in Section 7.3.2 [49]. Polyelectrolyte brushes represent a smart material coating, which can be either protein-resistant or can provide a mild, biocompatible environment depending on the ionic strength of the subphase [75]. Hence, protein adsorption at polyelectrolyte brushes is an interesting field of study [18, 49, 50, 52, 53, 75, 102–105, 116, 214, 215, 291, 293].

Self-assembled monolayers represent another way of surface functionalization. In general, surfactants are surface-active molecules composed of amphiphilic organic compounds. Active surfactants, whose headgroups have a specific affinity to a certain substrate, adsorb spontaneously at solid surfaces and form ordered molecular assemblies, so-called self-assembled monolayers (SAMs, Figure 4.6 c) [33, 165, 234, 235, 270]. The two most prominent examples of SAMs are

thiols on gold [226] and silane-based systems on silica [187], which were prepared by immersion coating. As the anchoring headgroup, the length of the alkyl chain, and the functional endgroup can be changed, a great variety of different SAM morphologies is established. Hence, SAMs represent ideal model systems for the study of interfacial phenomena, such as wetting, friction, corrosion, and adhesion [82, 162, 175, 189, 202, 237, 242].

In this work (cf. Chapter 8), SAMs composed of octadecyl trichlorosilane (OTS) on silica were used.[1] OTS films are characterized by a high degree of mechanical, thermal, and chemical stability. Due to their high internal order and extremely hydrophobic character, OTS films serve as ideal model substrate for protein adsorption studies [20, 89, 90, 204, 233, 237]. Moreover, OTS films are well-suited samples for X-ray and neutron reflectivity measurements [63, 71, 89, 90, 168, 201, 218, 259, 281, 282].

4.2 Experiments at the air-water interface

X-ray reflectivity measurements at the air-water interface were performed with a Bruker D8-Advanced diffractometer in $\theta - \theta$ geometry (Figure 4.7). The X-ray radiation was emitted from an X-ray tube (electrical current of 40 mA, electrical voltage of 40 kV) with a copper anode and was parallelized by a Goebel mirror. The energy of the X-ray beam is 8.048 keV ($\lambda = 1.54$ Å) with an energy resolution of $\Delta E/E = 2.5 \times 10^{-4}$. The beam size at the sample position was defined by a vertical and a horizontal slit with sizes of 0.1 mm and 10 mm, respectively. The scattered intensity was recorded by a NaI(Tl) scintillation detector. The angular resolution was calculated to 0.7 mrad. Specular reflectivity scans were performed by rotating the X-ray tube and the detector simultaneously, so that the angle of incidence equalled the exit angle of the radiation relative to the surface of the sample. In order to obtain the "true" specular reflectivity, diffuse scattering was measured by longitudinal-diffuse scans with a constant angular detector offset of 0.1°. A typical X-ray reflectivity measurement including an offset scan was recorded within 2 h and covered a dynamic range of seven orders of magnitude with Q ranging from 0.005 to 0.5 Å^{-1}. Before each measurement, the Langmuir trough mounted on the diffractometer (Figures 4.7 and 4.8) was cleaned thoroughly and filled with a freshly prepared sample solution.

Using reflectometers at synchrotron radiation sources (e.g., beamline BW1 at HASYLAB and beamline ID10B at ESRF), not only the vertical structure of the samples can be probed, but also information on the lateral organization of crystalline domains in thin films can be gained by grazing incidence X-ray diffraction (GIXD) [9, 119, 125, 126].[2] Recently, neutron reflectometry at liquid surfaces has also attracted attention, due to the construction of novel instruments, such as the Liquids Reflectometer at SNS [13] or FIGARO at ILL.

[1] The preparation of OTS films is described in Section 8.3 and in the literature [32, 71, 217, 244].
[2] Lately, GIXD measurements have also been performed at solid-liquid interfaces [171].

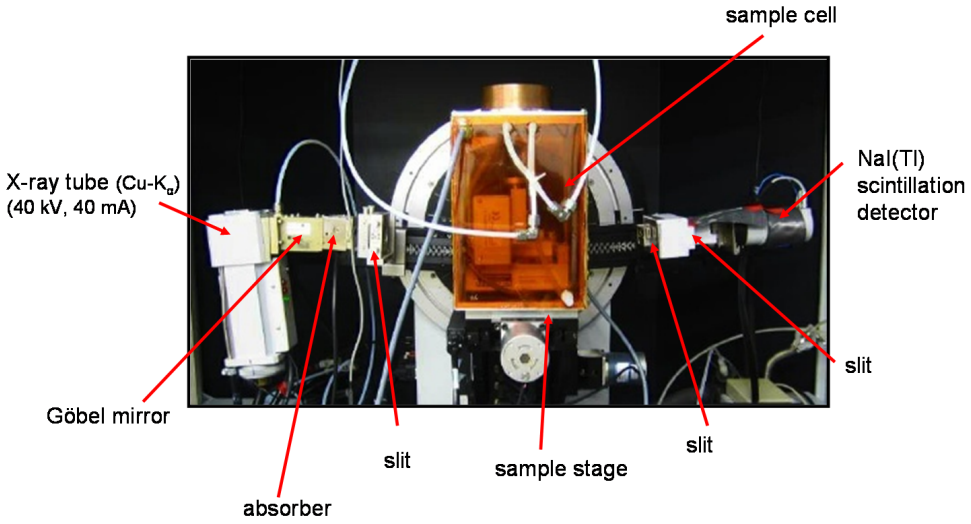

Figure 4.7: Experimental set-up of the D8 diffractometer for the study of air-water interfaces [112]. X-rays were generated in an X-ray tube equipped with a copper anode and were directed towards the sample position, where the photons were scattered. Both X-ray tube and detector could be rotated, so that reflectivity measurements of liquid surfaces became feasible in $\theta - \theta$ geometry.

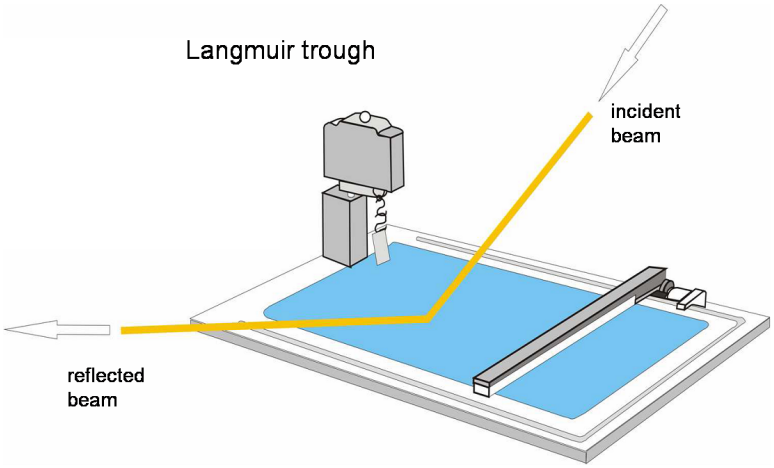

Figure 4.8: Schematic layout of the Langmuir trough inside the sample cell shown in Figure 4.7 [73]. The Langmuir trough could be equipped with a film balance and a surface barrier in order to measure and tune surface pressure and surface area of Langmuir films. The trough was mounted inside a sample cell with huge Kapton windows, which was mounted in the diffractometer (cf. Figure 4.7).

5 Effects of nonionic cosolvents on protein adsorption

In a recent study [143], nonionic cosolvents were found to lower the degree of protein adsorption at the silica-water interface. To further explore in how far nonionic cosolvents can be used to control protein adsorption, two studies are presented in this Chapter. In Section 5.1, the range of cosolvents is extended and their influence on protein adsorption at hydrophilic as well as at hydrophobic surfaces is studied [80]. Section 5.2 contains a study on the concentration-dependence of the cosolvent effect on protein adsorption at the air-water interface [113].

5.1 Effects of osmolytes on the structure of adsorbed proteins

5.1.1 Summary

Osmolytes are substances that affect osmosis and are used by cells to adapt to environmental stress. Here, we report a neutron reflectivity study on the influence of some osmolytes on protein adsorption at solid-liquid interfaces. Bovine ribonuclease A (RNase) and bovine insulin were used as model proteins adsorbing at a hydrophilic silica and at a hydrophobic polystyrene surface. From the neutron scattering data, the adsorbed protein layers were characterized in terms of layer thickness, protein packing density, and adsorbed protein mass in the absence and presence of urea, trehalose, sucrose, and glycerol. All data point to a clear effect of these nonionic cosolvents on the degree of protein adsorption. For example, 1 M sucrose leads to a reduction of the adsorbed amount of RNase by 36 % on a silica surface and by 71 % on a polystyrene surface. Trehalose was found to be of similar activity as sucrose. The changes in adsorbed protein mass can be attributed to a decreased packing density of the proteins in the adsorbed layers. Moreover, we investigated insulin adsorption at a hydrophobic surface in the absence and presence of glycerol. The degree of insulin adsorption is decreased by even 80 % in the presence of 4 M glycerol. The results of this study demonstrate that nonionic cosolvents can be used to tune and control nonspecific protein adsorption at aqueous-solid interfaces, which might be relevant for biomedical applications.

5.1.2 Introduction

Protein adsorption on solid surfaces has implications in such diverse fields as drug delivery, biocompatibility of implants, biofouling, food chemistry, contact lenses, and immunoassays [39, 59, 60, 134, 177]. The adsorption behavior of proteins at solid surfaces is ruled by a complex interplay between protein-protein and protein-surface interactions in an aqueous environment [50, 94, 163]. Hence, protein adsorption is and can be influenced by a number of factors, such as temperature, pH, and ionic strength of the protein solution [50, 94, 163]. Different strategies to control protein adsorption and, in particular, to design protein-resistant surfaces have emerged [139], because resistance to non-specific protein adsorption is a prerequisite for many biomaterials. For example, protein-repellent surface coatings like self-assembled monolayers (SAMs) presenting poly(ethylene glycol), oligo(ethylene glycol), or poly(ethyleneimine) groups have been developed [91, 98, 175, 235]. Furthermore, polyelectrolyte brushes composed of poly(acrylic acid) (PAA) represent another smart material coating. The protein affinity of a PAA brush can be "switched" by changing the salt concentration of the protein solution [95, 105, 214, 294]. Recently, Kane et al. [132] have suggested that SAMs presenting groups derived from kosmotropes exhibit protein-resistant behavior, since kosmotropes are substances that are preferentially excluded from a protein surface (cf. Figure 5.1).

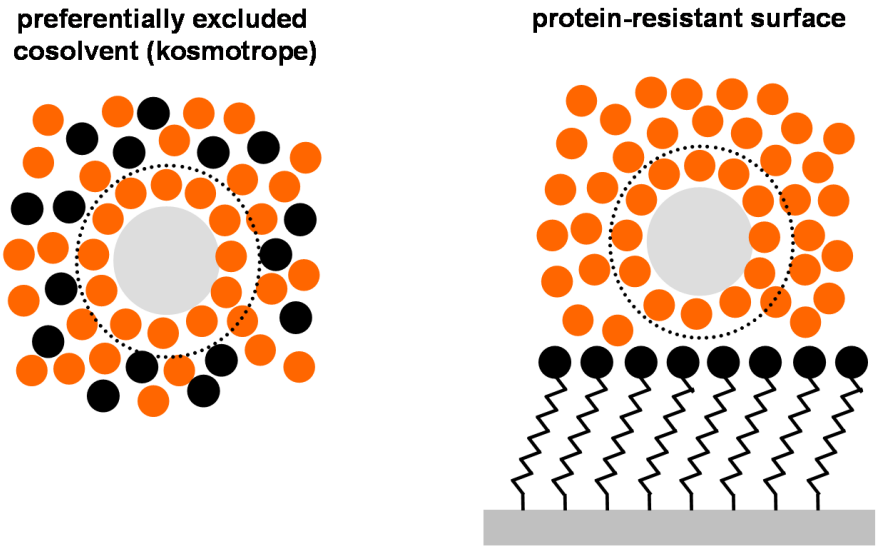

Figure 5.1: Kosmotropes can form the basis of protein-resistant surfaces [132]. (Left) The cosolvent molecules (black circles) are preferentially excluded from the protein surface, which is surrounded by a layer of hydration water. (Right) Kosmotropic cosolvents are attached onto a self-assembled monolayer on a Au substrate. Thus, protein-surface interactions are suppressed.

In a recent study [79], we could show that protein adsorption at a hydrophobic polystyrene surface is strongly affected by the kind of dissolved ions. Anions and cations are arranged in the so-called Hofmeister series according to their effectiveness in precipitating and stabilizing proteins [301]. Apparently, kosmotropic salts (stabilizing the folded structure) and chaotropic salts (destabilizing the folded structure) decrease the degree of protein adsorption, when added to a protein solution in molar concentrations [79]. Maximum protein adsorption is observed in the presence of "neutral" NaCl, which has neither kosmotropic nor chaotropic properties. However, there is also a series of nonionic cosolvents that act as kosmotropes or chaotropes. According to Timasheff [261, 263, 264], any chemical compound added to water or to an aqueous protein solution at molar concentrations may be termed "cosolvent", because up to 50 % of the solvent volume can be occupied by the cosolvent molecules. For example, glycerol is well-known to support the native structure of proteins in crystallography, whereas urea is routinely used to unfold proteins [84, 261, 265]. Osmolytes [297, 298], like amino acids, polyols and sugars, methylamines, and urea, are a special class of cosolvents, which usually (except for urea) have kosmotropic character. Nature uses these small molecules in cells of water-stressed organisms, such as bacteria, plants, and fish, in order to maintain their cell volume. In this context, trehalose, a naturally occurring disaccharide, has received special attention as a bioprotectant [99, 160, 296]. This sugar occurs in insects, desert plants, yeasts, algae, and fungi and facilitates their survival in an anhydrobiotic environment.

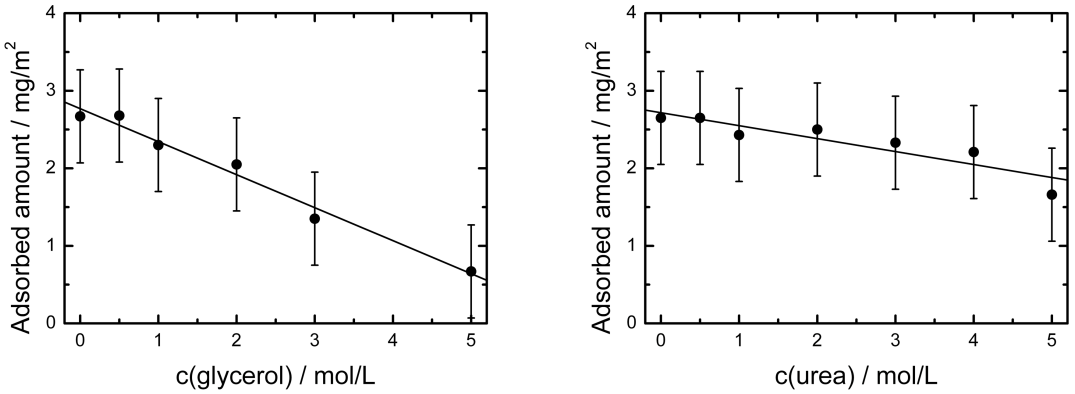

Figure 5.2: Adsorption of RNase at the silica-water interface in the presence of various glycerol and urea concentrations in the buffer, as obtained by optical reflectometry [143].

Here, we present a comprehensive study of the effects of various nonionic cosolvents on the degree of protein adsorption. The experiments were motivated in part by the finding that SAMs displaying groups of kosmotropes develop protein resistance [132]. Furthermore, a reduced degree of bovine ribonuclease A (RNase) adsorption was recently observed at the silica-water [143] and the air-water interfaces [113] in the presence of urea and glycerol (cf. Figure 5.2). Thus, to gain further insight into these phenomena, systematic neutron reflectivity measurements have been

performed in this study to investigate the effects of additional cosolvents, such as sucrose and trehalose, on protein adsorption at a silica surface. In addition, the effects of sucrose, trehalose, glycerol and urea on RNase adsorption at a hydrophobic poly(styrene) surface are presented here. RNase [206] is a pancreatic enzyme consisting of 124 amino acids; it has an isoelectric point of 9.3. The molecular dimensions are $22 \times 28 \times 38$ Å^3. The secondary structure of RNase comprises three α-helices, a four-stranded antiparallel β-sheet, and four disulfide bonds responsible for the high internal stability of RNase.

Besides RNase, we also report on the adsorption of bovine insulin at a hydrophobic poly(styrene) surface. Insulin is a 5.7 kDa peptide hormone. Its natural function is to lower the level of glucose in the blood. Lacking insulin can lead to diabetes mellitus type 1, which is usually treated by a lifelong medication with insulin injections. On the other hand, insulin is often used as a model protein to study the misfolding of proteins and the formation of amyloid fibrils [123, 127]. There is a series of diseases which are associated with the formation of amyloid fibrils, such as diabetes mellitus type 2, Creutzfeldt-Jakob and Alzheimer's disease [45, 62, 73, 286]. Although insulin does not form amyloid fibrils in vivo, this process can be triggered easily in vitro by lowering the pH-value and raising the temperature, by adding distinct organic solvents, or by agitation of insulin solutions in the presence of hydrophobic surfaces [29, 128, 246]. These activating conditions represent a severe issue in the production, storage, and handling of insulin. Therefore, it is interesting to analyze, if the adsorption of insulin at a hydrophobic poly(styrene) surface can be suppressed by adding cosolvents to the insulin solution.

We will show in this study that non-specific adsorption of RNase and insulin at an aqueous-solid interface can be reduced significantly by adding the osmolytes glycerol, sucrose, trehalose, and urea to the protein solution. The degree of adsorption and the structure of the formed protein adsorbates are characterized using neutron reflectometry. This technique is very useful in resolving aqueous-solid interfacial structures with Å-resolution, since neutrons can penetrate condensed matter on macroscopic scales. Furthermore, by applying the so-called contrast variation technique, thin protein layers can be sensed easily by neutron reflectometry, when the environment has been deuterated, e.g., by using D_2O as the solvent.

5.1.3 Experimental details

Materials

Bovine RNase (Sigma, R5500) and bovine insulin (I5500) were used without further purification. Protein solutions were prepared by dissolving 0.05 or 0.1 mg mL^{-1} RNase or insulin in a 10 mM morpholinopropane sulfonic acid (MOPS) buffer solution with D_2O as the solvent. The pD-value was adjusted to 7.4 (pD = pH-meter reading + 0.4) [47]. Glycerol, urea, sucrose, trehalose, and resveratrol were dissolved in the buffer solution with concentrations of 1, 2 or 4 mol L^{-1}. Substrate preparation is described in Section 4.1.3.

Neutron reflectivity experiments

The neutron reflectivity measurements were carried out at the Helmholtz-Zentrum Berlin (Germany) using the instrument V6 [167]. The experimental set-up is described in detail in Section 4.1.1. Data reduction and data analysis are outlined in Section 3.8.

5.1.4 Results

Data analysis

Bare silicon wafers and silicon wafers coated with a perdeuterated poly(styrene) (dPS) film were used as hydrophilic and hydrophobic model substrates for protein adsorption, respectively. In the case of hydrophobic substrates, the dPS film on each wafer was characterized before by recording a neutron reflectivity curve using a 3 : 1 D_2O-H_2O mixture as solvent (Figure 5.3). The interfacial structure of this system was described by a layer model, Si / dPS / solution. The scattering length densities (SLDs) of these components were fixed to $2.07{\cdot}10^{-6}$ Å^{-2} (Si), $6.42{\cdot}10^{-6}$ Å^{-2} (dPS), and $4.64{\cdot}10^{-6}$ Å^{-2} (D_2O-H_2O) [3, 224], whereas the layer thicknesses of the dPS film and the roughness of the Si-dPS interface were varied in the fitting process. Best fits could be obtained by simply using an enhanced Si-dPS roughness to model the thin SiO_2 layer on Si and by fixing the dPS-solution roughness to 5 Å in the presence of protein adsorbates. For the data shown in Figure 5.3, a typical dPS film thickness of 263 Å and a typical Si-dPS roughness of 11 Å have been found. The corresponding SLD profile of this interfacial structure is also shown in Figure 5.3.

In the next step, the D_2O-H_2O mixture was exchanged with a protein solution, for example, containing 0.05 mg mL^{-1} RNase in D_2O buffer solution (pD = 7.4). After one hour of equilibration, a neutron reflectivity curve was recorded, which is also plotted in Figure 5.3. Now, the reflectivity curve had to be analyzed using a 2-layer model, Si / dPS / adsorbed protein film / protein solution. In the fitting process, only the thickness and the SLD of the adsorbed protein film were varied. Its roughness could be modeled with a value of 5 Å. The SLD of the solution was fixed to $6.36{\cdot}10^{-6}$ Å^{-2} corresponding to D_2O. The SLD profile, after RNase has adsorbed at the dPS-solution interface, is also shown in Figure 5.3. It is important to note that adsorbed RNase can be detected with high sensitivity by neutron reflectometry, since the dPS film and the protein solution have nearly the same SLD. Due to this contrast matching (cf. Section 3.9.1), the observed Kiessig oscillations in the neutron reflectivity are directly related to the presence of the adsorbed protein film. From Figure 5.3, the structure and location of the RNase adsorbate is easily visible. In the same way, the effects of cosolvents on the adsorption of RNase at a dPS film were studied, each time using a new silicon wafer. When cosolvents are present in the solution, the SLD of the solution is changing. The correct value has been deduced from the position of the critical Q-value in the measured reflectivity curve. In the case of hydrophilic silicon wafers, it was necessary to include an explicit SiO_2 layer in the interfacial structure model, because the shape of the reflectivity curve is no longer dominated by the presence of a dPS film. The SLD

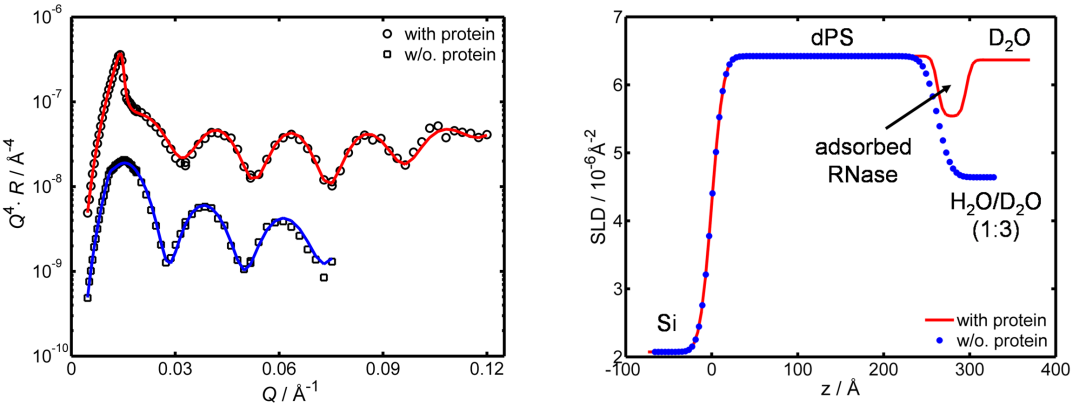

Figure 5.3: (Left) Typical neutron reflectivity curves of a silicon wafer coated with a perdeuterated poly(styrene) (dPS) film without and with adsorbed RNase and (Right) corresponding scattering length density profile [80]. Before protein adsorption, the dPS film thickness is characterized in contact with a 3 : 1 D_2O-H_2O mixture (open squares). Then, the D_2O-H_2O mixture is exchanged by a 0.05 mg/mL RNase solution with D_2O-buffer as the solvent (open circles). Fits based on structure models are shown as solid lines. For clarity, the reflectivity curves are shifted vertically. In the SLD profile, the symbols represent the interfacial structure in the absence of protein, and the solid line shows the interfacial structure in the presence of proteins. In this case, RNase proteins adsorb onto the dPS film.

of the SiO_2 layer and its roughness values on both sides were fixed to $3.48{\cdot}10^{-6}$ Å^{-2} and 5 Å, respectively [3, 224]. The thickness of the SiO_2 layer remains as a fitting parameter.

In an SLD profile, a protein adsorbate layer is characterized by its thickness, d, and scattering length density, $\rho_{\mathrm{adsorbate}}$. These parameters can be used to calculate the volume fraction, ϕ, of the protein molecules in the adsorbate layer and the adsorbed mass, Γ, as described in Section 3.9.2. The SLDs of the proteins are calculated by summing up the scattering lengths of all atoms of a protein molecule and dividing through the molecular volume. To this end, we used the scattering lengths published by NIST and the primary sequences of insulin and RNase [3, 192, 250]. For example, we obtained a value of $\rho_{\mathrm{RNase}} = 3.46{\cdot}10^{-6}$ Å^{-2} and $\rho_{\mathrm{insulin}} = 3.20{\cdot}10^{-6}$ Å^{-2} in a 2 molar glycerol-D_2O solution. For the RNase adsorbate shown in Figure 5.3, we obtain $\phi = 0.29$ and $\Gamma = 1.40$ mg m^{-2}.

RNase adsorption at the hydrophobic poly(styrene)-water interface

We have studied the effects of sucrose (1 M) and trehalose (1 M) as well as glycerol (2 M) and urea (2 M) on the adsorption of RNase at a hydrophobic dPS film. The corresponding neutron reflectivity curves are shown in Figure 5.4. As described above, each dPS film has been characterized before protein adsorption by measuring an additional neutron reflectivity curve

(data not shown). The interfacial structures of the RNase adsorbates as obtained from the fits (Figure 5.4) are listed in Table 5.1.

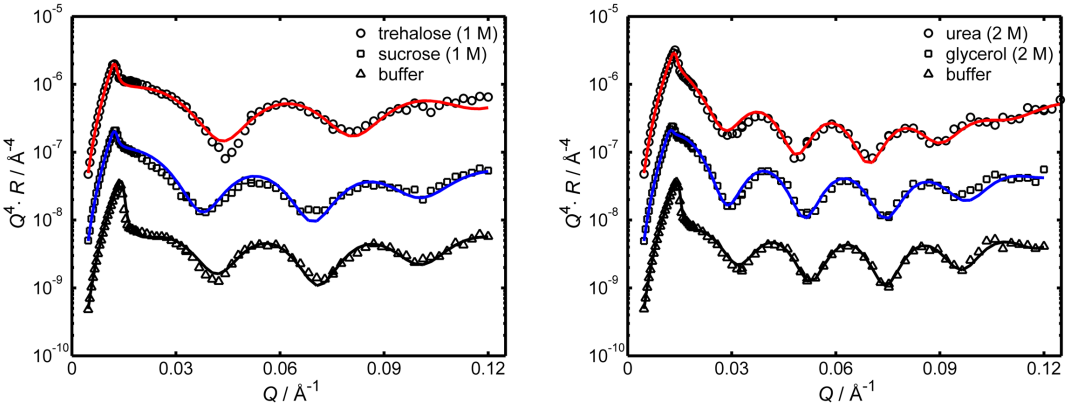

Figure 5.4: Neutron reflectivities of Si / dPS / RNase adsorbate / solution interfaces [80]. The solutions contained the protein RNase at a concentration of (Left) 0.1 mg mL^{-1} and (Right) 0.05 mg mL^{-1} and different cosolvents, as indicated in the legends. The symbols reflect the experimental data, the solid lines are fits based on a two-layer model of the interfacial structure. For clarity, the reflectivity curves are shifted vertically.

Table 5.1: Structure of RNase on a hydrophobic poly(styrene) surface, as derived from neutron reflectometry [80].[a]

solution condition	d / Å	ϕ	Γ / mg m^{-2}	degree of adsorption
pure buffer[b]	34	0.28	1.4	100 %
with 1 M sucrose[b]	35	0.09	0.4	29 %
with 1 M trehalose[b]	35	0.09	0.5	36 %
pure buffer[c]	34	0.29	1.4	100 %
with 2 M glycerol[c]	32	0.17	0.8	57 %
with 2 M urea[c]	36	0.14	0.7	50 %

[a] d is the thickness of the adsorbed protein layer, ϕ is the volume fraction of protein molecules inside the adsorbed protein layer, Γ is the mass of adsorbed protein. Maximum estimated errors are ± 3 Å for d and ± 0.2 mg m^{-2} for Γ. The degree of adsorption has an error of about ± 10 %.
[b] Protein solution concentration is 0.10 mg mL^{-1}.
[c] Protein solution concentration is 0.05 mg mL^{-1}.

Apparently, adsorbed RNase forms a monolayer under each solution condition with a layer thickness ranging from 32 Å to 36 Å, which matches the dimension of a hydrated RNase molecule. As can also be seen from Table 5.1, RNase has a surface concentration of 1.4 mg m^{-2} on the hydrophobic dPS film. However, a strong reduction of the degree of adsorption is observed, when sucrose or trehalose are dissolved at a concentration of 1 M in the RNase solution. Some-

what smaller effects, albeit remarkable, are found in the presence of glycerol (2 M) and urea (2 M). These cosolvent-induced reductions of non-specific RNase adsorption at a hydrophobic poly(styrene) surface can be ascribed to changes in packing density of the protein monolayer. Here, sucrose and trehalose are most effective as the volume fraction of RNase molecules is lowered from 0.28 to 0.09, when these sugars are present in the protein solution.

RNase adsorption at the silica-water interface

The neutron reflectivity curves measured after adsorption of RNase onto a hydrophilic silicon wafer with and without dissolved sucrose (1 M) or trehalose (1 M) are shown in Figure 5.5 together with the fits. In the presence of a protein adsorbate, the reflectivity is lowered, when compared to the reflectivity curve without proteins present (data not shown), and a broad Kiessig fringe with a minimum at about 0.065 $Å^{-1}$ occurs. The resolved interfacial structures of the studied protein adsorbates are listed in Table 5.2 along with the volume fractions and the masses of the adsorbed protein. For comparison, data of a previous study where RNase adsorbs in the presence of glycerol (2 M) and urea (2 M) have been included [143].

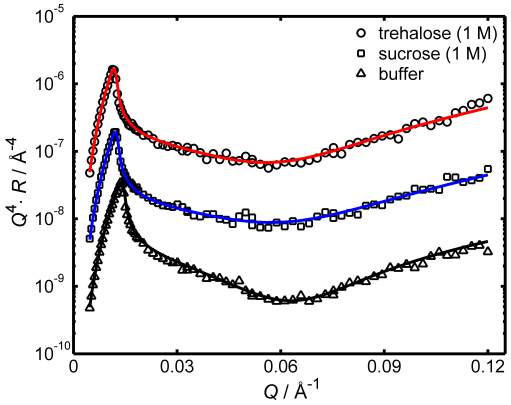

Figure 5.5: Neutron reflectivities of Si / SiO_2 / RNase adsorbate / solution interfaces [80]. The solutions contained the protein RNase at a concentration of 0.05 mg mL^{-1} and different cosolvents, as indicated in the legends. The symbols reflect the experimental data, the solid lines are fits based on a two-layer model of the interfacial structure. For clarity, the reflectivity curves are shifted vertically.

The data given in Table 5.2 reveal that RNase roughly forms a monolayer at the silica-water interface under the conditions studied, because the thickness of the adsorbed film matches the dimension of an RNase molecule. The observed thickness of the RNase layer is $38 - 41$ Å in the current study (Table 5.2). A slightly lower thickness of $32 - 34$ Å has been found in the earlier study [143], which may be explained by small variations of the temperature or the time-dependent structure of a freshly cleaned silica surface [156]. However, all cosolvents studied have a pronounced effect on the degree of RNase adsorption, i.e., their presence in the protein

Table 5.2: Structure of RNase adsorbed on a hydrophilic silica surface, as derived from neutron reflectometry [80].[a]

solution condition	d / Å	ϕ	Γ / mg m^{-2}	degree of adsorption
pure buffer	38	0.41	2.2	100 %
with 1 M sucrose	41	0.24	1.4	64 %
with 1 M trehalose	40	0.32	1.8	82 %
pure buffer[b]	34	0.56	2.7	100 %
with 2 M glycerol[b]	32	0.47	2.1	78 %
with 2 M urea[b]	32	0.43	1.9	70 %

[a] The protein solution concentration was 0.05 mg/mL. d is the thickness of the adsorbed protein layer,ϕ is the volume fraction of protein molecules inside the adsorbed protein layer, Γ is the mass of adsorbed protein. Maximum estimated errors are ± 3 Å for d and ± 0.2 mg m^{-2} for Γ. The degree of adsorption has an error of about ± 10 %.
[b] Data taken from [143].

solution leads to a partial reduction of the non-specific adsorption of RNase at the silica-water interface. Again, this reduction can be attributed to a lowering of the packing density of the protein molecules inside the adsorbate, as is reflected in the ϕ-values given in Table 5.2. It is interesting to note that in the absence of any cosolvent the surface concentration of RNase is higher at the hydrophilic silica surface (Table 5.2) as compared to the hydrophobic poly(styrene) surface (Table 5.1).

Insulin adsorption at the dPS-water interface

As already described in the Introduction 5.1.2, insulin can undergo a severe conformational change where it transforms from the native state to so-called amyloid fibrils [123], which are long aggregates of the protein molecules. It is also well-known that amyloid fibrils are formed when insulin solutions are agitated in the presence of hydrophobic surfaces [246]. In this way, it is interesting to study, if non-specific insulin adsorption at a hydrophobic surface can also be lowered by adding glycerol to the insulin solution.

In Figure 5.6, neutron reflectivity measurements are shown which reflect insulin adsorbates on a hydrophobic dPS film. They have been formed in the absence and presence of glycerol (2 M and 4 M). The fitting results and characteristics of the adsorbed layers are summarized in Table 5.3. The results show that insulin forms a monolayer of about 27 Å thickness at the dPS-water interface with a volume fraction of 0.39. In the presence of glycerol, the adsorbed amount is strongly lowered with increasing cosolvent concentration (Table 5.3). As also found for RNase (see above), the decreased degree of protein adsorption in the presence of glycerol is related to a decreased protein packing density in the adsorbed layer.

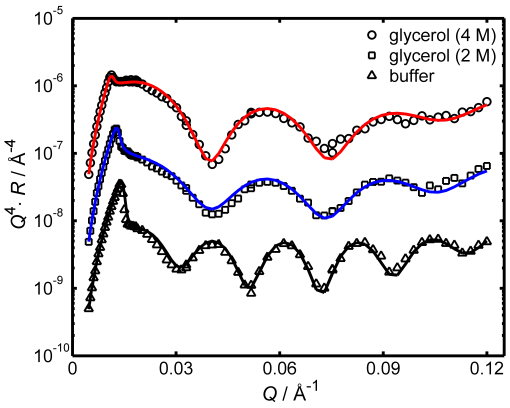

Figure 5.6: Neutron reflectivities of Si / dPS / insulin adsorbate / solution interfaces [80]. The solutions contained the protein insulin at a concentration of 0.1 mg mL^{-1} and different cosolvents, as indicated in the legends. The symbols reflect the experimental data, the solid lines are fits based on a two-layer model of the interfacial structure. For clarity, the reflectivity curves are shifted vertically.

Table 5.3: Structure of insulin adsorbates at a hydrophobic dPS interface, as derived from neutron reflectometry [80].[a]

solution condition	d / Å	ϕ	Γ / mg m^{-2}	degree of adsorption
pure buffer	27	0.39	1.4	100 %
with 2 M glycerol	24	0.17	0.6	40 %
with 4 M glycerol	25	0.07	0.3	20 %

[a] The protein solution concentration was 0.1 mg/mL. d is the thickness of the adsorbed protein layer, ϕ is the volume fraction of the protein molecules inside the adsorbed protein layer, and Γ is the mass of adsorbed protein. The maximum error of d and Γ are estimated to be ± 3 Å and ± 0.2 mg m^{-2}, respectively. The degree of adsorption has an error of about ± 10 %.

5.1.5 Discussion

Driving forces for RNase adsorption at hydrophilic and hydrophobic interfaces

As can be seen from Tables 5.1 and 5.2, RNase has a higher affinity to adsorb at a hydrophilic silica-water interface (about 2.5 mg m^{-2} on the average) than at a hydrophobic poly(styrene)-water interface (1.4 mg m^{-2}). With an isoelectric point of about 9.3, RNase has a positive net charge at pH = 7, while silica is negatively charged at neutral pH values. Therefore, electrostatic attraction between RNase and the silica surface will strongly contribute to the driving force for RNase adsorption at the silica surface. On the other hand, the hydrophobic effect is the main driving force for RNase adsorption at poly(styrene) films, due to the non-polar character of poly(styrene). The same trends have been observed for lysozyme, which has also a positive

net charge at neutral pH values. At a silica surface, a higher degree of lysozyme adsorption has been reported than at a hydrophobic silanized (OTS) surface [20].

The thickness of all studied RNase adsorbates varies between 32 Å and 41 Å (Tables 5.1 and 5.2). Assuming a hydration shell of approximately to 2 Å around dissolved RNase molecules, the molecular dimensions are approximately $26 \times 32 \times 42$ Å^3. Hence, the recovered adsorbate thicknesses are consistent with RNase monolayers. Moreover, this implies the absence of drastic adsorption-induced conformational changes, which can lead to alterations of the thickness and roughness of adsorbed protein films.

Effects of nonionic cosolvents on protein adsorption

Understanding cosolvent-protein interactions in solution is a prerequisite to explain their effect on protein adsorption. Timasheff and co-workers related the effect of cosolvents on protein hydration with their effect on the conformational stability of proteins in aqueous solutions [14, 84, 151, 261–265, 296]. The exclusion of cosolvents from the protein surface is entropically unfavorable, which shifts the equilibrium between the folded and the unfolded conformation towards the folded one, because the solvent accessible surface area of the folded state is smaller than that of the unfolded state. It has been noted that kosmotropicity of osmolytes might be favored by evolution [132, 262, 297, 298]. Kosmotropic osmolytes are preferentially excluded from the protein surface, inducing a preferential hydration of the protein. Urea, on the other hand, is a chaotropic osmolyte and a common protein denaturant. Urea binds to a protein surface and thus favors the unfolded state with a larger solvent accessible surface area. A lot of animals, like cartilaginous fish in which urea is the major osmolyte, also have certain methylamines (e.g., trimethylamine N-oxide, TMAO) that counteract the denaturing effect of urea [11, 159, 166].

The presence of 2 M glycerol has a strong effect on the degree of protein adsorption: The adsorbing mass of RNase is reduced by 43 % and 22 % at hydrophobic and hydrophilic surfaces, respectively (Tables 5.1 and 5.2), while that of insulin is even reduced by 60 % at a hydrophobic surface (Table 5.3). Glycerol strongly interacts with water and tends to be preferentially excluded from the surface of a protein. Thus, the protein becomes preferentially hydrated, and the folded conformation is stabilized [84, 272]. For RNase, this has been demonstrated by thermodynamic and dielectric relaxation spectroscopy measurements [26, 84]. This preferential hydration of proteins might hinder direct protein-surface contacts and adsorption-induced conformational changes. Therefore, it can be qualitatively understood why the interfacial affinity of a protein is diminished in the presence of glycerol. In complete analogy, sucrose and trehalose are also preferentially excluded from a protein surface. Regarding protein-surface interaction, these sugars are quite effective in reducing the degree of adsorption: 1 M of sucrose or trehalose leads to a decrease of 71 % or 64 % at a hydrophobic surface (Table 5.2). This may be explained in part by their larger molecular volume and higher number of hydroxyl groups (8) as compared to glycerol (3).

Urea, is a chaotropic cosolvent [111, 265]. However, in order to denature proteins, rather

high concentrations of urea are necessary. For example, fluorescence measurements have shown [190] that 7 M urea is the concentration at which half of the RNase molecules are denatured in solution. In the adsorption measurements described above, which have been performed at a urea concentration of only 2 M, the folded conformation of RNase is only slightly reduced. As urea directly binds to the protein surface, the solubility of hydrophobic protein surface patches in water is increased and hydrophobic interactions between the protein and a substrate surface are weakened. Hence, the surface concentration of RNase is decreased in the presence of urea (Tables 5.1 and 5.2). A change of the water structure and a concomitant weakening of hydrophobic interactions between protein molecules and aqueous-solid interfaces might even be a general aspect of cosolvent effects on protein adsorption.

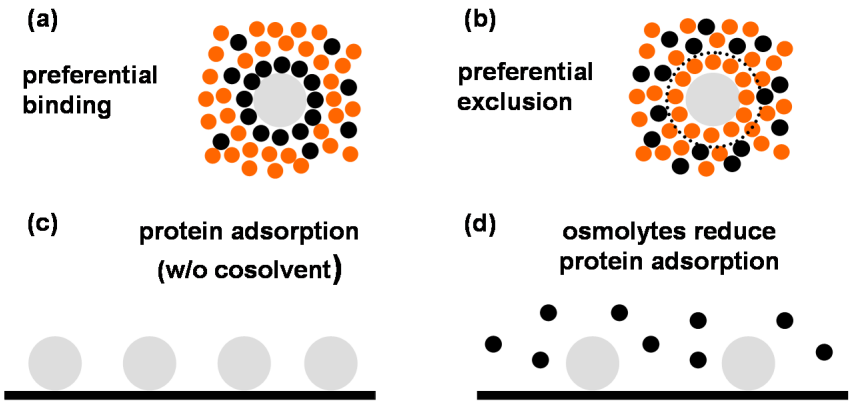

Figure 5.7: Protein solutions in the presence of cosolvents [80, 263]: (a) preferential binding of the cosolvent molecules (small black circles) to the protein molecule (large grey circle) or (b) preferential exclusion of cosolvent molecules from the protein surface with exclusion volume (dotted circle). Protein adsorption in the presence of cosolvents [80]: (c) Without cosolvents present in the protein solution, proteins form a densely packed monolayer at the solid-liquid interface. (d) In the presence of osmolytes, protein adsorption is significantly reduced by lowering the packing density of the adsorbed layer.

5.1.6 Conclusion

We have studied the adsorption of RNase and insulin at hydrophilic and hydrophobic aqueous-solid interfaces in the absence and presence of various osmolytes. The effects of these nonionic cosolvents on protein adsorption at aqueous-solid interfaces, as reported here, are in line with effects observed in other interfacial systems studied recently [143]: In the presence of kosmotropic and chaotropic salts (e.g., $(NH_4)_2SO_4$ and $Ca(SCN)_2$), the degree of RNase adsorption at a

hydrophobic poly(styrene) surface is also reduced [79]. Moreover, the degree of RNase adsorption at the air-water interface is also reduced in the presence of glycerol and urea [113]. These findings call for a quite general picture of the underlying mechanism, which is probably related to the cosolvent effects on protein hydration, as illustrated in Figure 5.7 in a schematic way. The results suggest a further function of osmolytes: the reduction of the interfacial affinity of proteins, which provides another means to reduce non-specific protein adsorption.

5.2 Effects of urea and glycerol on the adsorption of ribonuclease A at the air-water interface

The results presented in this Section are published in *Langmuir* [113]. The measurements were performed and the data were analyzed by Anne K. Hüsecken [112]; idea and design of the experiment, further analysis and data interpretation are part of this thesis.

5.2.1 Summary

This study reports on the influence of nonionic cosolvents on the interfacial structure of ribonuclease A (RNase) adsorbed at the air-water interface. We applied X-ray reflectometry to obtain detailed volume fraction profiles of the adsorbed layers and to follow the effect of glycerol and urea on the adsorbate structure as a function of cosolvent concentration. Under all conditions studied, the adsorbed RNase layer maintains its compact shape, and the adsorbed RNase molecules adopt a flat-on orientation at the interface. Both kosmotropic glycerol and chaotropic urea exert profound effects on the adsorbate: The surface excess decreases linearly with glycerol content and is also reduced at low urea concentration. However, at high urea concentration, parts of the adsorbed layer are dehydrated and become exposed to air. The electron density and volume fraction profiles of the adsorbed protein provide clear evidence that these effects are ruled by different mechanisms.

5.2.2 Introduction

In a biological cell, proteins are generally not solvated by pure water, but living cells are occupied by a lot of different proteins, nucleic acids, osmolytes, salts, and many other molecules. In this complex environment, crowding and confinement as well as cosolvents and interfaces may alter the stability, structure, and function of proteins [261, 302]. It is common to classify cosolvents in two groups regarding their effect on protein structure: protein-stabilizing cosolvents, such as SO_4^{2-} and glycerol, are called kosmotropes, and protein-destabilizing cosolvents, such as guanidinium, SCN^-, and urea, are called chaotropes or denaturants. While many studies deal with the structural and thermodynamic effects of cosolvents on proteins in solution [15, 22, 84, 87, 96, 124, 145, 153, 191, 196, 251, 261, 266, 272, 280, 301], their effect on protein adsorption remains largely unexplored. Moreover, small cosolutes may even drastically affect the folding and misfolding of amyloidogenic proteins which play a major role in the pathogenesis of, for example, diabetes mellitus type II and Alzheimer's disease [73, 74, 174]. For example, it has been reported that glycerol accelerates the conformational transition of amyloid β required for amyloid formation [299], and urea modulates the growth of amyloid β fibrils [138].

Protein adsorption at model interfaces is not only of fundamental interest in understanding physiological processes like blood coagulation [39, 134], but also of industrial and biotechno-

logical significance, for example, in stabilizing foams and food emulsions [61] or in designing biocompatible implants [39, 134].

Natively folded, globular proteins are roughly composed of a hydrophobic core and a hydrophilic shell of polar and charged amino acid groups, because entropy is gained by burying the hydrophobic residues in the interior of proteins due to the hydrophobic effect. Upon adsorption at the air-water interface, the lowest energy structure can change, so that some hydrophobic residues are exposed to the air. Therefore, protein adsorption at the air-water interface can lead to structural rearrangements or even to surface-induced denaturation. Hence, the air-water interface represents a model surface for the study of protein folding and protein conformation. In order to investigate protein-surface interactions, X-ray and neutron reflectivity techniques serve as powerful tools for exploring the interfacial structure, the adsorbed amount, and the volume fraction profile of proteins and biomolecules at solid-liquid [76, 117, 170, 245] and air-water interfaces [85, 157, 161, 197, 300].

In previous studies, first experiments on the effects of ionic and nonionic cosolvents have been performed, focusing on the adsorption of ribonuclease A (RNase) at the hydrophilic silica-water and the hydrophobic poly(styrene)-water interface by optical and neutron reflectometry [79, 143] (cf. Section 5.1). In the presence of both the kosmotropic glycerol and the chaotropic urea, less RNase is adsorbing at the silica-water interface [143] and at the poly(styrene)-water interface [80], while no major change in the adsorbate layer thickness could be detected (cf. Section 5.1). Moreover, we could show that the adsorption of insulin at a poly(acrylic acid) brush is largely suppressed in the presence of glycerol [75] (cf. Chapter 7). One may argue that proteins become preferentially hydrated in the presence of kosmotropic cosolvents [84, 261], thereby disfavoring conformational changes at the interface, whereas chaotropic cosolvents are accumulated at the protein surface and weaken hydrophobic protein-substrate interactions [22, 41, 227]. Interestingly, the effect of the chemical denaturants guanidinium chloride and urea on the adsorption of β-lactoglobulin (βLg) at the air-water interface was studied by Perriman et al. [198]. They observed a distinct increase in the thickness of the protein adsorbate, while the surface excess did not change systematically with denaturant concentration. In view of the different results obtained at the air-water and solid-liquid interfaces, the effects of nonionic colsolvents on the structure of protein adsorbates at hydrophobic-aqueous interfaces need to be clarified.

RNase is a pancreatic enzyme with a molecular mass of 13.7 kDa and an isoelectric point of 9.3 [206]. The crystal [295] and solution structure [229] of RNase are well-known. The molecular dimensions are $22 \times 28 \times 38$ Å^3. RNase comprises three α-helices, a four-stranded antiparallel β-sheet and four disulfide bonds responsible for its high internal stability.

In this study, we investigate how RNase adsorption to the air-water interface is altered in the presence of nonionic cosolvents. The effects of glycerol and urea on the structure and surface excess of RNase adsorbed at the air-water interface are determined by X-ray reflectivity measurements at different cosolvent concentrations. We discuss if the effects of cosolvents observed for RNase at solid surfaces (decreasing surface excess and roughly constant layer thickness) or βLg

at the air-water interface (increasing layer thickness and approximately constant surface excess) are also valid for RNase adsorption at the air-water interface. Thus, this study will contribute to elucidating the mechanisms of cosolvent-controlled protein adsorption.

5.2.3 Experimental methods

Materials

RNase (Sigma, R5500), glycerol (Sigma, G6279), and urea (Merck, 1.08488) were used as received. Protein solutions were prepared by dissolving RNase in a 10 mM phosphate buffer ($H_2PO_4^-$ / HPO_4^{2-}) adjusted to pH 7.0. The protein concentration was 0.1 mg mL^{-1} in the absence and the presence of cosolvents. Different cosolvent concentrations between 0 and 6 mol L^{-1} were used. The solutions were spread in a sealed Langmuir trough at 22 °C mounted in the diffractometer. Reflectivity measurements were performed after equilibrating the adsorbed layer for at least 16 h, because it is known from dynamic surface tension measurements that this equilibration might take up to 15 h [269].

X-ray reflectivity experiments

The X-ray reflectivity measurements were performed with a Bruker D8-Advanced diffractometer in a $\theta - \theta$ geometry, as described in Section 4.2.

Data reduction and analysis

Data reduction and data analysis are described in Section 3.8. Reflectivity data are normalized to the Fresnel reflectivity, R_F, in order to highlight features stemming from the adsorbed protein layers according to Equation (3.19). The interfacial structure of adsorbed protein films in electron density profiles is described by a layer model, air / protein adsorbate / subphase. In our study, a model consisting of two layers representing the adsorbed proteins explains the reflectivity data adequately; models consisting of only one layer do not yield appropriate refinements of the data. In order to reduce the number of fitting parameters, reference measurements without protein (data not shown) have been performed and analyzed; the values obtained for the roughness and electron density of the subphase have been used and kept constant when fitting the measurements with protein. The errors of the fitting parameters have been estimated by allowing a variation of 5% from the χ^2 of the best fit.

5.2.4 Results

Time evolution of the interfacial structure of RNase

As previous dynamic surface tension experiments have shown, it can take up to 15 h until RNase adsorption at the air-water interface has reached equilibrium [269]. Therefore, experiments on the cosolvent effects were performed after an equilibration time of at least 16 h. After 16 h,

subsequent reflectivity measurements of a distinct sample do not vary significantly from each other.

Figures 5.8 and 5.9 present experiments on the adsorption of RNase without cosolvent at selected time points of three separately prepared samples. As can be seen in Figure 5.8, after equilibration, the protein adsorbate causes a broad Kiessig fringe with a maximum at $Q = 0.13$ Å^{-1} in the reflectivity curve. The electron density (Figure 5.8) and volume fraction profiles (Figure 5.9) of the two curves taken 20 and 25 h after preparation do not vary significantly, indicating a high reproducibility of the adsorbate structure after equilibrium adsorption is reached. However, the measurement performed immediately after preparation differs substantially. The peak in the reflectivity curve is found at $Q = 0.17$ Å^{-1}, indicating a thinner adsorbed layer (see Table 5.4). Thus, it is shown that structural rearrangements in the adsorbed layer take place during the adsorption process until equilibrium adsorption is reached. These rearrangements, in particular, lead to a higher adsorbed amount and a thicker adsorbed layer with a compact protein conformation as shown in Figure 5.9.

Table 5.4: Structures of RNase adsorbed at the air-water interface at selected time points after preparation characterized by X-ray reflectivity [113].[a]

time	d / Å	Γ / mg m^{-2}
0 h	27.0 (1.2)	1.45 (0.12)
20 h	32.0 (0.9)	1.95 (0.12)
25 h	32.6 (1.2)	2.00 (0.22)

[a] The total layer thickness of the protein adsorbate and the surface excess are denoted as d and Γ, respectively.

Without proteins present in the bulk solution, the electron density increases sharply at the air-water interface from zero in air up to the electron density of the subphase (Figure 5.8). If proteins are present in the bulk solution, a protein film is formed spontaneously at the air-water interface; the interfacial structure is modeled by two adsorbate layers (Figure 5.8): a dense upper adsorbate layer ($z \approx 0 - 17$ Å; thickness, d_1) adjacent to the air-water interface with an electron density close to that of the pure protein as well as a diffuse layer ($z \approx 17 - 34$ Å; thickness, d_2) with a lower electron density. The corresponding volume fraction profiles in Figure 5.9 reveal that the upper layer has a volume fraction of approximately one and the lower layer has a decreased ϕ-value. It is important to note that the roughnesses of the adsorbate with air, σ_0, and the water subphase, σ_2, also have to be accounted for in order to obtain the total layer thickness of the protein adsorbate [76], d, which is given by

$$d = d_1 + d_2 + \sigma_0 + \sigma_2. \tag{5.1}$$

Thus, the equilibrium value of total thickness for the adsorbed layer in Figure 5.9 is 32 Å (Table 5.4) matching the dimensions of an RNase molecule.

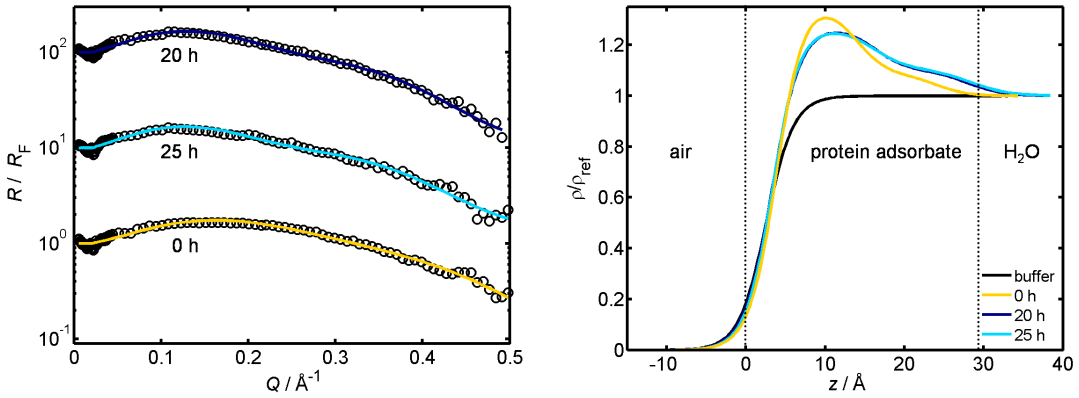

Figure 5.8: (Left) X-ray reflectivity curves (open circles) and fits (solid lines) and (Right) real-space electron density profiles normalized to the electron density of the subphase of RNase adsorbed at the air-water interface in a pure buffer solution [113]. Measurements were performed immediately after preparation, after 20 h and after 25 h. The X-ray reflectivity curves are shifted for clarity. The different parts of the electron density profile are separated by dotted vertical lines. The electron density profile of a pure air-water (buffer) interface is shown for comparison.

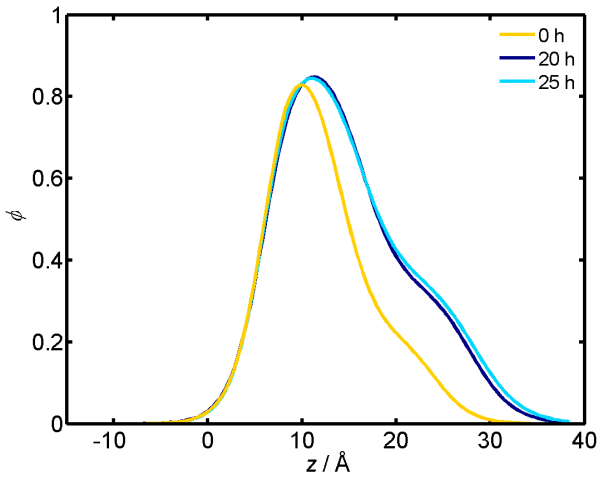

Figure 5.9: Volume fraction profiles of RNase adsorbed at the air-water interface in a pure buffer solution [113]. Measurements were performed immediately after preparation, after 20 h and after 25 h.

Effect of glycerol on the RNase adsorbate structure

In order to investigate the effect of glycerol on RNase adsorption at hydrophobic interfaces, X-ray reflectivity measurements were conducted with glycerol concentrations ranging from 0 to 4 mol L^{-1}. Figure 5.10 displays the corresponding X-ray reflectivity data. All reflectivity curves in Figure 5.10 have a similar shape, thus hinting at a common structure in the electron density profile. The curves differ only in small changes of the amplitude of the Kiessig oscillation. In fact, the interfacial structures in the electron density (Figure 5.10) and the volume fraction profiles (Figure 5.11) resemble those of the pure protein adsorbate without cosolvent. However, the absolute volume fraction decreases continuously with increasing glycerol concentration. As the adsorbed amount is given by the integral over the volume fraction profile, the same trend is observed for the adsorbed amounts (Table 5.5). The effect of increasing glycerol concentration on the total layer thickness and the amount of adsorbed protein is illustrated in Figure 5.12. The layer thickness remains approximately constant with varying glycerol concentration. Fitting yields a mean layer thickness of 31.9 (0.3) Å. The decrease of the adsorbed amount with increasing glycerol concentration shows apparently a linear behavior with a reduction rate of -0.21 (0.02) mg m^{-2} RNase per 1 mol L^{-1} glycerol. This value is a bit lower than the reduction rate obtained at the hydrophilic silica-water interface of -0.42 mg m^{-2} RNase per 1 mol L^{-1} glycerol obtained by optical reflectivity [143].

Table 5.5: Structures of RNase adsorbed at the air-water interface in the presence of glycerol characterized by X-ray reflectivity [113].[a]

c_{glycerol} / mol L^{-1}	ρ_1 / e Å^{-3}	ρ_2 / e Å^{-3}	d / Å	Γ / $mg\ m^{-2}$
0	0.387 (0.003)	0.449 (0.003)	32.0 (0.9)	1.95 (0.12)
0.1	0.382 (0.003)	0.432 (0.003)	32.6 (1.0)	1.90 (0.15)
1	0.374 (0.004)	0.419 (0.003)	31.2 (0.8)	1.61 (0.18)
2	0.392 (0.003)	0.426 (0.003)	32.8 (1.4)	1.41 (0.15)
3	0.383 (0.003)	0.400 (0.002)	31.7 (1.2)	1.30 (0.08)
4	0.376 (0.002)	0.403 (0.002)	30.9 (0.9)	1.07 (0.05)

[a] c_{glycerol} is the concentration of glycerol in the RNase solution, ρ_1 and ρ_2 are the electron densities of the adsorbed protein layer, d is the total layer thickness of the protein adsorbate, and Γ is the surface excess.

Effect of urea on the RNase adsorbate structure

Figure 5.13 shows X-ray reflectivity experiments of RNase adsorbed at the air-water interface in the presence of various urea concentrations in the protein solution illustrating the effect of the chaotropic cosolvent on the adsorption process. The reflectivity curves for low urea concentrations up to 2 mol L^{-1} resemble the curve of RNase without cosolvent, and for higher concentrations from 3 up to 6 mol L^{-1} further Kiessig fringes appear with minima and maxima roughly at $Q = 0.25$ Å^{-1} and $Q = 0.35$ Å^{-1}, suggesting a significant modification of the interfacial structure of

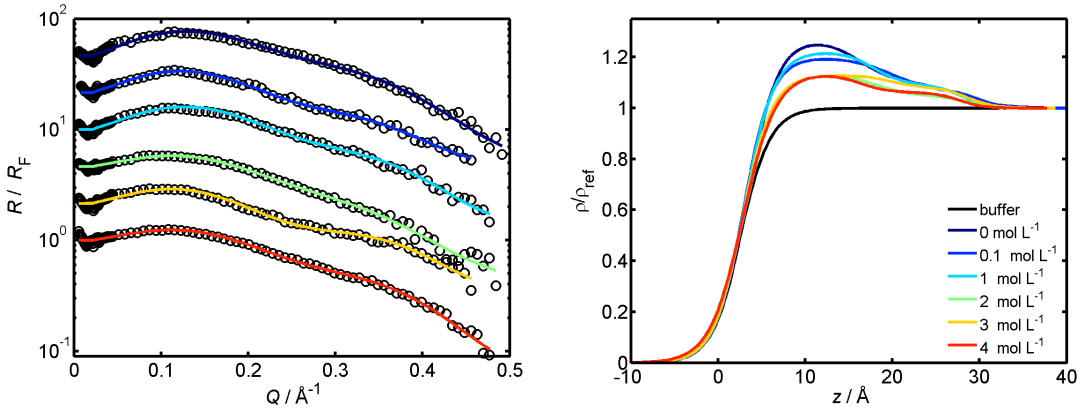

Figure 5.10: (Left) X-ray reflectivity curves (open circles) and fits (solid lines), and (Right) real-space electron density profiles normalized to the electron density of the subphase for RNase adsorbed at the air-water interface containing various glycerol concentrations as indicated [113]. The X-ray reflectivity curves are shifted for clarity.

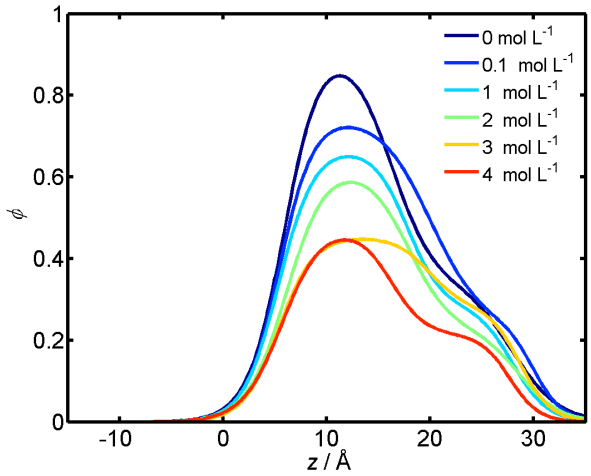

Figure 5.11: Volume fraction profiles for RNase adsorbed at the air-water interface containing various glycerol concentrations as indicated [113].

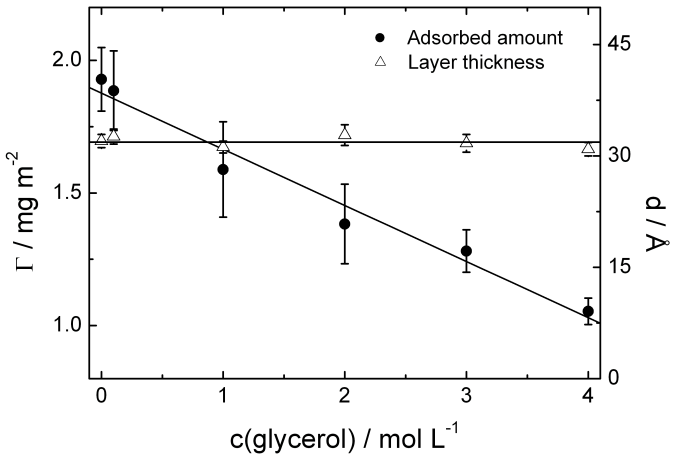

Figure 5.12: Variation of adsorbed mass, Γ (filled circles), and total layer thickness, d (open triangles), of RNase adsorbed at the air-water interface as a function of glycerol concentration in the protein solution [113]. The variation of the adsorbed mass with glycerol content was fitted linearly (line), yielding a reduction rate of -0.21 (0.02) mg m^{-2} RNase per 1 mol L^{-1} glycerol; the layer thickness as a function of glycerol concentration was fitted by a constant (horizontal line) resulting in a mean adsorbate thickness of 31.9 (0.3) Å.

the adsorbate. These differences become evident in the electron density profiles (Figure 5.13) and the volume fraction profiles (Figure 5.14). The dense upper layer of the adsorbate whose volume fraction has decreased for increasing urea concentration has nearly the same volume fraction at 2 mol L^{-1} as the diffuse layer protruding into the subphase. For 3, 4, and 6 mol L^{-1} urea in the solution, the electron density of this upper layer is lower than that of water, indicating that parts of the protein are outside the subphase and exposed to air. Due to this exposure, the adsorbed proteins are not fully hydrated at high urea concentrations, and therefore, it is not possible to subtract the reference profile according to the methodology described above (cf. Section 3.9.2). Hence, ϕ-profiles and adsorbed amounts are only calculated for urea concentrations ranging from 0 to 2 mol L^{-1} (Table 5.6), assuming a full hydration under these conditions. Interestingly, the total thickness of the adsorbate remains approximately constant as a function of urea concentration with a mean thickness of 31.5 (0.2) Å (Figure 5.15).

5.2.5 Discussion

The experiments on RNase adsorption at the air-water interface without cosolvent present in the solution show that the RNase adsorbate has a total layer thickness of 32 Å. With a hydration shell of approximately 2 Å around the dissolved RNase molecules, the molecule dimensions are approximately $26 \times 32 \times 42$ $Å^3$. Therefore, it can be concluded that adsorbed RNase molecules have a flat-on orientation toward the air-water interface with the long axis parallel to the interface, and

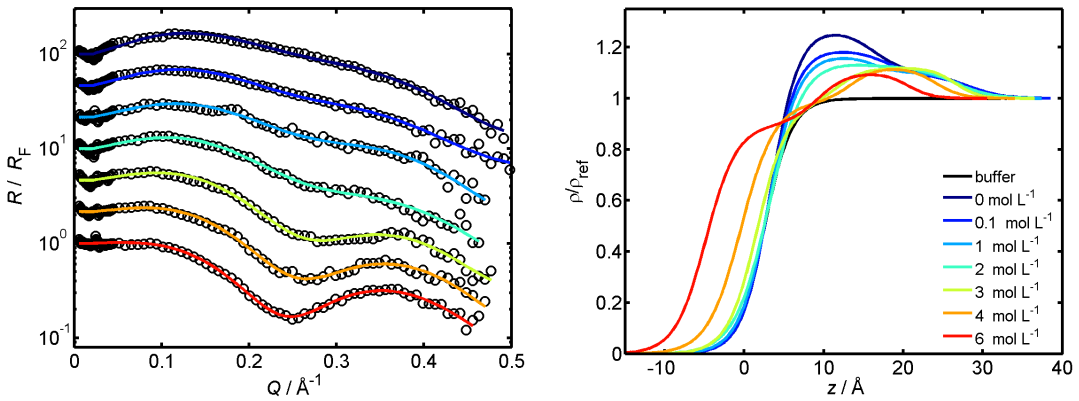

Figure 5.13: (Left) X-ray reflectivity curves (open circles) and fits (solid lines), and (Right) real-space electron density profiles normalized to the electron density of the subphase for RNase adsorbed at the air-water interface containing various urea concentrations as indicated [113]. The X-ray reflectivity curves are shifted for clarity. It is noted that the electron density profiles are shifted along the z-axis in order to superimpose the air-water interface at urea concentrations of $0 - 2$ mol L^{-1}. At higher urea concentrations, the air-water interface cannot be located precisely.

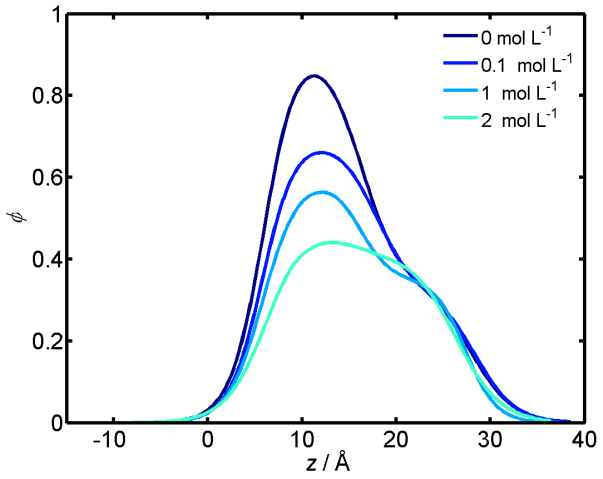

Figure 5.14: Volume fraction profiles for RNase adsorbed at the air-water interface containing various urea concentrations as indicated [113].

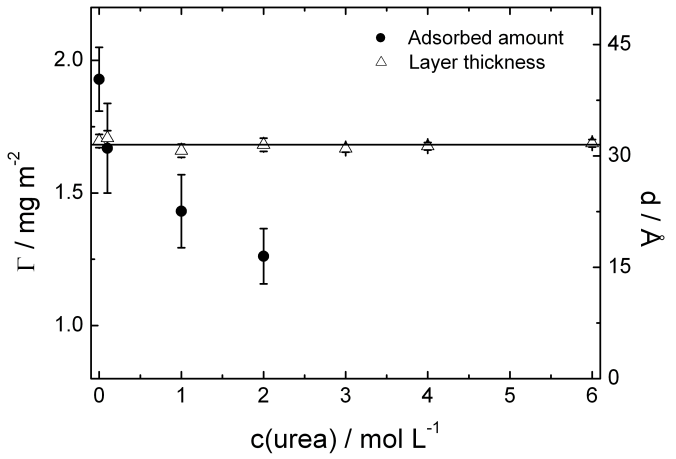

Figure 5.15: Variation of adsorbed mass, Γ (filled circles), and total layer thickness, d (open triangles), of RNase adsorbed at the air-water interface as a function of urea concentration in the protein solution [113]. The layer thickness as a function of urea concentration was fitted by a constant (horizontal line) resulting in a mean adsorbate thickness of 31.5 (0.2) Å.

Table 5.6: Structures of RNase adsorbed at the air-water interface in the presence of urea characterized by X-ray reflectivity [113].[a]

c_{urea} / mol L^{-1}	ρ_1 / e $\mathrm{Å}^{-3}$	ρ_2 / e $\mathrm{Å}^{-3}$	d / Å	Γ / $mg\ m^{-2}$
0	0.387 (0.003)	0.449 (0.003)	32.0 (0.9)	1.95 (0.12)
0.1	0.389 (0.004)	0.427 (0.003)	32.4 (1.0)	1.69 (0.17)
1	0.391 (0.004)	0.398 (0.003)	30.7 (0.9)	1.45 (0.14)
2	0.394 (0.004)	0.400 (0.004)	31.5 (0.9)	1.28 (0.10)
3	0.406 (0.003)	0.354 (0.003)	31.0 (0.5)	
4	0.404 (0.003)	0.354 (0.003)	31.3 (0.5)	
6	0.413 (0.002)	0.335 (0.002)	31.7 (0.5)	

[a] c_{urea} is the concentration of urea in the RNase solution, ρ_1 and ρ_2 are the electron densities of the adsorbed protein layer, d is the total layer thickness of the protein adsorbate, and Γ is the surface excess.

that RNase forms a monomolecular layer upon adsorption at the air-water interface. Moreover, it is suggested that the compact, globular shape of RNase and, in particular, most of its tertiary structure are maintained upon adsorption at the air-water interface. Similar adsorbate structures with a compact, globular structure of adsorbed RNase have been found at the hydrophilic silica-water interface [143] and at the hydrophobic poly(styrene)-water interface [79, 80] by neutron reflectivity. This clue is in line with spectroscopic studies that have shown that the α-helix and β-sheet content of RNase is only slightly reduced upon adsorption at a polyelectrolyte brush [291] and that the β-sheet content is decreased upon adsorption at a hydrophilic germanium crystal [23]. Besides, experiments on RNase denaturation in solution using small-angle X-ray

scattering and Fourier transform infrared spectroscopy have shown that RNase retains residual secondary structure in the chemically and thermally denatured state [251]. Hence, even at the extremely hydrophobic air-water interface, RNase may adsorb maintaining most of its tertiary structure. This might also be due to the high stability of RNase with an unfolding free energy of $\Delta G_0 = 7.9$ kcal mol^{-1}, as determined by circular dichroism spectroscopy [241], owing to its four disulfide bonds. Analogously, it has been suggested that the air-water interface provides a near-native environment for the adsorption of lysozyme and βLg [162, 197, 198]. However, it should be mentioned here that surface-induced denaturation of proteins, for example, myoglobin and lysozyme, at the air-water interface has also been observed [107, 300].

Considering the dimensions of hydrated protein molecules, the time-evolution of the adsorbed layer as shown in the ϕ-profile in Figure 5.9 can be ascribed to a change in the orientation as illustrated in Figure 5.16, which is in analogy with a study of RNase adsorption at mica [150]. At first, RNase molecules adapt a flat-on orientation with the smallest axis perpendicular to the surface because the layer thickness of 27 Å exactly (within $\pm$ 1 Å) matches the smallest axis of RNase. After sufficient equilibration time, the orientation of the adsorbed molecules has changed, leading to an orientation with the other small axis (32 Å) perpendicular to the interface as described above. The change in orientation allows for a denser packing of the adsorbed molecules and, hence, a higher surface excess. However, the adsorbate thickness is only an indirect parameter to draw conclusions on protein orientations at interfaces. Hence, the scheme shown in Figure 5.16 represents a reasonable suggestion for a structural model which is consistent with the data.

Glycerol is known to interact strongly with water and tends to be excluded from the protein-water interface [84, 272]; thus, the protein becomes preferentially hydrated, as has been shown for RNase by thermodynamic and dielectric relaxation spectroscopy measurements [26, 84]. While hydrophobic interactions are strengthened in this way, the adsorbed amount of RNase does not rise but is reduced continuously with increasing glycerol content (Figure 5.12). This observation might be explained as glycerol stabilizes the native protein conformation. Thus, the protein's interfacial affinity is weakened, because a direct protein-interface contact and conformational changes upon adsorption are suppressed. Hence, glycerol protects the protein's globular shape from drastic structural changes due to exposure at the hydrophobic interface. This interpretation is directly corroborated by the experimental data presented in Figure 5.11, since all volume fraction profiles share a common shape with a mean adsorbate thickness of 31.9 (0.3) Å analogous to that of the control experiment without cosolvent. Thus, the mechanism of reduced adsorption in the presence of glycerol formerly proposed for glycerol-protein interactions at hydrophilic interfaces is supported [143].

The use of urea to denature proteins is now commonplace [22, 87]. However, the molecular basis of protein denaturation by urea is still under debate [22, 37, 41, 83, 111, 227]. It is thought that protein denaturation by urea may involve direct hydrogen-bonding interactions with the protein. The transition of RNase into the denatured state in solution sets in at about 6 mol L^{-1}

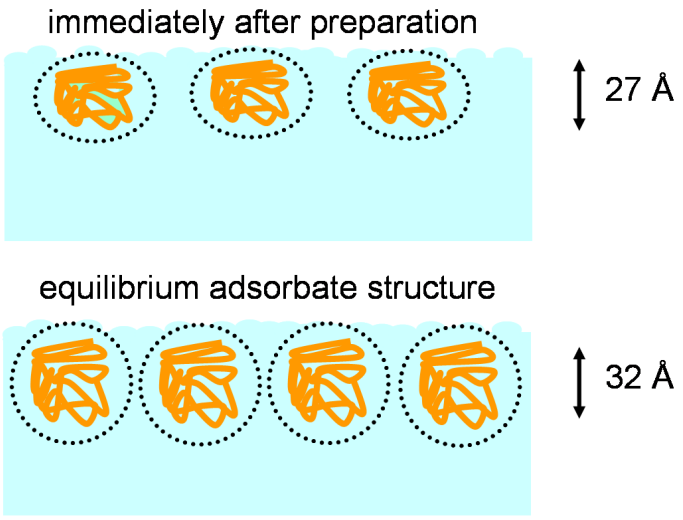

Figure 5.16: Simple model for the time-evolution of the adsorbed RNase layer (see Figure 5.8 and Table 5.4) [113]. The measurement performed directly after preparing the solution suggests that RNase forms an adsorbed monolayer with its smallest axis (26 Å) perpendicular to the interface. After equilibratium is reached, a structural reorganization of the adsorbed layer occurs, so that the molecules are oriented flat-on with their other small axis (32 Å) perpendicular to the interface allowing for a more densely packed adsorbate. Hence, the structural rearrangement of the adsorbed layer might be directly correlated with a change of protein orientation at the interface.

and the denatured state is reached at about 8 mol L^{-1}, as has been shown by optical rotation measurements [87]. Moreover, the concentration, $c_{1/2}$, at which half of the protein molecules in solution at pH 7 have been denatured by urea has been determined to be 7 mol L^{-1}, as obtained by fluorescence measurements [190], or 8 mol L^{-1}, as deduced from circular dichroism [241]. However, it has been shown that adsorption at the air-water interface [198] or at silica nanoparticles [241] might reduce the $c_{1/2}$ value. It can be assumed that RNase is not denatured in solution in our measurements with a maximum urea concentration of 6 mol L^{-1}. However, the adsorbate structure at high urea concentrations ($3-6$ mol L^{-1}) might indicate that RNase is, in part, denatured at the interface, although the thickness of the adsorbate is approximately constant.

Since urea is known to preferentially bind to the protein-water interface [261], certain conformational changes of the protein might occur. Moreover, urea weakens hydrophobic interactions, thus increasing the solubility of hydrophobic protein residues in water [41, 48]. Therefore, the hydrophobic interaction between RNase and the air-water interface might be diminished and the decrease of the adsorbed amount (up to 2 mol L^{-1}) is understood in a qualitative way and in line with earlier findings at the hydrophilic silica-water interfaces [143]. However, at urea concen-

trations of 3 mol L^{-1} and higher, the electron density profiles in Figure 5.13 exhibit adsorbate layers with electron densities below that of water, which means that the volume fraction profiles cannot be calculated unambiguously. At these concentrations, urea-driven rearrangements must have led to an exposure of parts of the protein to air. Similar dehydration layers have been observed previously for βLg adsorbed at the air-water interface in 6 mol L^{-1} urea solution in the presence of dithiothreitol that removes the disulfide bonds [198].

Similar mechanisms have been suggested for the effect of kosmotropic and chaotropic ions on the interfacial structure of protein adsorbates [79], where kosmotropic salts may disfavor conformational changes of proteins and chaotropic salts may accumulate at the protein surface. In comparison with earlier studies on the effect of chemical denaturants on protein adsorption at the air-water interface, it is striking that in the case of RNase the total layer thickness remains approximately constant while the adsorbed amount decreases with increasing cosolvent concentration, whereas a significant increase in film thickness and an almost constant surface excess were observed for βLg in the presence of urea and guanidinium hydrochloride [198].

In this study, the different scenarios observed upon RNase adsorption at the air-water interface under the different conditions studied are illustrated in the simple model presented in Figure 5.17: Without cosolvents present in the subphase (Figure 5.17a), RNase forms a densely packed monomolecular layer at the air-water interface with a total layer thickness of 32 Å, matching the dimensions of an RNase molecule with a lower part protruding into the subphase and an upper part in contact with the air-water interface. In the presence of glycerol in Figure 5.17b, RNase proteins become preferentially hydrated, while glycerol molecules are excluded from the hydration shell, which is indicated by the dotted circle. With increasing glycerol content, glycerol is still excluded from the protein's hydration shell, so that the volume fraction of the adsorbate and, hence, the surface excess decrease. At low urea concentration as in Figure 5.17c, urea molecules attach to hydrophobic patches of the protein and may thus lead to a varied protein conformation. However, the X-ray data suggest that the compact shape of the adsorbed layer is maintained even in the presence of urea. In the presence of high urea concentration as in Figure 5.17d, hydrophobic parts of the protein, which become available by urea-induced protein destabilization, are exposed to air. Figure 5.16 and 5.17 give only a simple view of the interfacial adsorbate structure. Molecular details of such structures are likely to be more complex [172].

5.2.6 Conclusion

In this study, we found that the affinity of RNase to adsorb at the air-water interface can be drastically altered by the presence of nonionic cosolvents. Glycerol and urea at low concentrations cause a continuous reduction of the adsorbed amount, while the overall strucure of the adsorbed layer is maintained. However, in the presence of high urea concentrations, parts of the adsorbed layer are exposed to the air while the total layer thickness also remains constant. The electron density and volume fraction profiles of the protein adsorbates provide indications for the different mechanisms underlying the effects of kosmotropic and chaotropic cosolvents. While

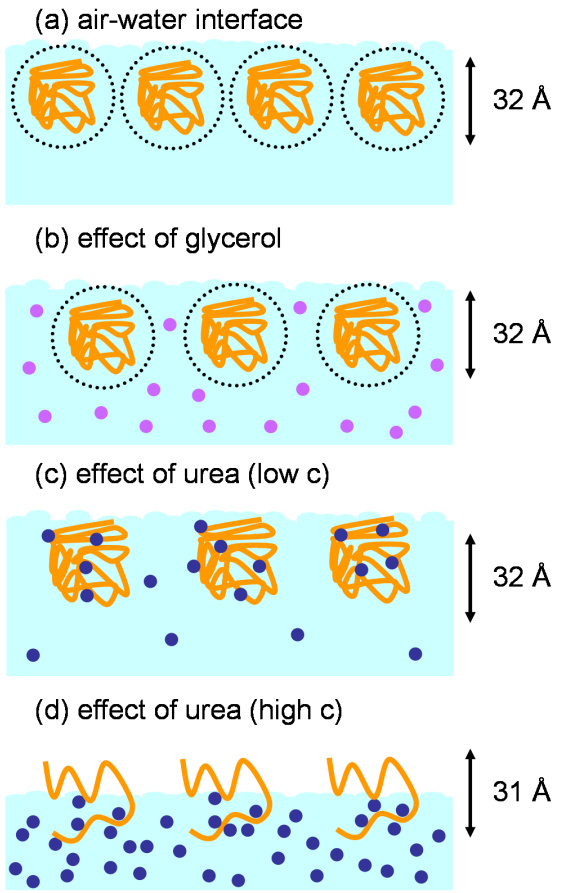

Figure 5.17: Simple model for the adsorption of RNase at the air-water interface (a) [113]. The effect of glycerol (b) and urea at low (c) and high concentration (d) are also visualized. Under all conditions studied, RNase forms a monomolecular adsorbate layer with a flat-on orientation and a layer thickness matching one of the small axes of the molecule. Both without cosolvent and in the presence of glycerol, the proteins are surrounded by a hydration shell (dotted circle). In the presence of glycerol, the volume fraction of the adsorbed layer is reduced as well as in the presence of low urea concentrations, although urea preferentially binds to the surface of the proteins and may lead to conformational changes. In the presence of high urea concentrations, parts of the adsorbed layer are dehydrated and exposed to the air.

protein stabilizing cosolvents induce a preferential hydration of the proteins protecting their conformation, protein destabilizing cosolvents accumulate at the protein-water interface and weaken hydrophobic interactions. These data agree well with earlier studies in which the effects of ionic cosolvents at hydrophobic surfaces and the effect of nonionic cosolvents at hydrophilic surfaces were probed.

6 Effects of ionic cosolvents on the structure of adsorbed protein films

The presence of ions in a protein solution can alter the adsorption behavior of proteins. In this Chapter, two studies on the effect of ions on protein adsorption are reported. The first study (Section 6.1) shows that high concentrations of NaCl can lead to increased adsorption at hydrophobic polystyrene surfaces [78]. In the second study (Section 6.2), salts selected from the Hofmeister series were used, and it was found that both kosmotropic and chaotropic salts could lower the degree of protein adsorption at a hydrophobic surface [79].

6.1 Effect of salt on the adsorption of BSA at hydrophobic surfaces

The study presented in this Section has been published in *European Physical Journal Special Topics* [78].

6.1.1 Summary

In a biological cell, proteins face a highly complex environment comprising crowding and confinement effects as well as interactions with interfaces, cosolvents, and other biomolecules. In this study, the X-ray reflectivity technique has been used for the in situ characterization of adsorbed protein layers at solid-liquid interfaces. The adsorption of bovine serum albumin at the hydrophobic polystyrene-water interface has been investigated in the presence and in the absence of salts. The data indicate that enhanced adsorption occurs at high salt concentrations.

6.1.2 Introduction

Biological cells provide a very complex environment for proteins, in which crowding and confinement effects can lead to enormous alterations of the conformational stability or the biological activity of proteins [67, 173]. Besides, proteins interact with various interfaces, cosolvents or other biomolecules present in the cell. However, studying protein adsorption onto solid surfaces is not only of considerable academic interest, but also of great importance in everyday life – in a favourable or in an unfavourable way [50]. Undesirable effects are, e.g., the induction of blood clotting onto medical devices or the formation of biofilms onto contact lenses that can lead

to immunological reactions [39, 134], whereas solid-phase immunoassays exemplify favourable a application [288].

Probing the interfacial structure of the adsorbed protein layers in situ is the essential prerequisite for elucidating the mechanisms of protein adsorption. Standard techniques such as ellipsometry, optical reflectometry, fluorescence spectroscopy, and surface plasmon resonance spectroscopy can assess the amount of adsorbed protein [50]. However, these methods do not allow for the investigation of interfacial structures with high resolution. X-ray reflectometry is a unique method for in situ interface characterization on atomic length scales [267]. Since solid or liquid phases can be penetrated by high-energy photons, buried interfaces can be probed [76, 168, 170, 194, 212]. Therefore, X-ray reflectivity serves as a powerful tool for determinating the structure and composition of protein layers at solid-liquid interfaces [76, 194].

Whenever an aqueous protein solution is exposed to a solid surface, protein molecules will generally tend to adsorb spontaneously at the solid-liquid interface. This can affect their structure and flexibility and thus their biological function [50, 143]. Hence, it is of special interest to study how the structure of protein adsorbates is influenced by modifying the surface chemistry of the subtrate or by varying the protein solution properties by adding salts. Such information may contribute to a detailed understanding of how to control protein adsorption, e.g., the way to control protein interfacial affinity or to create protein-resistant surfaces [50, 143, 271].

Proteins in nature are not only solvated by water, but intracellular solutions are crowded with cosolvents like salts, osmolytes or other molecules that can have profound effects on structure, stability, and function of proteins [22, 124, 141, 146, 261]. Thus, studies of hydrophobic surfaces and the influence of cosolvents play a crucial role in revealing the mechanisms of biochemical and biotechnological processes.

In this study, the structure of adsorbed layers of bovine serum albumin (BSA) is obtained by in situ X-ray reflectometry. We show that the structure of protein adsorbates in their native environment can be probed with high resolution by high-energy X-rays. To this end, the adsorption of BSA at the hydrophobic polystyrene (PS)-water interface is monitored in the presence and in the absence of salts. Surprisingly, BSA adsorption at the hydrophobic, nonpolar PS surface is favored by high salt concentrations.

6.1.3 Experimental section

BSA was obtained from Sigma (Taufkirchen, Germany) and was used without further purification. The proteins were dissolved in aqueous buffer solutions with a protein concentration of 0.1 mg/mL. The buffer solutions were prepared with 10 mM morpholinopropanesulfonic acid (MOPS) and adjusted to pH 7 using NaOH solution.

In order to study the structure of adsorbed protein layers at buried solid-liquid interfaces, high-energy X-ray reflectometry has been employed. The X-ray reflectivity measurements were performed at the synchrotron light source DELTA (Dortmund, Germany) using the high-energy

reflectivity setup of beamline BL9 [144], as described in [194]. Further experimental details are described in Section 4.1.2.

6.1.4 Results and discussion

Data were analyzed by a least square fitting routine using the effective density model [267] and by simultaneously fitting the Fourier transform of the data [236]. The vertical structure of the system was described by a layer model, Si / SiO_2 / PS / protein adsorbate / protein solution. In the framework of a box model, the adsorbed protein layer is modeled as a homogeneous layer with electron density (ρ_{ads}), layer thickness (d_{ads}), and roughness (σ_{ads}). The structure of the substrate was determined in a pre-measurement of the hydrophobic polystyrene-water interface (without proteins present in the subphase) and kept constant during the refinement of the data. Reflectivities are calculated by Parratt's algorithm [193]. Thereafter, the resulting density profile is varied by stochastic displacements of the electron density in order to improve the quality of the refined reflectivity curve [230, 267]. Small 'bumps' with a maximum amplitude of 0.1 e/Å^3 and a full width at half maximum of 5 Å were introduced to the best box model fit. Thus, the electron density profile is not changed significantly except for small layering effects in the PS film. In order to compare our results with other methods, the volume fraction of the protein, ϕ, and the adsorbed mass of protein per surface area, Γ, are calculated, as described in Section 3.9.2.

The adsorption of BSA onto hydrophobic polystyrene was investigated in situ in the presence and absence of salts. A buffer solution with 1 M NaCl was prepared for the X-ray reflectivity measurement in the presence of salt. This high salt concentration has been chosen, because not very much about protein adsorption in the presence of high salt concentration is known yet. The results are shown in Figure 6.1 and Table 6.1. In order to emphasize the Kiessig oscillation of the adsorbed layer, R/R_F is shown instead of the pure reflectivity R. Thus, both the Kiessig fringes and the density contrast as indicated by the oscillation amplitude become pronounced. The drastically different oscillation amplitudes in Figure 6.1 can, in part, be attributed to slightly different electron densities of the PS films, as obtained from the pre-measurements.

Table 6.1: Interfacial structure of BSA films adsorbed poly(styrene), as obtained from X-ray reflectometry [78].[a]

solution condition	Γ / mg/m^2	ρ_{ads} / e/Å^3	d_{ads} / Å	σ_{ads} / Å
without NaCl	0.24 (0.10)	0.338 (0.003)	39.9 (0.5)	8.0 (1.0)
with 1 M NaCl	0.96 (0.10)	0.350 (0.003)	43.1 (0.5)	9.0 (1.0)

[a] Γ, ρ_{ads}, d_{ads}, and σ_{ads} denote the surface excess, layer thickness, electron density and interfacial roughness of the adsorbed BSA layer, respectively.

In the absence of NaCl, BSA adsorbs only to a very small extent at this pH (Table 6.1).

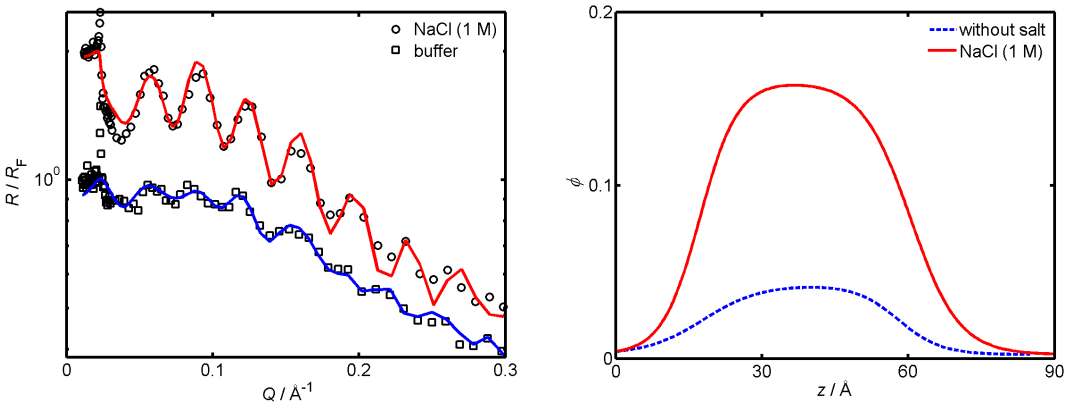

Figure 6.1: (Left) X-ray reflectivity data for the adsorption of BSA at the hydrophobic polystyrene-water interface in the presence and absence of NaCl [78]. Measured data are dotted; fits are shown as solid lines. The reflectivity curves are shifted by a constant factor for clarity. (Right) Volume fraction profiles of BSA adsorbed at PS in the absence and presence of 1 M NaCl. For clarity, the volume fraction profiles are shifted along the z-axis [78].

Moreover, the PS surface is rather hydrophobic, and therefore, one might expect adsorption-induced conformational changes of BSA, which is a "soft protein" [163]. However, as the thickness of the adsorbed layer matches the dimensions of a BSA molecule, one can assume that BSA denatures only to a small extent upon adsorption at the PS surface at this pH if at all. For an adsorbed layer composed of denatured proteins, one would expect distinct changes in both the layer thickness and the electron density, as has been observed for protein adsorption at silanized silicon wafers (cf. Chapter 8). Hence, we propose that the structure of the adsorbed layer is mainly composed of a monolayer of procumbent BSA molecules. In essence, the observed value for Γ is consistent with similar studies [255, 256].

In general, protein adsorption at hydrophobic surfaces is governed by hydrophobic interactions as the main driving force [40, 50]. In our case, the BSA molecules carry a negative net-charge at pH 7 (cf. Table 2.1); hence, electrostatic protein-protein interactions within the adsorbed layer are important as well. This delicate balance of protein-surface and protein-protein interactions can be altered in the presence of small ions [50, 141, 146]. Ions are distributed in the interfacial layer, resulting in charge screening effects that can alter both attractive and repulsive electrostatic interactions, and thus, the surface excess can be affected. In the literature, the effect of NaCl on the adsorption of lysozyme at the silica-water interface has been discussed [254, 278]. Increasing the concentration of NaCl leads to reduced lysozyme adsorption or even to a complete removal of the adsorbed layer [254].

In the presence of NaCl, the Kiessig fringes of the reflectivity curve shown in Figure 6.1 become more pronounced. Although this might partially be due to a slightly different density of the PS layer, the drastic effect of salt on the protein layer is shown in the volume fraction profile in

Figure 6.1. Accordingly, Γ is drastically enhanced in the presence of 1 M NaCl. In comparison to former studies with moderate salt concentrations, this fact is new [254] and highlights the complexity of ion-water interactions at interfaces [141, 146]. An enhanced adsorption at a hydrophobic surface in the presence of salts underpins that the hydrophobic effect acts as the dominating driving force for protein adsorption in this case.

6.1.5 Conclusion

In this study, the interfacial structure of BSA adsored at the hydrophobic polystyrene-water interface has been characterized in situ in the presence and the absence of NaCl by X-ray reflectometry. We have shown that adding salt to protein solutions can affect the adsorption behavior by increasing the amount of adsorbed protein and the packing density of the adsorbed molecules. Hence, it can be deduced that the hydrophobic effect is the dominating driving force. High-energy X-ray reflectometry is able to investigate buried solid-liquid interfaces with an accuracy in the angstrom regime which is of particular interest for probing interfacial aspects of manifold biophysical systems.

6.2 Hofmeister effect on the density profile of protein adsorbates

The results presented in this Section are published in *Journal of Physical Chemistry B* [79].

6.2.1 Summary

The effects of various salts on the adsorption of ribonuclease A (RNase) at a hydrophobic poly(styrene) film were analyzed in this study applying neutron reflectometry. It has been found that both the kosmotropic salts, $(NH_4)_2SO_4$ and Na_2SO_4, and the chaotropic salts, NaSCN and $Ca(SCN)_2$, significantly reduce the amount of adsorbed protein. Maximum adsorption is observed in the presence of NaCl. Apparently, there is no single Hofmeister effect on the degree of protein adsorption at an aqueous-solid interface which ranges from kosmotropic to chaotropic ions. The observed variations in the adsorbed amount can be attributed to variations in the packing density of the adsorbed protein molecules. The results suggest that kosmotropic salts reduce the degree of protein adsorption by disfavoring a conformational adaptation and a dehydration of the protein molecules at a hydrophobic poly(styrene) film. On the other hand, chaotropic salts shield hydrophobic interactions between the protein molecules and the substrate by saturating hydrophobic patches on the protein surface. Remarkably, the results of this study corroborate earlier findings on the effects of nonionic cosolvents on protein adsorption [143].

6.2.2 Introduction

In 1888, Hofmeister described a ranking of ions according to their effectiveness in precipitating hen egg-white proteins [101]. This so-called Hofmeister series has also been found to rule the conformational stability of native proteins in aqueous solutions. In the case of anions, the following order is often reported [266]:

$$SO_4^{2-} > F^- > CH_3COO^- > Cl^- > Br^- > I^- > ClO_4^- > SCN^-.$$

Ions on the left side of this series are called kosmotropes. They are strongly interacting with water molecules (via hydrogen bonds) and stabilize the compact folded structure of protein molecules. In contrast, ions located on the right side of this series tend to unfold proteins in aqueous solution. They are called chaotropes. There is also a corresponding series for cations:

$$Mg^{2+} > Ca^{2+} > Na^+ > K^+ > Rb^+ > NH_4^+.$$

Kosmotropic and chaotropic cations are located on the left and the right side, respectively. The effect of cations is usually much weaker than that of the anions. The effectiveness of cations in stabilizing proteins is sometimes described in a reversed way, i. e., Mg^{2+} and Ca^{2+} lower the stability and NH_4^+ raises the stability of the native protein conformation [35, 261]. However,

there is clear experimental evidence that Ca^{2+} ions can be used to denature proteins [96, 276]. Na^+ and Cl^- are generally considered to act in an almost neutral way [46].

In this study, we were interested in the effects of different ions, selected from the Hofmeister series, on the adsorption process of proteins at aqueous-solid interfaces. It is well-known that proteins undergo more or less severe conformational changes upon adsorption on a solid surface [16, 240, 274]. These changes adapt the protein to its new environment and optimize the interfacial contact area. On the other hand, as outlined above, kosmotropic and chaotropic ions have a profound effect on the conformational stability of dissolved protein molecules. Therefore, it can be expected that the degree of protein adsorption and the structure of a protein adsorbate at an aqueous-solid interface depend on the kind of ions present in solution. In a previous study, it has been observed that the presence of glycerol and urea significantly reduces the degree of protein adsorption at a silica-water interface [143]. This result is remarkable, since glycerol and urea have rather opposite solution properties: glycerol is stabilizing and urea is destabilizing the native folded structure of a protein. Thus, it is of great interest, if kosmotropic and chaotropic ions act in the same way as glycerol and urea do. As before [143], we use ribonuclease A (RNase) and silicon wafers as model system. However, in order to exclude electrostatic interactions between the protein and the interface, which depend on the ionic strength of the protein solution, the silicon wafers were coated with a thin non-polar poly(styrene) film. Protein adsorption is then driven mainly by hydrophobic interactions. As will be shown in this study, the adsorption of the RNase is strongly dependent on the kind of added salt. Moreover, both kosmotropic and chaotropic salts lower the degree of adsorption as also found for glycerol and urea.

6.2.3 Experimental section

RNase was obtained from Sigma-Aldrich (catalog no. R5500). Protein solutions were prepared by dissolving 0.05 mg mL^{-1} RNase in a 10 mM morpholinopropane sulfonic acid (MOPS) buffer solution. D_2O was used as the solvent. The pD-value was adjusted to 7.4 (pD = pH-meter reading + 0.4) [47]. The salts $(NH_4)_2SO_4$, Na_2SO_4, NaCl, NaSCN, and $Ca(SCN)_2$ were also obtained from Sigma-Aldrich and were dissolved in the protein solution with concentrations of 0.67 or 2 mol L^{-1} (except for Na_2SO_4 which has a maximum solubility of 1.3 mol L^{-1} at 20 °C) [188]. Substrate preparation is described in Section 4.1.3.

Neutron reflectivity measurements were performed at the Helmholtz-Zentrum Berlin (Berlin, Germany), using the instrument V6 [167], as described in Section 4.1.1.

6.2.4 Results and discussion

At first, the dPS film on each silicon wafer was characterized by recording a neutron reflectivity curve using a 3 : 1 D_2O-H_2O mixture as solvent (Figure 6.2). The experimental curve has been analyzed by fitting a calculated curve to the data (Figure 6.2). The Parratt algorithm was applied and a 2-layer model, Si / SiO_2 / dPS / solution, was used. The scattering length densities of the

four components were fixed to $2.07 \cdot 10^{-6}$ Å^{-2} (Si), $3.48 \cdot 10^{-6}$ Å^{-2} (SiO_2), $6.42 \cdot 10^{-6}$ Å^{-2} (dPS), and $4.64 \cdot 10^{-6}$ Å^{-2} (D_2O-H_2O) [3, 224], whereas the layer thicknesses of SiO_2 and dPS were varied in the fitting process. Interlayer roughnesses were all fixed to 5 Å. For the data shown in Figure 6.2, thicknesses of 22 Å and 229 Å have been found for the silicon oxide and the dPS layer, respectively. The scattering length density profile representing this structure is also shown in Figure 6.2.

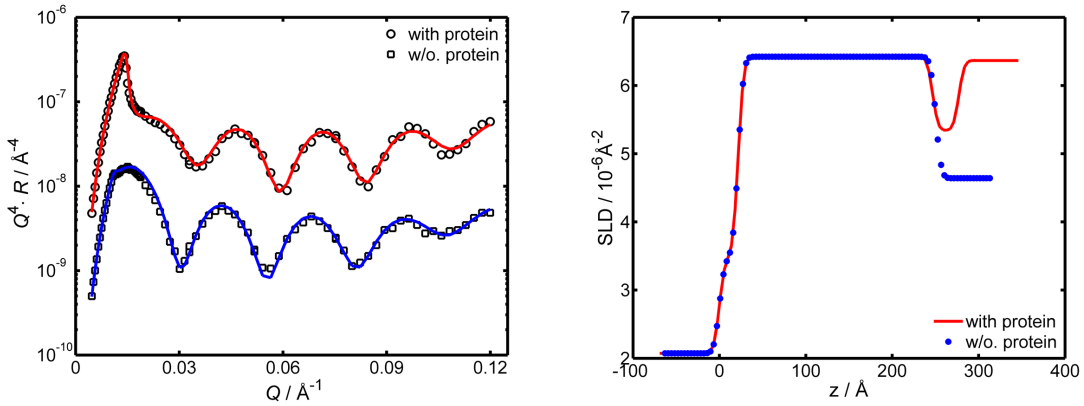

Figure 6.2: (Left) Typical neutron reflectivity curves of a silicon wafer, which is coated with a perdeuterated poly(styrene) film [79]. The film is in contact with a 3 : 1 D_2O-H_2O mixture (open squares) or with an RNase solution containing 2 mol L^{-1} NaCl (open circles). The solid lines show fits based on layer models for the interfacial structures. The reflectivity curves are shifted for clarity. (Right) Corresponding scattering length density (SLD) profiles of a silicon wafer coated with a dPS film [79]. The symbols represent the interfacial structure in the absence of protein using a 3 : 1 D_2O-H_2O mixture. In contact with an RNase-D_2O solution, protein molecules adsorb onto the dPS film (solid line).

In the next step, the D_2O-H_2O mixture was exchanged by a protein solution containing 0.05 mg mL^{-1} RNase and, for example, 2 mol L^{-1} NaCl in D_2O buffer solution (pD = 7.4). After one hour of equilibration, a neutron reflectivity curve was recorded, which is also plotted in Figure 6.2. Now, the reflectivity curve had to be analyzed using a 3-layer model, Si / SiO_2 / dPS / protein adsorbate / protein solution. In the fitting process, the thickness and the scattering length density of the protein adsorbate were varied. Its roughness was set to 5 Å. The scattering length density of the solution was a further fitting parameter, which is associated with the critical Q-value of a neutron reflectivity curve. The obtained scattering length density profile, when RNase has adsorbed in the presence of 2 mol L^{-1} NaCl, is shown in Figure 6.2. From this plot, the structure and location of the RNase adsorbate is easily visible. In the same way, the effects of NaSCN, $Ca(SCN)_2$, Na_2SO_4, and $(NH_4)_2SO_4$ on the adsorption of RNase at a dPS film were studied, each time using a new silicon wafer. All salts were dissolved at two concentrations, 0.67 mol L^{-1} and 2 mol L^{-1}, except for Na_2SO_4 which has a maximum solubility of 1.3 mol L^{-1}

at 20 °C [188] and was thus dissolved at a concentration of 0.67 mol L^{-1} only. The neutron reflectivity curves measured after adsorption of RNase in the presence of the salts are shown in Figure 6.3 together with the fits. The interfacial structures corresponding to these fits are listed in Table 6.2. The calculated mass of RNase adsorbed at a hydrophobic dPS film, Γ, is plotted in Figure 6.4 for all samples studied.

Table 6.2: Structures of Si / SiO_2 / dPS / protein adsorbate / protein solution interfaces characterized by neutron reflectometry [79].[a]

dissolved salt	c_{salt} / mol L^{-1}	$d_{adsorbate}$ / Å[b]	$\rho_{adsorbate}$ / 10^{-6} Å^{-6}	$\rho_{solution}$ / 10^{-6} Å^{-6}
NaCl	0.67	32	5.39	6.37
NaSCN	0.67	34	5.44	6.37
$Ca(SCN)_2$	0.67	37	5.13	5.80
Na_2SO_4	0.67	33	5.61	6.37
$(NH_4)_2SO_4$	0.67	27	5.38	6.00
NaCl	2	30	5.34	6.37
NaSCN	2	35	5.32	6.00
$Ca(SCN)_2$	2	31	4.64	5.00
$(NH_4)_2SO_4$	2	32	5.08	5.70

[a] c_{salt} is the salt concentration in the RNase solution, $d_{adsorbate}$ is the thickness of the RNase adsorbate layer,$\rho_{adsorbate}$ and $\rho_{solution}$ are the scattering length densities of the RNase adsorbate and the solution, respectively.
[b] The maximum error is estimated to be ± 3 Å.

As can be clearly seen from Figure 6.4, the maximum adsorbed amount of RNase at an aqueous-poly(styrene) interface is observed in the presence of NaCl. The Na^+ and Cl^- ions are generally regarded as the neutral midpoints in the Hofmeister series of anions and cations. Remarkably, in the presence of chaotropic salts (NaSCN and $Ca(SCN)_2$) and kosmotropic salts (Na_2SO_4 and $(NH_4)_2SO_4$), the degree of adsorption is significantly decreased. The measured thickness of the RNase adsorbate layer formed in the presence of salts is in the range of about $30 - 34$ Å (Table 6.2). Taking into account that the adsorbate layer has a roughness of a few angstroms, the overall thickness of the adsorbate layer matches the diameter of an RNase molecule (assuming a spherical shape, RNase has a diameter of 37 Å) [153]. This suggests that RNase is roughly forming a monolayer and maintains its native shape at the water-poly(styrene) interface under all solution conditions studied. Therefore, the variations in the adsorbed mass of RNase (Figure 6.4a) must be attributed to variations in the volume fraction of RNase in the adsorbate layer, which is also plotted in Figure 6.4b. Apparently, kosmotropic and chaotropic salts lower the packing density of RNase at a water-poly(styrene) interface by decreasing the protein-interface attraction and/or increasing the protein-protein repulsion. This result is in full agreement with an earlier study, where the adsorption of RNase was studied in the presence of glycerol and urea [143]. Both the protein-stabilizing glycerol and the protein-destabilizing urea were found to lower the volume fraction of RNase molecules in an adsorbate layer. It is likely

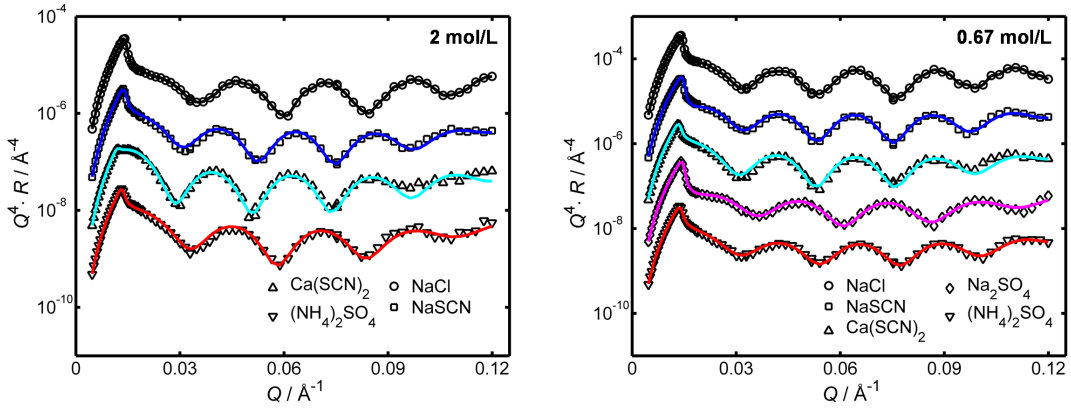

Figure 6.3: Neutron reflectivities of Si / SiO_2 / dPS / RNase adsorbate / solution interfaces [79]. The solutions contained the protein RNase and different salts, as indicated in the legends. The symbols reflect the experimental data, the solid lines are fits based on a three-layer model of the interfacial structure.

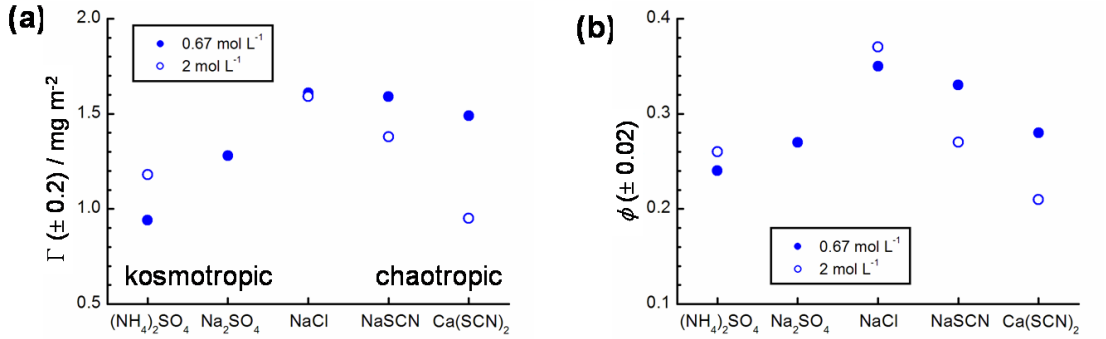

Figure 6.4: (a) Adsorbed mass of RNase at a water-poly(styrene) interface, Γ, and (b) volume fraction of RNase within the adsorbate layer, Φ [79]. The protein adsorption was performed in the presence of various salts at two different concentrations as indicated in the legend. The RNase concentration was kept constant at 0.05 mg mL^{-1}.

that protein-stabilizing cosolvents, such as kosmotropic salts and glycerol, reduce the degree of protein adsorption by disfavoring a conformational change and a dehydration of the protein molecules (they become preferentially hydrated). A conformational change and a dehydration of a protein molecule enable hydrophobic interactions, which represent a dominant driving force for protein adsorption at aqueous-solid interfaces [50]. On the other hand, chaotropic salts and urea can accumulate at the protein molecular surface [41, 195, 266]. Thus, hydrophobic interactions between the protein molecules and the substrate are probably shielded.

6.2.5 Conclusion

In this study, it has been found that both kosmotropic and chaotropic salts lower the degree of protein adsorption at a hydrophobic surface by decreasing the volume fraction of the protein within the adsorbate. Since both kinds of salts exert the same effect on protein adsorption, the current data do not support the idea of a single Hofmeister effect ranging from kosmotropic to chaotropic ions. However, when kosmotropic or chaotropic ions are considered separately, a Hofmeister effect might exist, which needs to be clarified by future experiments. The reported data are in excellent agreement with an earlier study, where the effects of glycerol and urea on protein adsorption were examined. Thus, there seem to be general mechanisms how protein stabilizing and destabilizing cosolvents influence the process of protein adsorption at aqueous-solid interfaces.

7 Adsorption and aggregation of insulin at poly(acrylic acid) brushes

The study discussed in this Chapter is published in *Physical Chemistry Chemical Physics* [75]. The results obtained by ATR-FTIR spectroscopy were performed and analyzed by Dr. Christian Reichhart [213].

7.1 Summary

A planar poly(acrylic acid) (PAA) brush provides an unusual substrate for the unspecific immobilization of proteins on material surfaces. At neutral pH-values, proteins adsorb at a PAA brush when the ionic strength of the protein solution is low. In contrast, raising the ionic strength to a few 100 mM transforms a PAA brush into a rather protein-resistant surface coating. Moreover, a PAA brush represents a mild environment for adsorbed proteins which preserves their secondary structure and biological activity. In this study, we focus on the biocompatibility of a PAA brush with an insulin solution. Insulin can form amyloid fibrils, which may also be triggered by interfaces. Using neutron reflectometry and attenuated total reflection-Fourier transform infrared (ATR-FTIR) spectroscopy, the effects of pD-value, ionic strength, and glycerol concentration on the density profile and the secondary structure of adsorbed insulin molecules at a PAA brush have been studied. At pD 7, insulin adsorbs at a PAA brush despite its negative net charge. As has been found for other proteins in earlier studies, increasing the ionic strength of the insulin solution to 500 mM decreases the amount of adsorbed insulin drastically. In contrast, at pD 2, addition of salt to the insulin solution induces a thick insulin adsorbate at a PAA brush suggesting both protein-brush and protein-protein interactions, i. e., insulin adsorption and aggregation to be effective. However, in the presence of 2 M glycerol, insulin adsorption is largely suppressed. Furthermore, no major alterations of the secondary structure of insulin can be detected by ATR-FTIR spectroscopy under all conditions studied. Hence, the performed experiments do not provide any evidence for the formation of insulin amyloid structures qualifying a PAA brush as a potential biocompatible material coating for insulin.

7.2 Introduction

The natural function of insulin is to lower the level of glucose in the blood. Lacking insulin can cause diabetes mellitus type 1, which is usually treated by a lifelong medication with insulin injections. On the other hand, insulin is often used as a model protein to study the misfolding of proteins and the formation of amyloid fibrils. There is a series of diseases which are associated with the formation of amyloid fibrils, such as diabetes mellitus type 2, Creutzfeldt-Jakob and Alzheimer's disease [62, 74, 286]. Although insulin does not form amyloid fibrils in vivo, this process can be triggered easily in vitro by lowering the pH-value and raising the temperature, by adding organic solvents, or by agitation of insulin solutions in the presence of hydrophobic surfaces [29, 128, 179, 246]. These activating conditions represent a severe issue in the production, storage, and handling of insulin. In a series of studies, distinct aggregation pathways of insulin are discribed ending up in different amyloid fibril morphologies [65, 108, 247]. Generally, by lowering the pH-value insulin, hexamers are broken up into dimers and monomers [287]. Raising the temperature leads to a destabilization of the native conformation of insulin molecules, which favors the formation of amyloid structures rich in β-sheet contents. Furthermore, adding salt to an insulin solution shields the electrostatic repulsion of the positively charged insulin molecules at low pH-values, thereby facilitating their aggregation.

Coating a material surface with a poly(acrylic acid) (PAA) brush provides an interesting tool to control the unspecific adsorption of proteins. A PAA brush consists of PAA chains which are densely grafted to a solid support [18, 293] or to a colloidal sphere, as sketched in Figure 7.1. When the ionic strength of the protein solution is low, protein molecules adsorb at a PAA brush at neutral pH-values, even if they are carrying a negative net charge, such as bovine serum albumin or α-lactalbumin [102, 105, 294]. The protein molecules deeply penetrate the PAA brush and show a maximum packing density where the density of the PAA chains is highest [105, 222]. Thus, adsorption is driven by protein-PAA interactions only. Remarkably, by increasing the ionic strength of a protein solution to a few 100 mM, the protein molecules desorb from the PAA brush, which becomes largely protein resistant [102, 294]. It has been argued that this salt effect is a direct evidence for a release of counterions as driving force for protein adsorption at a PAA brush [293]. Moreover, proteins that are incorporated in a PAA brush do not show major changes of their secondary structures [214, 291] and maintain their biological activity to a high degree [92, 215].

In this study, we analyze the biocompatibility of a PAA brush with insulin solutions. It has been reported that amyloid fibril formation can be observed in insulin solutions which are in contact with a hydrophobic surface, such as that of Teflon or air [246]. Thus, it is of great interest, if the biocompatibility of a PAA brush, as found so far for a series of proteins, also fully applies to insulin. First experimental investigations have already shown that insulin, when adsorbed at a PAA brush, does not form amyloid fibrils at pD 2 and 60 °C, where fibrillation is triggered in solution [214]. However, as outlined above, an increased ionic strength also favors amyloid fibril formation of insulin in acidic solutions. Therefore, we have performed extended experiments,

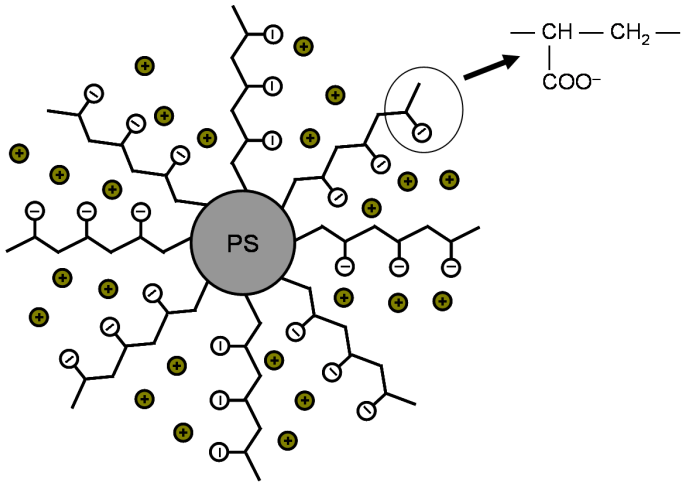

Figure 7.1: Sketch of a spherical polyelectrolyte brush. Long linear poly(acrylic acid) chains are grafted to a colloidal poly(styrene) sphere [294].

in which the pD-value and the ionic strength are varied. Using neutron reflectometry (NR), we present for the first time the effects of these parameters on the scattering length density profile of insulin at a PAA brush. Indeed, as shown in this study, a very thick insulin adsorbate is formed at a PAA brush at pD 2 and 500 mM NaCl concentration, suggesting aggregation of insulin molecules at the interface. In order to examine the nature of this adsorbate, the secondary structure of insulin has been estimated by applying attenuated total reflection-Fourier transform infrared (ATR-FTIR) spectroscopy. In addition, we have chosen glycerol as a cosolvent of the insulin solution, because it may be used as a probe for the kind of insulin aggregation taking place at a PAA brush. Glycerol is known to be inefficient in dissolving insulin amyloid fibrils [29]. On the other hand, it is a potent agent to suppress protein adsorbates at interfaces [143]. In this way, a normal protein adsorbate may be distinguished from protein amyloid fibrils. As will be shown in this study, all experimental results gathered so far do not provide any evidence that a PAA brush might induce the formation of insulin amyloid fibrils.

7.3 Experimental section

7.3.1 Sample solution preparation

Bovine insulin was purchased from Sigma (I5500) and was used without further purification. An insulin stock solution was prepared in D_2O (pD 2.4) at a concentration of 1 mg mL^{-1}. Insulin sample solutions with a concentration of 0.1 mg mL^{-1} were prepared by tenfold dilution of the stock solution using D_2O-buffer solutions adjusted to pD 2.4 or 7.4. A pD-value of 2.4 was achieved by adding concentrated HCl solution. A pD-value of 7.4 was buffered with 10 mM

morpholinopropanesulfonic acid (MOPS). A pD-value was measured by using a conventional pH-electrode, calibrated in H_2O, and by adding 0.4 to the pH-meter reading (pD = reading + 0.4) [47].

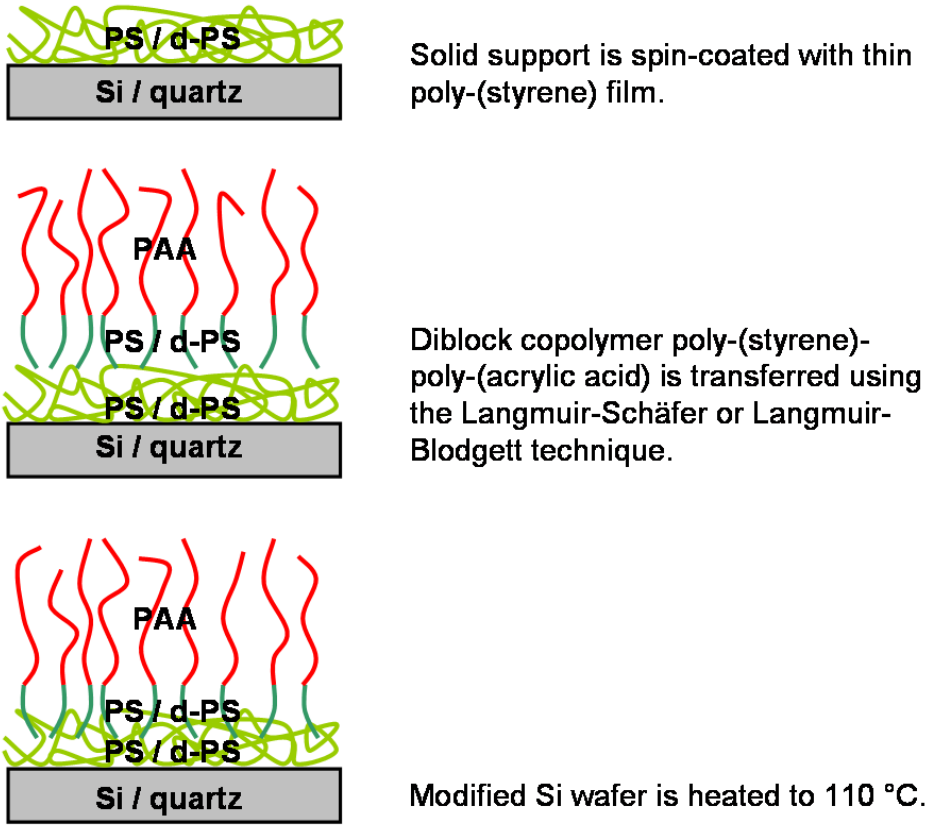

Figure 7.2: Preparation of a planar polyelectrolyte brush, according to [49]. At first, a silicon wafer is coated with a poly(styrene) film. Then, the diblock copolymer poly(styrene)-poly(acrylic acid) is transferred to the PS-coated silicon block by the Langmuir-Schaeffer technique. In the end, the wafer was heated to 110 °C for 10 min, in order to create a stable and irreversibly fixed poly(acrylic acid) brush.

7.3.2 PAA brush preparation

The preparation of a planar poly(acrylic acid) (PAA) brush was performed according to the literature [49] with some modifications (cf. Figure 7.2). Silicon blocks were used as substrates in the NR and the ATR-FTIR experiments. They were cleaned in a 1 : 1 : 4 mixture of NH_3 (30 %), H_2O_2 (30 %), and H_2O followed by intensive rinsing with pure water. For ATR-FTIR studies,

a thin film of poly(styrene) (PS) from Aldrich (Taufkirchen, Germany) with a molar weight of 44000 g mol^{-1} was deposited on one of the large, polished sides of a silicon block by spin-coating using a 6 mg mL^{-1} polymer solution in toluene (spin-coater KW-4A from Chemat Technology). A film thickness in the range of $250 - 300$ Å is obtained in this way [103]. Five milligrams of the diblock copolymer poly-(styrene)-poly(acrylic acid) (PSPAA) from Polymer Source (Montreal, Canada) was dissolved in 3 mL 1,4-dioxane and 2 mL toluene. The copolymer consisted of 32 styrene and 278 acrylic acid monomers. The PSPAA solution was spread on the surface of a water subphase in a Langmuir trough (model 611D from Nima) to generate a PSPAA monolayer with a packing density of about 0.1 chains per nm^2. The pH-value of the water subphase was lowered to about 4 with concentrated HCl solution to reduce the charge of the copolymer and to stabilize the copolymer monolayer on the water surface. For neutron reflectometry studies, perdeuterated poly(styrene) (dPS) from Polymer Standards Service (Mainz, Germany) was deposited on a silicon block by spin-coating using a 6 mg mL^{-1} polymer solution in toluene. Instead of PSPAA, the deuterated diblock copolymer poly(styrene-d8)-poly(acrylic acid) (dPSPAA) from Polymer Source (Montreal, Canada) was used. This copolymer consisted of 49 styrene-d8 and 222 acrylic acid monomers (mean values). For both applied techniques, ATR-FTIR and NR, the copolymer was transferred to the PS- or dPS-coated silicon block applying the Langmuir-Schäfer technique. The silicon surface was tilted by a few degrees relative to the copolymer monolayer on the subphase letting the liquid contact line move slowly across the PS- or dPS-film upon lowering and lifting the silicon block. This results in a very homogeneous transfer of the copolymer. A transfer ratio of about 1 was observed. Finally, the modified silicon blocks were heated to 110 °C for 10 min, which leads to a diffusion of the PS or dPS chains of the copolymer into the PS or dPS film, thereby creating a stable and irreversibly fixed PAA brush.

7.3.3 Neutron reflectometry

The neutron reflectivity measurements were performed at the Helmholtz-Zentrum Berlin (Germany) using the instrument V6 [167], as illustrated in Section 4.1.1.

7.3.4 ATR-FTIR spectroscopy

ATR-FTIR spectra were recorded with the Nicolet 6700 Fourier transform infrared spectrometer from Thermo Fisher Scientific at a spectral resolution of 2 cm^{-1}. Spectra are derived from 128 successive interferograms. The used ATR accessory includes a liquid jacketed flow cell with a silicon crystal as internal reflection element (Pike Technologies, Madison, Wisconsin, USA). The silicon crystal has a size of $80 \times 10 \times 4$ mm^3 and is of trapezoidal shape with 45° bevel angles at each end of the crystal. It is coated with a PAA brush on the largest side (80×10 mm^2). The flow cell was rinsed with buffer or sample solutions using a syringe or a peristaltic pump. Temperature was kept constant at 23.5 °C. At the beginning of each series of measurements, a background spectrum of buffer solution was recorded that was subtracted from all following measured spectra.

GRAMS software (Thermo Fisher Scientific) was used for spectrum processing and peak-fitting. In this peak-fitting, the amide I'-band (in D_2O) is decomposed into six sub-bands of Gauss-Lorentz type (variable ratio). Initial peak positions were determined from second derivative spectra and by Fourier self-deconvolution (FSD). Only spectra showing similar peak positions applying these two methods were used for peak-fitting. Peak positions were not allowed to move further than 2 cm^{-1} during peak-fitting, as recommended in literature [238]. The deviations between the measured amide I'-bands and the fitted curves are very small.

7.4 Results and discussion

7.4.1 Neutron reflectometry

In Figure 7.3a, a neutron reflectivity curve of a silicon-dPS-PAA-D_2O interface is shown. Since dPS and D_2O are characterized by approximately the same scattering length density (SLD), the observed Kiessig fringes indicate the presence of the non-deuterated PAA chains. A further neutron reflectivity curve has been measured after rinsing and filling the sample cell with a 0.1 mg mL^{-1} insulin solution (pD 7) to probe the adsorption of insulin at the PAA brush (Figure 7.3a). Finally, a 0.1 mg mL^{-1} insulin solution containing 500 mM NaCl was brought into contact with the PAA brush, and a third neutron reflectivity curve was measured (Figure 7.3a). Under this condition of elevated ionic strength, insulin is expected to desorb from the PAA brush, as has been observed for other proteins [102, 105].

In order to analyze these data, layer models for the interfacial structures have been used. The first layer represents the dPS film, which is directly deposited on the silicon wafer. The density profile of the PAA chains, which are grafted to the dPS film, has been modelled by additional layers. In the fitting process, some structure parameters were fixed to known values. The scattering length densities of the Si wafer, the dPS film, and the solution (D_2O) were set to $2.07 \cdot 10^{-6}$ $Å^{-2}$, $6.42 \cdot 10^{-6}$ $Å^{-2}$, and $6.37 \cdot 10^{-6}$ $Å^{-2}$, respectively [3]. In addition, the thickness of the layers representing the PAA brush was fixed to 60 Å, and the roughness of the layers was fixed at 7 Å. In some cases it has been needed to divide a 60 Å layer into two 30 Å layers to optimize the fit of the experimental data. During the fitting process, the roughness of the silicon wafer, the thickness of the dPS film, and the scattering length densities of the PAA layers were varied. The data fits obtained in this way are shown as solid lines in Figure 7.3a, and the corresponding scattering length density profiles are plotted in Figure 7.3b.

From the SLD profiles, it can be seen that insulin is deeply penetrating the PAA brush upon adsorption (Figure 7.3b). A maximum insulin density is found at $z = 250 - 400$ Å, where the PAA chain density is highest. It is noted that the isoelectric point of insulin is reported at pH 5.3 [290]. Thus, at pD 7, insulin adsorbs with a negative net charge and interacts with the negatively charged PAA chains. In the presence of 500 mM NaCl, the SLD profile clearly indicates desorption of insulin from the PAA brush (Figure 7.3b). This salt effect can be traced back to a release of counterions as the main driving force for protein adsorption at a PAA brush

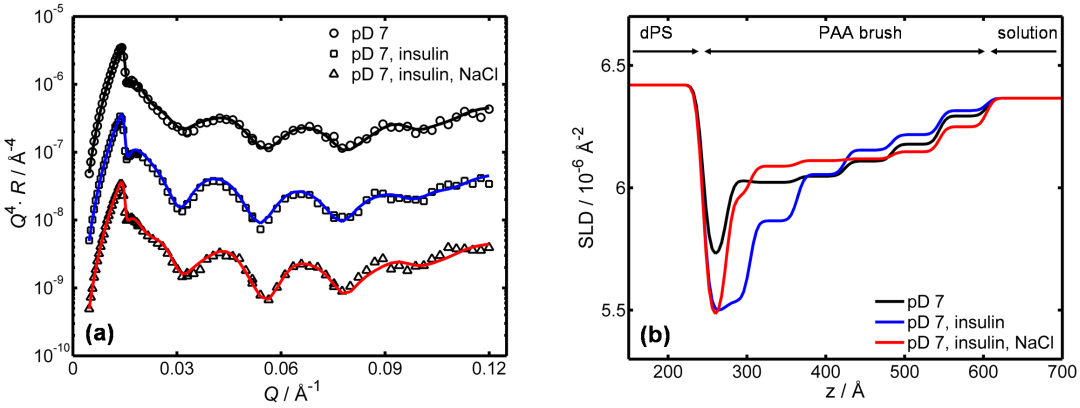

Figure 7.3: (a) Neutron reflectivity curves of a Si-dPS-PAA-solution interface [75]. Experimental data (symbols) have been obtained with a pure D_2O-buffer solution at pD 7, a solution containing 0.1 mg mL^{-1} insulin, and a solution containing insulin with 500 mM NaCl, as indicated in the figure legend. Solid lines are fits based on layer models for the interfacial structures. (b) Scattering length density (SLD) profiles as derived from the neutron reflectivity fits shown in Figure 7.3a [75]. z is the distance from the Si surface. At z = 200 Å, the SLD indicates the dPS film. For z > 600 Å, the profiles reach the solution with an SLD of $6.37{\cdot}10^{-6}$ $Å^{-2}$ corresponding to D_2O. Upon addition of 500 mM NaCl to the insulin solution, insulin desorbs from the PAA brush.

under neutral pH-value conditions. A detailed explanation and discussion of this driving force can be found in a series of papers [104, 152, 293].

However, at about z = 400 Å, the SLD profiles with and without adsorbed insulin cross each other, indicating some rearrangement of PAA chains when they interact with adsorbing insulin molecules (Figure 7.3b). Unfortunately, due to this rearrangement, no volume fraction profile of adsorbed insulin can be calculated, as has been done for α-lactalbumin [105]. However, it is possible to calculate the total amount of adsorbed insulin. To do so, the SLD profile with adsorbed protein is decomposed into contributions from the insulin molecules (ins), the PAA chains (PAA), and the solvent (sol):

$$\mathrm{SLD}(z) = \rho_{\mathrm{ins}}\phi_{\mathrm{ins}}(z) + \rho_{\mathrm{PAA}}\phi_{\mathrm{PAA}}(z) + \rho_{\mathrm{sol}}\left[1 - \phi_{\mathrm{ins}}(z) - \phi_{\mathrm{PAA}}(z)\right]. \tag{7.1}$$

ρ_i and ϕ_i are the scattering length density and the volume fraction of component i. In the absence of adsorbed insulin, this equation becomes:

$$\mathrm{SLD}'(z) = \rho_{\mathrm{PAA}}\phi'_{\mathrm{PAA}}(z) + \rho_{\mathrm{sol}}\left[1 - \phi'_{\mathrm{PAA}}(z)\right], \tag{7.2}$$

where the prime ($'$) indicates altered values due to a PAA rearrangement. Since the number of

PAA chains remains constant upon insulin adsorption, we may write:

$$\int [\phi_{\mathrm{PAA}}(z) - \phi'_{\mathrm{PAA}}(z)]\,\mathrm{d}z = 0. \tag{7.3}$$

The integration is performed over the z-range of the PAA brush. Thus, if we integrate over the difference of the scattering length density profiles obtained in the presence and the absence of insulin, the PAA contribution is cancelled, and the adsorbed mass of insulin per surface area, Γ, can be calculated:

$$\int \left[\mathrm{SLD}(z) - \mathrm{SLD}'(z)\right] \mathrm{d}z = [\rho_{\mathrm{ins}} - \rho_{\mathrm{sol}}] \int \phi_{\mathrm{ins}}(z)\mathrm{d}z, \tag{7.4}$$

$$\Gamma = \frac{1}{v} \int \phi_{\mathrm{ins}}(z)\mathrm{d}z, \tag{7.5}$$

where v is the specific volume of insulin. Using v= 0.717 cm^3 g^{-1} [248], ρ_{ins} = 3.27·10^{-6} Å^{-2}, and ρ_{sol} = 6.37·10^{-6} Å^{-2}, the adsorbed masses corresponding to the profiles shown in Figure 7.3b have been determined according to Equation (7.5). ρ_{ins} has been calculated using the primary sequence of insulin [250] and neutron scattering lengths published by the NIST [3].

Table 7.1: Salt effect on the insulin binding capacity of a PAA brush [75].[a]

	Γ / mg m^{-2} no NaCl	Γ / mg m^{-2} 500 mM NaCL
pD 7	1.1	0.3
pD 2	4.0	20
pD 2, 2 M glycerol	2.0	3.9

[a] Insulin concentration in solution is 0.1 mg mL^{-1}.

As can be seen from Table 7.1, 1.1 mg m^{-2} of insulin adsorbs at a PAA brush at pD 7 from a 0.1 mg mL^{-1} insulin solution. When 500 mM NaCl is added to the insulin solution, insulin desorbs from this PAA brush into the insulin solution. Only 0.3 mg m^{-2} of insulin remain adsorbed (Table 7.1). In this way, the well-known salt effect on the protein binding capacity of a PAA brush can be confirmed using insulin.

Since insulin can form amyloid fibrils in solution at pH 2 and 60 °C [128, 248], we have also analyzed the adsorption of insulin at a PAA brush under acidic conditions. In an earlier study, no amyloid fibril formation of insulin could be detected at a PAA brush at pD 2 and 60 °C [214]. However, an elevated ionic strength facilitates the aggregation of positively charged insulin molecules and increases the rate of nucleation substantially [29]. Therefore, we also present data on the effect of salt on adsorbed insulin at pD 2. In Figure 7.4a, neutron reflectivities of a planar PAA brush are shown that have been measured at pD 2 with solutions containing pure buffer, 0.1 mg mL^{-1} insulin, and 0.1 mg mL^{-1} insulin with 500 mM NaCl. Apparently, these data curves look much different to those obtained at pD 7 (Figure 7.3a). In particular, when NaCl

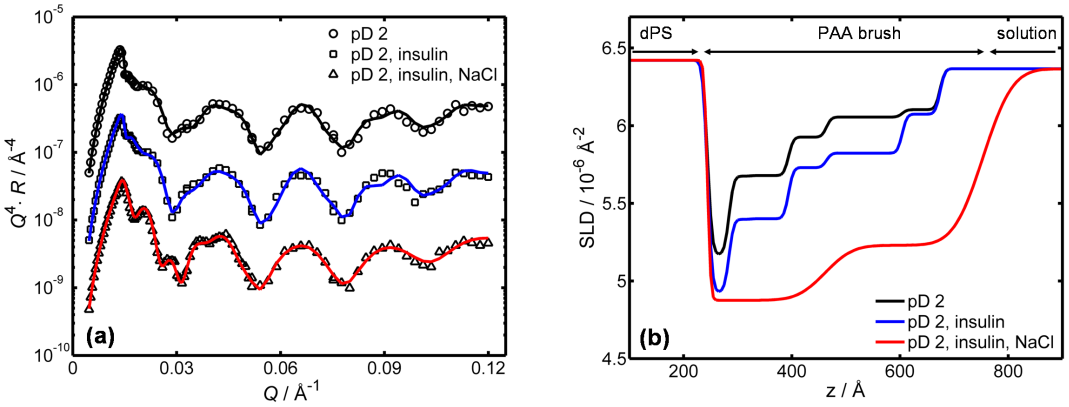

Figure 7.4: (a) Neutron reflectivity curves of a Si-dPS-PAA-solution interface [75]. Experimental data (symbols) have been obtained with a pure D_2O solution at pD 2, a solution containing 0.1 mg mL^{-1} insulin, and a solution containing insulin with 500 mM NaCl, as indicated in the figure legend. Solid lines are fits based on layer models for the interfacial structures. (b) Scattering length density (SLD) profiles as derived from the neutron reflectivity fits shown in Figure 7.4a [75]. z is the distance from the Si surface. At z = 200 Å, the SLD indicates the dPS film. For z > 700 Å, the profiles reach the solution with an SLD of $6.37 \cdot 10^{-6}$ $Å^{-2}$ corresponding to D_2O. Upon addition of NaCl to the insulin solution, a drastic increase of the adsorbed amount of insulin is observed.

is added to the insulin solution at pD 2, Kiessig fringes with smaller Q-spacing can be observed indicating a significantly stronger adsorption of insulin at a PAA brush. The neutron reflectivity curves measured at pD 2 have been analyzed in the same way as those at pD 7 (see above), except that the reflectivity curve measured with 500 mM could be modelled using only two thick layers. Scattering length density profiles extracted from this analysis are shown in Figure 7.4b, and the amounts of adsorbed insulin are also given in Table 7.1.

At pD 2, the PAA chains, which have a pK_a-value of about 4.5 [29, 88], are completely neutralized. Therefore, the above-mentioned counterion release can no longer act as driving force for protein adsorption at a PAA brush at pD 2. However, strong adsorption of insulin is observed (blue curve in Figure 7.4b). The scattering length density profile found with an insulin solution deviates from that found with a pure buffer solution over the whole z-range of the PAA brush. Thus, insulin again penetrates the PAA brush and preferentially interacts with the PAA chains even at pD 2. It is likely that hydrogen bonds and van der Waals interactions are responsible for this insulin binding. Remarkably, when 500 mM NaCl is added to the insulin solution, the adsorbed amount is increasing from 4.0 to 20 mg m^{-2} (Table 7.1). From the inspection of the corresponding scattering length density profile (red curve in Figure 7.4b), it can be concluded that the insulin adsorbate formed at pD 2 with 500 mM NaCl is extending further into the solution than the PAA chains. Therefore, attractive protein-protein interactions

must exist that add to protein-PAA interactions. I.e., at pD 2 and 500 mM salt concentration, adsorption and aggregation of insulin molecules take place at a PAA brush.

The thick insulin adsorbate formed at pD 2 in the presence of salt (Figure 7.4b) might suggest the existence of amyloid fibrils. In order to study the nature of this adsorbate, insulin adsorption experiments were also carried out with 2 M glycerol as cosolvent. Glycerol is known to be inefficient in dissolving insulin amyloid fibrils [29]. Rather, acceleration of the conformational transition required for amyloid formation was observed with amyloid-β-peptide solutions containing 1.2 M glycerol [299]. On the other hand, glycerol substantially reduces the tendency of proteins to adsorb at a silica-water interface [143]. Glycerol is a protein stabilizing agent that preferentially interacts with water. With glycerol as cosolvent, proteins become strongly hydrated, and their native conformation is stabilized against unfolding [84, 261]. Probably, a preferential hydration and a conformational stabilization of protein molecules disfavor protein adsorption, because this process requires some degree of protein dehydration and conformational change [50, 143]. In this way, glycerol can be used as a sensitive chemical probe for the kind of insulin aggregation, i.e., amorphous or amyloidal, going on at a PAA brush. If insulin would form amyloid fibrils at a PAA brush, one would not expect glycerol to inhibit this process. If insulin forms an amorphous adsorbate layer, 2 M glycerol should lower the degree of adsorption significantly.

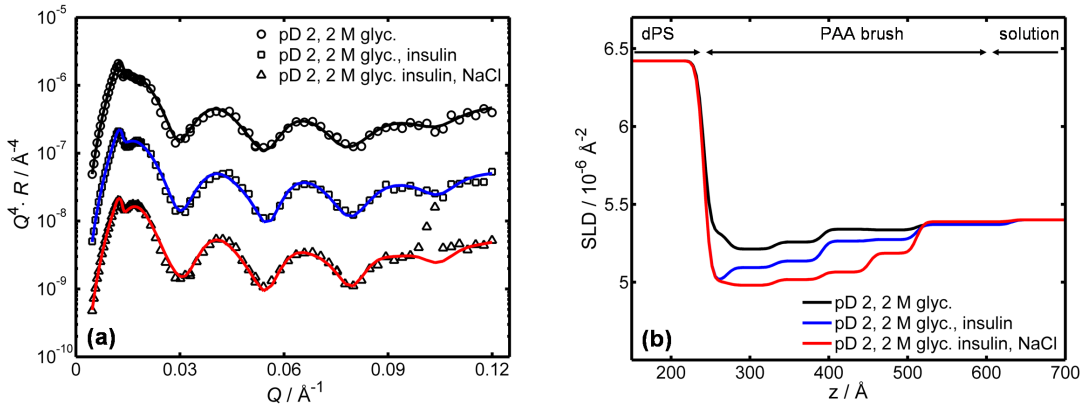

Figure 7.5: (a) Neutron reflectivity curves of a Si-dPS-PAA-solution interface [75]. Experimental data (symbols) have been obtained with D_2O containing 2 M glycerol at pD 2 as the solvent, with 0.1 mg mL^{-1} insulin, and with 0.1 mg mL^{-1} insulin and 500 mM NaCl, as indicated in the figure legend. Solid lines are fits based on layer models for the interfacial structures. (b) Scattering length density (SLD) profiles as derived from the neutron reflectivity fits shown in Figure 7.5a [75]. z is the distance from the Si surface. At z = 200 Å, the SLD indicates the dPS film. For z > 600 Å, the profiles reach the solution with an SLD of $5.4{\cdot}10^{-6}$ $Å^{-2}$ corresponding to D_2O with 2 M glycerol.

In Figure 7.5a, neutron reflectivity curves probing the adsorption of insulin at a PAA brush

in the presence of 2 M glycerol are shown. For data fitting, a reduced scattering length density of the solvent resulting from the exchangeable protons of the glycerol molecules had to be taken into account. Similarly, the scattering length density of insulin is reduced, which is needed to calculate the adsorbed mass per unit area. Values of $\rho_{\mathrm{ins}} = 3.1910^{-6}$ Å^{-2} and $\rho_{\mathrm{sol}} = 5.410^{-6}$ Å^{-2} have been used. The obtained scattering length density profiles are shown in Figure 7.5b, and the adsorbed amounts of insulin are given also in Table 7.1.

Remarkably, by adding 2 M glycerol to the insulin solution at pD 2, a drastic reduction of the adsorbed amount of insulin at a PAA brush can be found. At low ionic strength, 2.0 mg m^{-2} of insulin are adsorbed, whereas only 3.9 mg m^{-2} of insulin are adsorbed after adding 500 mM NaCl to the insulin solution (Table 7.1). Apparently, the previously observed inhibition effect of glycerol on protein adsorption at a silica-water interface can be confirmed for insulin adsorption at a neutral PAA brush. This result strongly suggests that the thick insulin adsorbate found at pD 2 in the presence of salt (Figure 7.4b) has a non-amyloidal structure. Adsorbed insulin molecules seem to interact weakly with each other in an amorphous way. This finding is corroborated by ATR-FTIR data which are presented in the following.

7.4.2 ATR-FTIR spectroscopy

The secondary structure of insulin adsorbed at a PAA brush has been estimated by ATR-FTIR spectroscopy. The so-called amide I-band in H_2O or amide I'-band in D_2O, located at $1600 - 1700$ cm^{-1}, can mainly be associated with the carbonyl vibration of the peptide bonds. The exact wavenumber of this carbonyl vibration depends on the secondary structure the peptide bond is involved in. Therefore, a decomposition of the amide I-band yields sub-bands which are representing the different secondary structure elements [34]. Assuming the transition dipole moments to be similar, the areas of the obtained sub-bands provide an estimate for the fractions of the secondary structure elements. In particular, the formation of amyloid fibrils is clearly seen as a huge increase in the β-sheet fraction at around 1629 cm^{-1} with values of about $60 - 70$ % in the case of insulin [108, 214].

In a previous publication, it has been already reported on the secondary structures of insulin in solution and adsorbed at a PAA brush at both pD-values 2 and 7 [214]. The main conclusion of these experiments can be summarized like this: At pD 7, all fractions of secondary structure elements remain the same upon adsorption at a PAA brush. The fraction of β-sheets is about 22 %. At pD 2, there is a small increase in β-sheet contents when insulin adsorbs at a PAA brush. However, this increase is too small to indicate the presence of amyloid fibrils.

In Figure 7.6, the amide I'-band of insulin ATR-FTIR spectra are shown. These spectra reflect the effects of NaCl and glycerol on the secondary structure of insulin that is adsorbed at a PAA brush at pD 2, in order to get further insight into the interfacial structures analyzed by NR (Figures 7.4b and 7.5b). Apparently, no major changes in the shape of the amide I'-band are detectable. In the presence of glycerol, the band is slightly shifted to larger wavenumbers. A

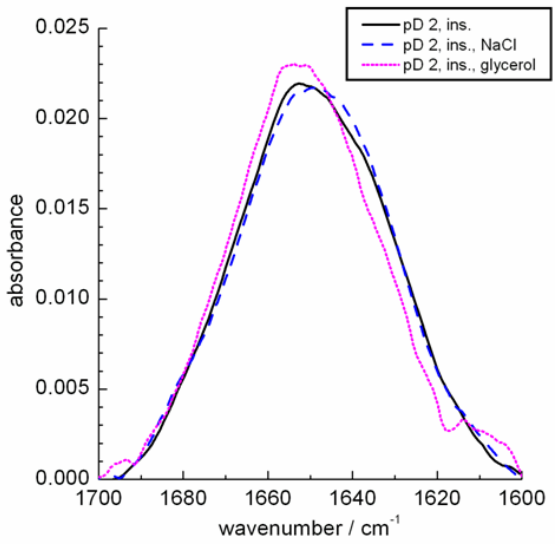

Figure 7.6: ATR-FTIR spectra of insulin adsorbed at a PAA brush (0.1 mg mL^{-1} insulin in solution, pD 2) showing the amide I'-band [75]. The shape of this band is sensitive to the fractions of secondary structure elements. The spectra are normalized to a band area of 1 cm^{-1}. NaCl has been added to the insulin solution at a concentration of 500 mM, glycerol at a concentration of 2 M, as indicated in the figure legend.

Table 7.2: Fractions of secondary structure elements of insulin in solution (2 mg mL^{-1}, pD 2) and adsorbed at a PAA brush (0.1 mg mL^{-1}, pD 2) [75].[a]

	turn 1681 cm^{-1}[c]	turn 1667 cm^{-1}	α-helix 1653 cm^{-1}	unordered 1641 cm^{-1}	β-sheet 1629 cm^{-1}	baseline[b] 1610 cm^{-1}
in solution	8	19	30	22	21	2
adsorbed	5	20	30	21	24	2
adsorbed, 500 mM NaCl	4	16	30	26	21	4
adsorbed, 2 M glycerol	6	23	33	20	15	4

[a] Fractions are given in percent with an error of ±2 %.
[b] Sub-band used for minor baseline correction.
[c] Wavenumbers used as starting values for band fitting.

quantitative analysis of the secondary structure of insulin, as deduced from a decomposition of the amide I'-band, is listed in Table 7.2.

As can be seen from Table 7.2, the fractions of secondary structure elements of insulin are very similar under the various conditions studied. An increase in β-sheet content upon adsorption at a PAA brush at pD 2, as reported earlier [214], is hardly detectable. This might be attributed to the use of a different insulin batch and/or to minor differences in the experimental conditions,

such as temperature, pD-value, or PAA brush grafting density. However, from an inspection of the data set of Table 7.2, a major increase of the β-sheet fraction of insulin, when it is adsorbed at a PAA brush at pD 2, can clearly be ruled out. In particular, the huge increase in the adsorbed amount of insulin by adding 500 mM NaCl at pD 2 (Figure 7.4b) is definitely not associated with the formation of amyloid fibrils. The thick adsorbate seems to exhibit an amorphous packing of insulin molecules. Furthermore, in the presence of 2 M glycerol, a decrease of the β-sheet fraction of insulin at a PAA brush can be observed. This might suggest a shift of the dimer-monomer equilibrium to the monomer side, since dimers are formed by intermolecular β-sheets [287]. This would be consistent with the effect of ethanol reported in the literature [29, 64]. Ethanol shifts the dimer-monomer equilibrium of insulin at pD 2 to the monomer side and breaks intermolecular β-sheets.

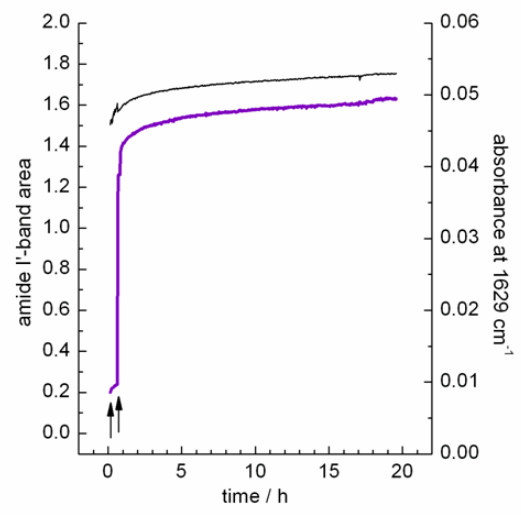

Figure 7.7: Long-term behavior of insulin adsorbed at a PAA brush at pD 2 [75]. The lower thick curve shows the total absorbance (area) of the amide I'-band. The upper thin curve indicates the absorbance at 1629 cm^{-1} which is normalized to the total absorbance. The ATR sample cell was filled with insulin solution (0.1 mg mL^{-1}, pD 2, left arrow) and insulin solution (0.1 mg mL^{-1}, pD 2) that contains 500 mM NaCl (right arrow).

Finally, the long-term behavior of insulin at a PAA brush at pD 2 in the presence of 500 mM NaCl has been studied using ATR-FTIR spectroscopy. In Figure 7.7, the total absorbance of the insulin amide I'-band is plotted as a function of time. The total absorbance is a measure for the adsorbed amount of insulin at the PAA brush. In the absence of salt, an initial absorbance of about 0.2 is observed. After rinsing the ATR sample cell with an insulin solution that contains 500 mM NaCl, the total absorbance is increasing to 1.5. From repeated measurements, the total absorbance has been found to increase by a factor of 6$\pm$1. This increase is in excellent agreement with the mass increase detected by NR (Table 7.1). The absorbance at 1629 cm^{-1}, which has been normalized to the amide I'-band area, is also plotted in Figure 7.7. The absorbance at this

wavenumber is sensitive to the fraction of β-sheets, which are the main component of insulin amyloid fibrils. Apparently, this normalized absorbance is only slightly increasing with time, suggesting a minor increase in β-sheet fraction only. Thus, the thick insulin adsorbate formed at pD 2 in the presence of 500 mM NaCl is not consisting of amyloid fibrils, and no such fibrils are formed over at least one day.

7.5 Conclusion

Aspects of the biocompatibility of a PAA brush have been demonstrated in a series of earlier studies. It has been shown that at neutral pH-values proteins do not change their secondary structure, i.e., they do not denature [214, 291]. Moreover, the activity of several enzymes has been found to be reasonably preserved [92, 215] considering the diminished reorientational mobility of proteins inside a PAA brush [105]. However, besides unfolding, some proteins misfold into amyloid fibrils which are associated with several diseases. Insulin is a prominent example which may form amyloid fibrils at low pH-values and elevated temperatures, in the presence of organic solvents, or in contact with hydrophobic interfaces [29, 128, 179, 246]. In this view, we have analyzed, if a PAA brush triggers the formation of insulin amyloid fibrils. So far, all performed experiments do not provide any evidence that this is the case. Insulin that is adsorbed at a PAA brush remains in a native-like conformation at low pH-values, elevated temperatures, increased ionic strength and in the presence of glycerol. The results of this study add to the list of properties that qualify a PAA brush as a biocompatible material coating.

8 Short- and long-range forces affect the interfacial structure of adsorbed protein films

The results presented in this Chapter arose from a tight cooperation with Hendrik Hähl and Prof. Dr. Karin Jacobs (Universität des Saarlandes, Saarbrücken, Germany). While experimental design and sample preparation were carried out by Hendrik Hähl, data reduction and data analysis were part of this work. Interpretation of the data was a collaborative work. As this project is still in progress and simulation studies are envisaged, only a brief interpretation of the obtained results is given here.

8.1 Summary

In many studies, biofilm formation at interfaces is explained by inter-protein and protein-surface interactions and the hydrophobic effect as main driving forces. However, long-range van der Waals dispersion interactions between atoms of proteins and surfaces are always present. In this study, a set of four different substrates is used to separate contributions of short- and long-range forces on the formation of adsorbed films of three different proteins. It is shown that long-range forces can exert subtle effects on the degree of protein adsorption. Moreover, depending on the surface chemistry, rather different interfacial structures can be formed: While thick, hydrated adsorbed layers, in which proteins retain most of their native conformation, are favored on hydrophilic surfaces, the presence of hydrophobic surfaces can cause denaturation of adsorbed proteins, resulting in thin adsorbed layers with high protein packing densities.

8.2 Introduction

First studies have shown that the enzymatic activity of adsorbed proteins [169], their orientation on the surface [56] and the kinetics of the adsorption process [20, 204] are strongly influenced by the substrate. Moreover, slight changes in the subsurface composition of substrates can affect adsorption dynamics. In this study, effects of changing the subsurface composition on the structure of adsorbed protein films are investigated.

Protein adsorption is sensitive to quite a number of parameters, such as pH value, ionic strength, temperature and protein concentration [50, 164, 277]. In most studies, the influence of the substrate on protein adsorption is described in terms of surface chemistry (that is, sign and value of surface charge as well as surface free energy) and interfacial roughness [164]. These properties are mainly related to the surface-nearest layer of atoms. However, van der Waals forces arising from the bulk substrate should not be neglected. Depending on the surface geometry, van der Waals forces can range over tens of nanometers [115, 176]. In this regard, it has been shown that van der Waals forces play a crucial role in the stability of thin polymer films [97, 237]. Furthermore, in contrast to pure Coulomb interactions, ions in aqueous solution cannot screen van der Waals forces. Hence, van der Waals forces should be a relevant driving force for the formation of adsorbed protein films.

Recently, effects of van der Waals forces on the adsorption kinetics of large, deformable proteins, such as α-amylase and bovine serum albumin (BSA), have been reported [204]. By using silicon wafers varying in silicon oxide thickness, long-range forces are affected, while the surface free energy is kept constant. As two types of adsorption kinetics could be distinguished, the influence of the subsurface composition of substrates is clearly demonstrated. Therefore, one might speculate that the interfacial structure of adsorbed protein films should also diversify (e.g., in protein content, film thickness, protein orientation or conformation) with different subsurface compositions. In order to explore the interfacial structure of adsorbed protein films in situ with angstrom resolution, X-ray reflectometry is applied here.

8.3 Experimental section

8.3.1 Materials and methods

Two different types of silicon wafers were used as substrates for protein adsorption: wafers with a native silicon oxide layer of 17 (3) Å (Wacker Siltronic AG, Burghausen, Germany) and wafers with a thermally grown amorphous silicon oxide layer with a thickness of 1510 (10) Å (Silchem, Freiberg, Germany), as characterized by ellipsometry. After the cleaning procedure, the wafers were hydrophilic with a water contact angle below 5° and were stored under water until usage.

In order to vary the surface chemistry of the substrates, both types of wafers were covered with a self-assembled monolayer (SAM) of octadecyltrichlorosilane (OTS, Sigma-Aldrich, Germany), using standard procedures [32, 282]. Wafers covered with OTS layers exhibit hydrophobic surfaces with water contact angles of 107° to 112° with a contact angle hysteresis of less than 5°. The surface chemistry of these types of substrates is analyzed in detail in earlier studies [20, 204]. In addition, the quality of the achieved hydrophobic layers was determined by X-ray reflectivity measurements (see below). The obtained values (cf. Table 8.1) agree well with literature [168, 260], indicating densely packed and homogeneous layers. OTS wafers were cleaned by sonication in ethanol and acetone before use.

Thus, a set of four different substrates was obtained, as illustrated in Figure 8.1: hydrophilic

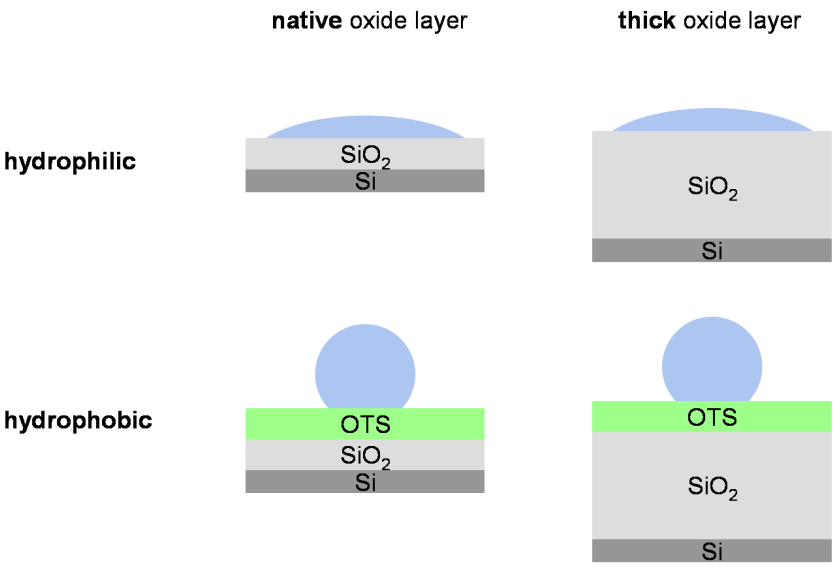

Figure 8.1: Sketch of the four different model substrates: hydrophilic and hydrophobic wafers (abbreviated as "phil" and "phob", respectively) with either a natively thin (called "N") or a thick (called "T") silicon oxide layer. Using this set of substrates, contributions of short- and long-range forces on biofilm formation at interfaces can be separated. The variation of the oxide layer thickness leads to different long-range forces, while short-range forces are changed between hydrophilic and hydrophobic surface chemistries.

and hydrophobic wafers (abbreviated as "phil" and "phob", respectively) with either a native, thin (called "N") or a thick, thermally grown (called "T") silicon oxide layer. ζ-potential measurements have shown that the difference in silicon oxide film thickness does not alter the surface charge of the substrates [20]. The isoelectric points of these surfaces are 1.8 for the hydrophilic and 3 for the hydrophobic surface. The roughness, as measured by atomic force microscopy in an $0.5 \times 0.5\,\mu m^2$ area, was below 2 Å for all types of wafers. This set of wafer types allows to separate the contribution of short- and long-range forces. Using the same surface chemistry (either phil or phob), but different silicon oxide layers, long-range forces arising from the different subsurface compostions are varied. On the other hand, varying surface chemistry (either on N or T substrates) changes short-range forces only, because van der Waals interactions are only marginally affected by molecularly thick OTS layers [118].

The proteins used in this study were α-amylase from human saliva (A0521), bovine serum albumin (BSA, A3059) and lysozyme from hen egg white (62971, all purchased from SigmaAldrich, Germany). The proteins were used as received without further treatment. Characteristics of the proteins are presented in Section 2.4.

α-amylase and BSA differ in their adsorption kinetics on thick compared to thin silicon oxide

wafers [20]. On thick silicon oxide wafers (phil and phob), the proteins showed Langmuir-like kinetics, whereas a 'stepped' kinetics with a distinct change in adsorption rate at low coverages was observed on thin silicon oxide wafers. Such a behavior was not recorded for lysozyme [204], which is gerenally regarded as a stiff protein [76, 163].

Proteins were dissolved in 10 mM phosphate buffer solution with a pH of 7 and an ionic strength of 20 mM. Moreover, an acetate buffer system at pH 4.7 and CAPS (3-(cyclohexylamino)-1-propanesulfonic acid) adjusted with NaOH to pH 11 were used to realize stable solution pH values at the isoelectric points of BSA and lysozyme, respectively. Appropriate amounts of NaCl were added to obtain the same ionic strength as for the phosphate buffer solutions.

The X-ray scattering experiments were conducted at the surface diffractometer of beamline BL9 at the synchrotron light source DELTA (Dortmund, Germany) using the high-energy scattering set-up [194], as described in Section 4.1.2.

The specially designed Teflon sample cell was equipped with a flow system containing a syringe pump and a switch with a sample loop (Rheodyne Manual Sample Injector) prior to the cell. Thus, protein solutions could be injected into the sample cell at a selected time, allowing for a minimum disturbance of the system. The final protein concentration in the sample cell was 0.1 mg/mL. Before analyzing the adsorbate structure, reflectivity curves of each new wafer were taken. After adding protein solution, the system was equilibrated for at least 1 h.

8.3.2 Analysis of the X-ray reflectivity data

Data reduction and data analysis are described in Section 3.8. The interfacial structure of the samples is described by a layer model: (Si / SiO_2 / solution) at hydrophilic wafers and (Si / SiO_2 / OTS head / OTS tail / solution) at hydrophobic wafers. For the hydrophobic substrates, two layers are introduced to the model representing the head and tail of the OTS film [168, 218]. Moreover, for the characterization of an OTS/water interface, an additional layer accounting for depletion at the "hydrophobic gap" has to be introduced [168]. Adsorbed protein films could adequately be described by a single layer.

In order to minimize the number of fitting parameters, the following strategies are applied: At first, each substrate is characterized under pure buffer without protein, and thus parameters describing the substrate were constrained when fitting the measurements with proteins present in the system. Hence, only the parameters of the adsorbed protein layer and, in the case of hydrophobic substrates, the parameters of the hydrophobic gap are varied when refining the reflectivity curves. Furthermore, the electron densities of the silicon substrate, the silicon oxide layer and the water subphase are set to the theoretical values, as obtained from CXRO [1]. To model the structure of OTS films, values from the literature [168] are used as starting values and are varied over a narrow range. The thickness of the silicon oxide layer is varied between 5 Å and 15 Å for native SiO_2, and a value of 1500 Å is used as a starting value for the thickness of the thermally grown SiO_2 layer. As an example for the complex layer models and the methodology

of data analysis, Figure 8.2 and Table 8.1 present the results for BSA adsorption at the Nphob substrate.

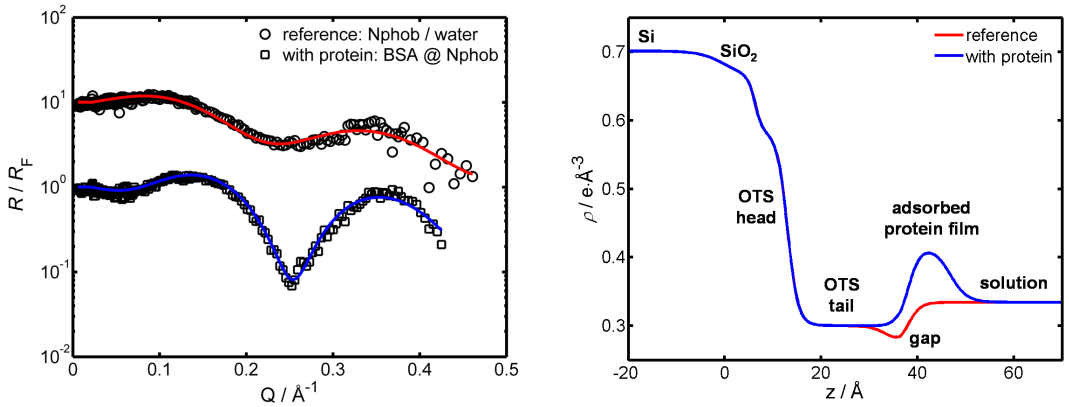

Figure 8.2: (Left) Reflectivity curves of the Nphob substrate in the absence and presence of BSA. Data and fits are displayed as open symbols and solid lines, respectively. Fits are based on layer models, as described in the text. For clarity, reflectivity curves are shifted vertically. (Right) Electron density profiles obtained from fitting the reflectivity data. The different layers (Si / SiO_2 / OTS head / OTS tail / gap / adsorbate / solution) are indicated. Before analyzing protein adsorption, reference measurements without protein are analyzed, and parameters of the substrates are kept constant when refining the data in the presence of protein adsorbates. In this way, the number of fitting parameters is reduced considerably, and only parameters of the adsorbed protein film and the gap have to be varied.

Table 8.1: Interfacial structure of the Nphob substrate (hydrophobic wafer with a native SiO_2 layer) under water and after adsorption of BSA, as characterized by X-ray reflectometry (Figure 8.2).[a]

	Si	SiO_2	OTS head	OTS tail	gap (under water)
ρ / e Å^{-3}	0.702	0.663	0.579 (0.006)	0.300 (0.004)	0.262 (0.007)
d / Å	–	6.2 (2.0)	6.8 (0.4)	21.5 (0.4)	3.2 (0.4)
σ / Å	4.7 (0.9)	1.3 (0.5)	2.0 (0.2)	3.2 (1.6)	2.3 (0.5)

	gap (after adsorption)	adsorbate
ρ / e Å^{-3}	0.296 (0.007)	0.416 (0.005)
d / Å	3.3 (0.2)	8.9 (0.5)
σ / Å	2.3 (0.4)	3.2 (0.5)

[a] ρ, d, and σ denote the electron density, film thickness, and roughness of the layers, respectively. Errors of the fitting parameters are determined by allowing a variation of 5 % from the best fit. ρ_{Si} and ρ_{SiO_2} were set to theoretical values [1].

The calculation of volume fraction profiles and the surface excess is described in Section 3.9.2.

Both nominal film thickness, d, and interfacial roughness, σ, contribute to the effective layer thickness, d_{eff}, of adsorbed protein films, as outlined in Section 5.2.

8.4 Results

8.4.1 Protein adsorbates in different surface potentials

The adsorption of α-amylase (αAMY), BSA, and lysozyme (LYS) has been studied on four different types of substrates. Therefore, scans of the substrates without and with proteins present in the subphase have been performed. Reflectivity data for all systems studied at neutral pH value are shown in Figure 8.3, and the corresponding volume fraction profiles are displayed in Figure 8.4.

X-ray reflectivity curves in the absence of proteins (Figure 8.3) show specific features: Reflectivity curves of substrates with thermally grown oxide layer (T) show a pronounced kink near Q_c and a high frequency oscillation, which is related to the thick oxide layer (cf. inset in Figure 8.6). Oscillations in the curves of phob substrates are related to the OTS structure and the hydrophobic gap. Raw data in the absence and presence of adsorbed protein films are compared with each other in Figure 8.3. Since differences of the curves in the absence and presence of proteins can only be related to features stemming from adsorbed protein films, X-ray reflectometry provides high sensitivity to the structure of protein adsorbates. Depending on the density contrast of the adsorbed protein film to the substrate and to the subphase, oscillations in the reflectivity curve can become pronounced in the presence of proteins. In the case of BSA and αAMY adsorption at silica, the density contrast is weak, and the presence of adsorbed protein films is dominated by a lowering of the reflectivity curves. Details of interfacial adsorbate structures can be deduced from data fitting and analysis. From the fits shown in Figure 8.3 electron density profiles are obtained, which can be compared to the profiles in the absence of proteins (as exemplified in Figure 8.2). Then, volume fraction profiles can be calculated, according to Equation (3.27).

From the ϕ-profiles shown in Figure 8.4, several trends can be extracted, which hold true for all three proteins studied. At hydrophobic wafers, the maximum volume fraction is larger at wafers with native oxide layer than at the ones with thermally grown layer. At hydrophilic wafers, this trend is reversed. Comparing adsorbed protein layers on hydrophilic and hydrophobic surfaces, it is striking that protein adsorbates on hydrophobic substrates are much thinner (cf. Figure 8.5) and have a high maximum volume fraction. Despite different protein structures and different conformational stabilities, in almost all cases, the effective film thickness of protein films adsorbed at hydrophobic substrates is on the order of $13-18$ Å, which is well below the smallest diameter of each protein studied. Hence, protein conformation changes drastically upon adsorption at OTS surfaces. Upon adsorption at hydrophilic wafers, protein films are thicker than those at hydrophobic wafers (cf. Figure 8.5).

In view of the adsorbed amount Γ (cf. Figure 8.5), another tendency becomes visible. Comparing the surface excess of proteins adsorbed at wafers with native and thick silicon oxide layer,

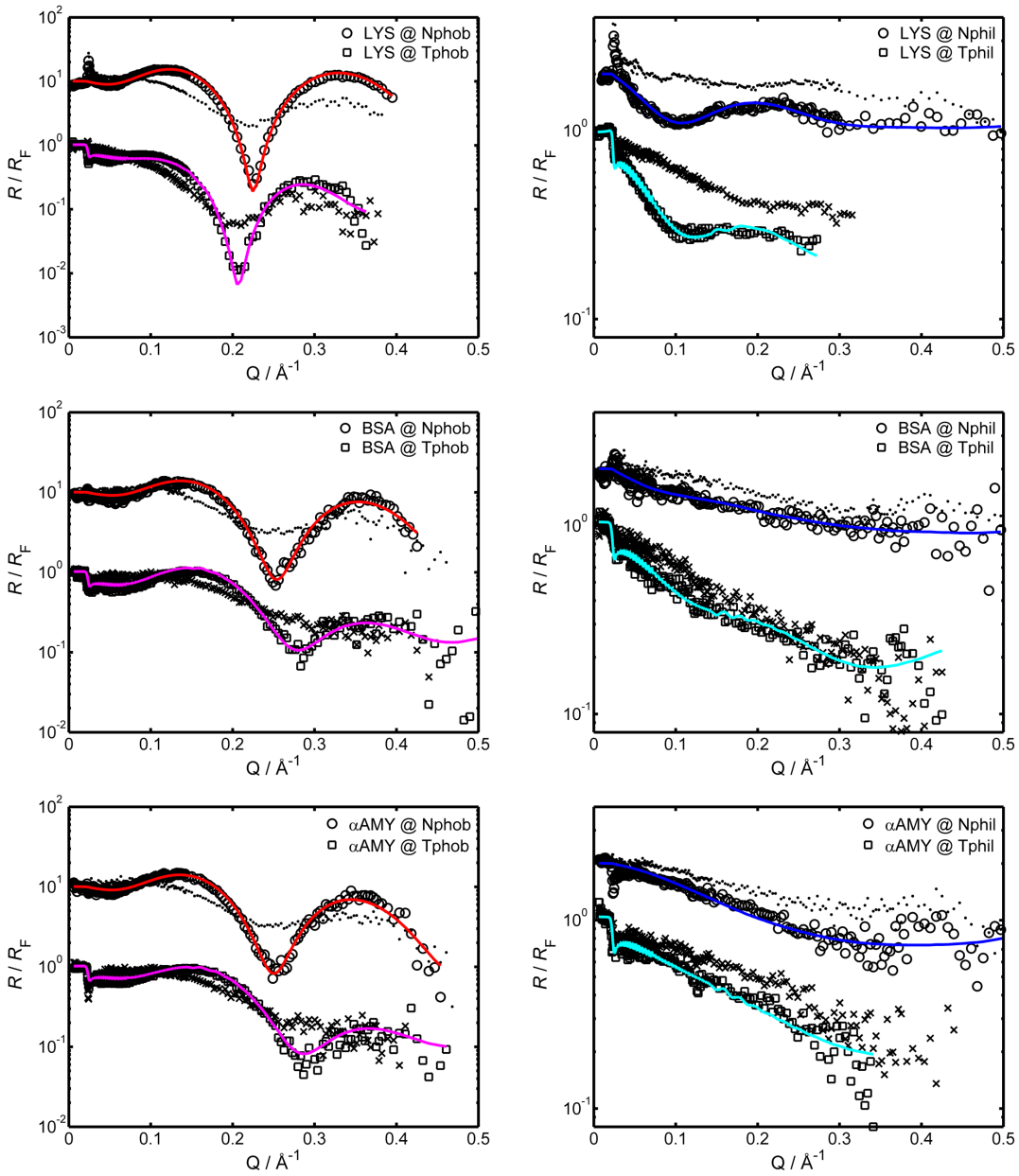

Figure 8.3: Reflectivity data for the adsorption of lysozyme (LYS, top), bovine serum albumin (BSA, middle), and α-amylase (αAMY, bottom) on four different types of substrates: silicon wafers with native (N) and thermally grown (T) oxide layer serve as hydrophilic (phil) substrates, and were also covered with a self-assembled monolayer of OTS to provide a hydrophobic (phob) environment. Data for phob and phil systems are shown on the left and right hand side, respectively. At first, all substrates were characterized in the absence of protein (data shown as "$\cdot$" for N and "$\times$" for T wafers; fits of reference measurements were omitted in order to increase the visibility of data on adsorbed protein films). After equilibration, measurements in the presence of adsorbed proteins are performed; data (open symbols) and fits (solid lines) are shown. For clarity, reflectivity curves are shifted vertically.

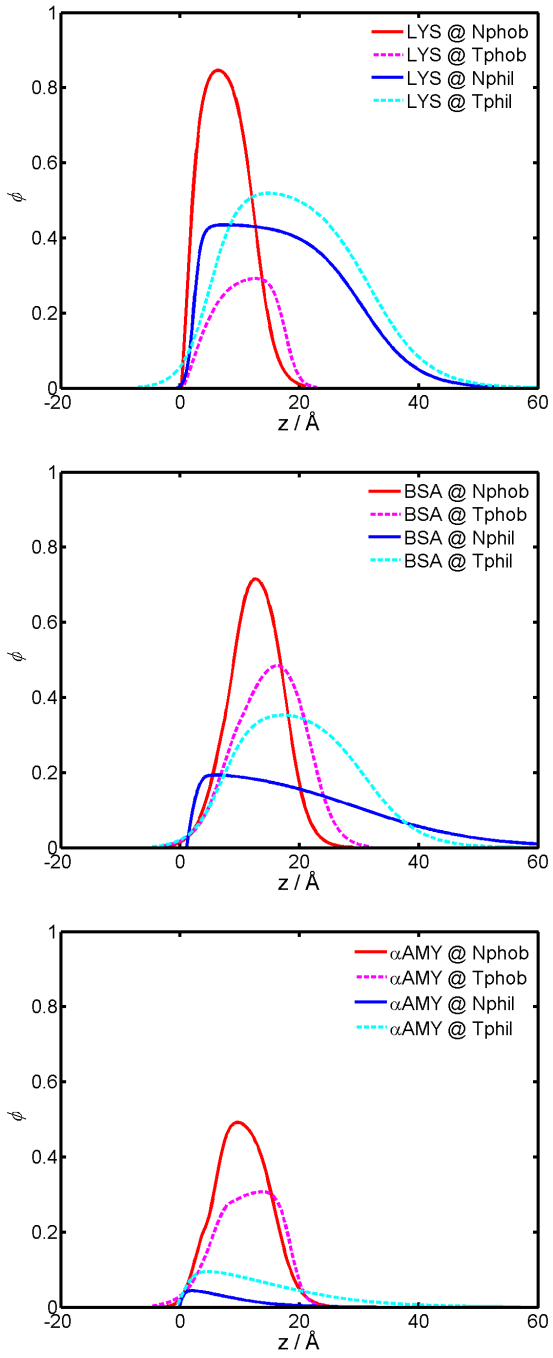

Figure 8.4: Volume fraction profiles for the adsorption of lysozyme (LYS, top), bovine serum albumin (BSA, middle), and α-amylase (αAMY, bottom) on four different types of substrates: silicon wafers with native (N) and thermally grown (T) oxide layer serve as hydrophilic (phil) substrates, and were also covered with a self-assembled monolayer of OTS to provide a hydrophilic (phob) environment. The profiles were calculated from the data shown in Figure 8.3, based on the methodology described in Section 3.9.2.

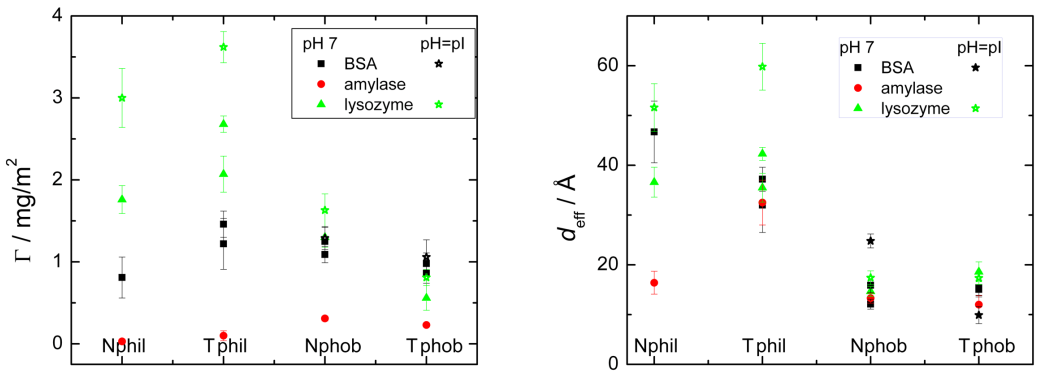

Figure 8.5: (Left) Adsorbed mass and (Right) effective layer thickness (d_{eff}) of lysozyme, BSA, and amylase adsorbed at the four different substrates.

trends in the data of hydrophobic and hydrophilic surfaces differ significantly. Using hydrophobic surfaces, more proteins adsorb at substrates with a thin SiO_2 layer than at those with a thick layer. This trend in Γ is inverted when changing the surface chemistry from hydrophobic to hydrophilic. On the hydrophilic substrates, thin oxide layers are covered by less adsorbed proteins as compared to their thick oxide counterparts.

Although, given a distinct surface, the surface excess varies from protein to protein, it is important to note that the trend in Γ holds true for all proteins studied. The different adsorbed amounts can be attributed to their different structures and isoelectric points (cf. Section 2.4). Therefore, inter-protein as well as protein-surface Coulomb forces are different for any combination of protein and surface. In order to control inter-protein Coulomb interactions, measurements for BSA and lysozyme adsorption have been performed at their isoelectric points, which are shown together with the volume fraction profiles in Figure 8.6. Obviously, maximum adsorption of BSA and lysozyme occurs at their isoelectric points. Moreover, the tendency of different protein adsorption behavior at N and T substrates is enhanced in going to the isoelectric points of the proteins.

8.5 Discussion

This study is meant to clarify the contributions of various driving forces of protein adsorption. To this end, the interfacial structures of three different proteins adsorbed at a set of four different substrates have been investigated by X-ray reflectometry. In this way, even slight differences of their interfacial structures become visible.

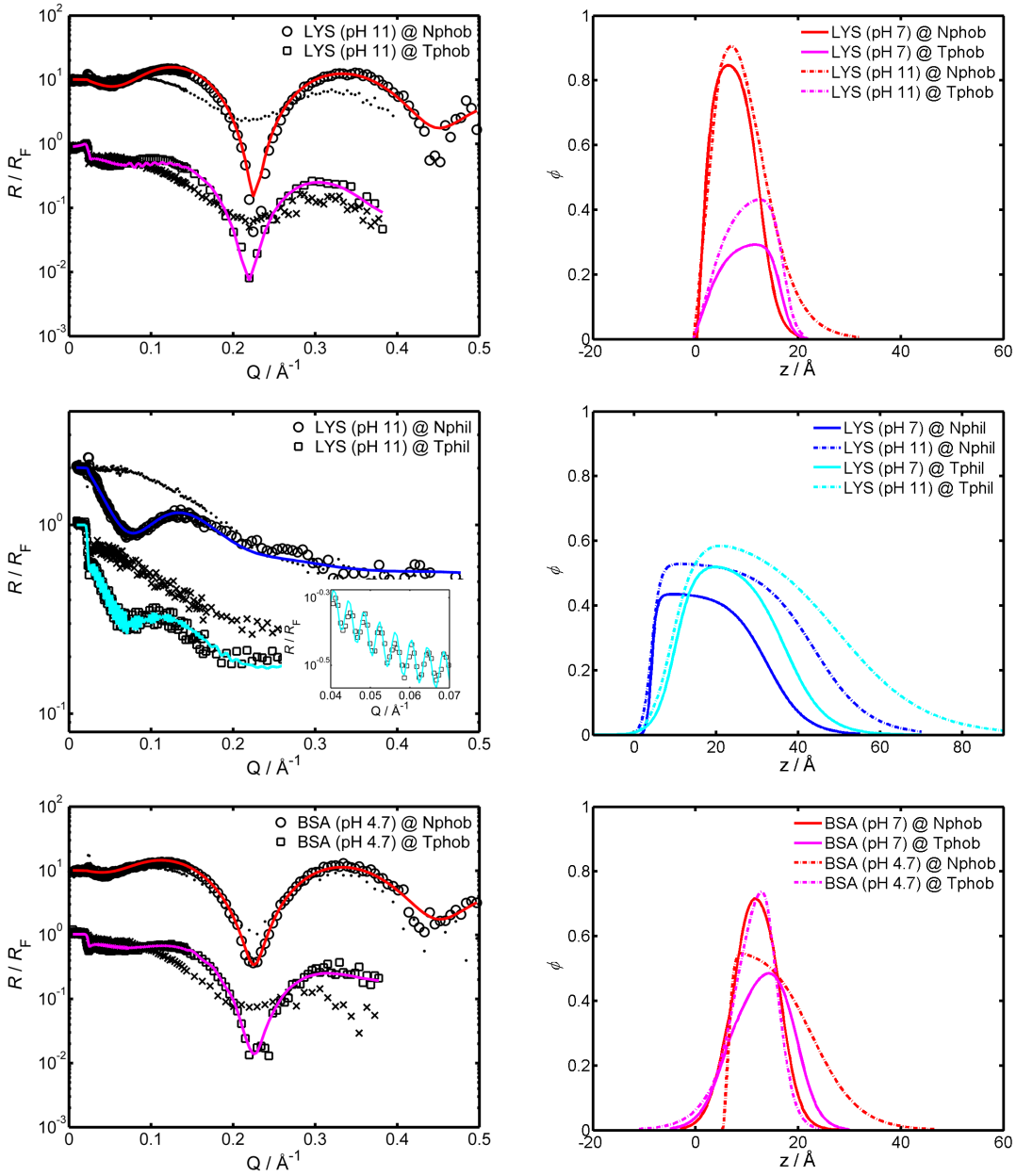

Figure 8.6: In the case of lysozyme and BSA, additional measurements on the adsorption behavior at the isoelectric points of these proteins are performed. (Left) Reflectivity measurements and fits of these systems as well as (Right) corresponding volume fraction profiles are displayed. For clarity, data in the absence of proteins (dots and crosses) are shown, and reflectivity curves are shifted vertically. For comparison, volume fraction profiles at neutral pH values are added. Oscillations stemming from the thick thermally grown silicon oxide layer are highlighted in the inset.

8.5.1 The influence of subsurface composition on protein adsorption

As outlined above, a set of four functionally different model surfaces has been chosen. Given the same solution conditions, the analysis of protein adsorption on the four different surfaces enables to elucidate the effect of subsurface composition on the structure and surface excess of adsorbed protein films.

For all proteins studied, a higher surfaces excess is found at Nphob than at Tphob substrates (cf. Figure 8.5). This finding can be related to an enhanced protein packing density inside the adsorbed layers, as shown in Figure 8.4, because the film thickness does not differ drastically between adsorbed films at Nphob and Tphob substrates. Since experimental conditions of the protein solutions were identical for protein adsorption at Nphob and Tphob substrates, the trend is caused by the different subsurface compositions of the substrates. In the case of the Nphob sample, attractive dispersion forces arising from the buried silicon still influence adsorbed protein molecules. On the other hand, at the Tphob sample, dispersion interactions mediated through the thick silicon oxide layer are far too weak to affect adsorbing proteins. Using hydrophilic substrates, the trend is reversed (increased adsorption at phil as compared to phob substrates). However, an explanation for this effect is still lacking and subject of further studies.

8.5.2 The influence of surface chemistry on the interfacial structure and surface excess of adsorbed protein films

The results of this study underpin that protein molecules can undergo drastic conformational changes upon adsorption, depending on the surface chemistry of the substrate. The thickness of nearly all adsorbed protein films at hydrophobic surfaces is in the range of $13 - 18$ Å, whereas protein films adsorbed at hydrophilic substrates are much thicker (with one exception). At hydrophobic surfaces, both small film thickness and increased volume fraction strongly suggest a certain degree of protein denaturation. This finding is in good agreement with previous neutron reflectometry and simulation studies of lysozyme adsorption at hydrophobic surfaces [162, 205].

Moreover, with respect to protein adsorption at hydrophobic surfaces, two additional aspects are notable: (i) Proteins of different sizes and different isoelectric points form adsorbed films with thicknesses distributed in a narrow range, suggesting a similar degree of adsorption-induced denaturation for all three proteins studied. (ii) At neutral pH value, lysozyme and BSA adsorb to a similar extent. In view of these two aspects, electrostatic interactions can only play a minor role in protein adsorption at hydrophobic surfaces. Instead, lysozyme and BSA adsorption at OTS surfaces is mainly driven by hydrophobic interactions. Moreover, the level of surface-induced conformational changes might be related to the interfacial energy of the surface. This hypothesis is further corroborated by a study on BSA adsorption at poly(styrene) [78].

On hydrophilic surfaces, however, adsorbed protein films are thicker, and the volume fraction profiles (cf. Figure 8.4) have a rather asymmetrical shape, due to the large roughness of the adsorbate-solution interface. In many cases, the effective film thicknesses of adsorbed protein

films at hydrophilic surfaces (cf. Figure 8.5) is on the order of the smallest diameter of the respective protein. With regard to the asymmetric ϕ-profiles, the following picture seems to be consistent with the data: At hydrophilic surfaces, adsorbed proteins retain most of their native conformation. However, at the adsorbate-solution interface, adsorbed proteins are flattened with some parts protruding into the subphase. Moreover, low volume fraction values indicate that proteins might conserve their hydration shell upon adsorption at hydrophilic interfaces.

In the case of lysozyme adsorption at pH 11, the effective thickness of the adsorbed layer is by a few angstroms larger than the largest axis of a lysozyme molecule. Hence, thick lysozyme films can be explained by bilayer adsorption, which was also found in previous studies [76, 117, 278]. At pH 7, electrostatic protein-surface and protein-protein interaction result in a thinner film and a lowering of the adsorbed mass.

In essence, concerning the influence of surface chemistry on protein adsorption, the results presented here are in line with recent studies; yet the results have further implications, since the detailed surface *and* subsurface composition of the samples used is investigated. In most previous studies, this issue has been neglected, and hence, this study might shed light on open question and contradictory results in the field of protein adsorption.

8.5.3 Discussion of sample impurities and difficulties of data analysis

Figure 8.5 shows that the adsorbed amounts found for α-amylase are quite low in comparison to those of BSA and lysozyme. It is important to mention here that the α-amylase powder used comprises a protein content of approximately 10 % only. A crude precipitation test has shown that the rest of the powder mainly consists of stabilizing agents, e.g., sulfate ions. Due to the presence of high ion concentrations, electrostatic protein-surface interactions might be diminished, especially at the pH of 7, which is very close to the isoelectric point of α-amylase. Recently, it has been shown that the addition of kosmotropic salts can lead to reduced protein adsorption [79]. Nevertheless, the ϕ-profiles of α-amylase show the same trends as those of lysozyme and BSA. Therefore, the data on amylase adsorption also corroborate the notion that differences in the interfacial structure of proteins adsorbed on N and T substrates are mainly caused by long-range van der Waals forces.

In the cases of BSA and amylase adsorption at hydrophilic surfaces, changes in the reflectivity curves (when compared to those of the pure substrates) are weak, and surface coverages are extremely low. Hence, the adsorbed films might not be adequately described as homogeneous layers, and results obtained from fitting layer models to these systems are not unambiguous. However, although layer thickness and volume fraction are strongly correlated parameters in this scenario, a precise determination of the surface excess is possible [147].

OTS surfaces have received a special attention, due to the density-depletion layer at OTS-water interfaces [168]. Therefore, it is rather interesting to study how the hydrophobic gap is altered in the presence of adsorbed proteins. Recently, protein adsorption data have been anaylzed maintaining the gap structure without proteins [216]. On the other hand, changes

of the gap structure are expected, as adsorbed proteins can unfold at OTS surfaces, exposing their hydrophobic patches to the surface. However, two aspects obstruct a detailed answer to this question in this study: (i) As the hydrophobic gap is a thin layer of low density contrast, reflectivity curves covering a very large Q-range are necessary, in order to draw valid conclusions. (ii) A lot of reference measurements (data not shown) lead to the notion that the preparation of OTS layers and, therefore, the (more or less) perfect packing of OTS films influences the width and depth of the hydrophobic depletion zone. Moreover, these data suggest that, depending on the substrate quality and on solution conditions, the density depletion can be decreased or increased after adsorption [114].

8.6 Conclusion

Altogether, the results of the comprehensive study presented in this Chapter can be summed up as follows: Notably, long-range van der Waals forces affect the degree of adsorbed protein films. To this end, an extensive investigation using three model proteins has been performed. On hydrophobic OTS surfaces, enhanced protein adsorption is found at substrates with a thin native SiO_2 layer, where van der Waals interactions contribute to the formation of protein adsorbates. However, on hydrophilic surfaces, this trend is reversed; explanations for this reversion are still under discussion. Moreover, concerning the influence of surface chemistry on protein adsorption, the results of this study clearly demonstrate that hydrophilic surfaces represent a mild environment, where proteins can retain most of their native conformation. On the other hand, protein adsorption at hydrophobic OTS surfaces can cause significant conformational changes, resulting in very thin adsorbed layers with very high protein packing densities.

9 Summary and Outlook

In this Chapter, the main results of this thesis are reflected, and future perspectives in the field of protein adsorption are discussed. In the following, the four main findings of this work are summarized:

- In two detailed studies (Chapter 5), the potential of osmolytes to reduce protein adsorption has been revealed. For three functionally different model interfaces, it has been shown that the addition of nonionic cosolvents to protein solutions leads to a decreased surface excess by lowering the protein packing density inside the adsorbed protein layer. Hence, these results provide a means to control the interfacial affinity of proteins.

- Furthermore (Chapter 6), the addition of ionic cosolvents to protein solutions alters attractive and repulsive electrostatic interactions between proteins and surfaces as well as between proteins inside the adsorbed layer. In the presence of NaCl, protein adsorption at hydrophobic surfaces can be increased, whereas the presence of kosmotropic and chaotropic salts leads to reduced protein adsorption. In particular, this study addresses Hofmeister effects on protein adsorption.

- Polyelectrolyte brushes (Chapter 7) are an interesting tool to control non-specific protein adsorption. In this investigation, the properties of a poly(acrylic acid) brush in the presence of insulin are analyzed. It is shown that poly(acrylic acid) brushes can provide a biocompatible environment even for aggregation-prone peptides.

- Moreover, the influence of surface chemistry and substrate composition on protein adsorption is discussed (Chapter 8). The results clearly show that protein adsorption at hydrophobic surfaces can lead to drastic conformational changes of adsorbed proteins, and that van der Waals forces can exert significant effects on protein adsorption.

The results of this work pave the way for further research projects in the field of protein adsorption: The effects of nonionic cosolvents have been studied thoroughly in the case of RNase; these results might be complemented by using spectroscopic techniques to determine the influence of cosolvents on the secondary structure of adsorbed proteins and by studying the influence of nonionic cosolvents on the adsorption of "soft" proteins. Moreover, the results on the influence of specific and non-specific ionic interactions on protein adsorption might serve as a starting point for extensive further studies on ion effects in protein adsorption. Furthermore, in the case

of protein adsorption at hydrophobic OTS surfaces, the role of the hydrophobic gap on protein adsorption is still debated.

Studying protein adsorption by X-ray and neutron scattering techniques provides many perspectives for future research. Advances in data analysis and instrumental improvements might lead to a deeper understanding of time-dependent phenomena, such as protein adsorption kinetics [76, 300]. Combining scattering experiments with the molecular details of proteins can meliorate the resolution and validity of density profiles [178, 197]. Moreover, computational studies and simulations will contribute to a molecular-scale picture of protein adsorption [44, 149, 208, 223]. In particular, the combination of scattering experiments with simulations will help gaining insight into the structure and thermodynamics of soft matter systems [68]. In some cases, proteins or peptides form ordered two-dimensional assemblies at interfaces; the lateral structure of these systems can be analyzed by grazing incidence diffraction [42, 43, 66, 140, 155]. Besides, in a recent neutron reflectometry study, the adhesion of live cells on quartz has been investigated [249], which is a new research topic for applying surface scattering techniques. In view of the variety of proposed further projects, protein adsorption will remain a challenging area of research in the future.

Bibliography

[1] Center for X-Ray Optics. http://henke.lbl.gov/, 2010.

[2] National Human Genome Research Project. www.genome.gov, 2010.

[3] National Institute of Standards and Technology. http://www.ncnr.nist.gov/resources/n-lengths/list, 2010.

[4] Protein Data Bank. http://www.pdb.org/, 2010.

[5] UCSF Chimera. http://www.cgl.ucsf.edu/chimera/, 2010.

[6] F. Abelès. Recherches sur la propagation des ondes électromagnétiques sinsoidales dans les milieux stratifiés. *Annales de Physique*, pages 596–640, 1950.

[7] M. Abramowitz and I. A. Stegun. *Handbook of Mathematical Functions with Formulas, Graphs, and Mathematical Table*. New York, 1972.

[8] B. Alberts, D. Bray, and K. Hopkin. *Lehrbuch der Molekularen Zellbiologie*. Weinheim, 2005.

[9] J. Als-Nielsen, D. Jacquemain, K. Kjaer, F. Levellier, M. Lahav, and L. Leiserowitz. Principles and applications of grazing incindence x-ray and neutron scattering from ordered molecular monolayers at the air-water interface. *Physics Reports*, 246:251–313, 1994.

[10] J. Als-Nielsen and D. McMorrow. *Elements of Modern X-ray Physics*. New York, 2001.

[11] G. Anand, S. N. Jamadagni, S. Garde, and G. Belfort. Self-Assembly of TMAO at Hydrophobic Interfaces and Its Effect on Protein Adsorption: Insights from Experiments and Simulations. *Langmuir*, 26:9695–9702, 2010.

[12] J. D. Andrade, editor. *Surface and interfacial aspects of biomedical polymers*. New York, 1985.

[13] J. F. Ankner, X. Tao, C. E. Halbert, J. F. Browning, S. Michael Kilbey, O. A. Swader, M. S. Dadmun, E. Kharlampieva, and S. A. Sukhishvili. The SNS Liquids Reflectometer. *Neutron News*, 19:14–16, 2008.

[14] T. Arakawa and S. Timasheff. The stabilization of proteins by osmolytes. *Biophysical Journal*, 47:411–414, 1985.

[15] R. Baldwin. How Hofmeister ion interactions affect protein stability. *Biophysical Journal*, 71:2056–2063, 1996.

[16] A. Ball and R. A. L. Jones. Conformational changes in adsorbed proteins. *Langmuir*, 11:3542–3548, 1995.

[17] V. Ball, A. Bentaleb, J. Hemmerle, J.-C. Voegel, and P. Schaaf. Dynamic Aspects of Protein Adsorption onto Titanium Surfaces: Mechanism of Desorption into Buffer and Release in the Presence of Proteins in the Bulk. *Langmuir*, 12:1614–1621, 1996.

[18] M. Ballauff and O. Borisov. Polyelectrolyte brushes. *Current Opinion in Colloid & Interface Science*, 11:316–323, 2006.

[19] A. Baszkin and W. Norde, editors. *Physical Chemistry of Biological Interfaces*. New York, 2000.

[20] M. Bellion, L. Santen, H. Mantz, H. Hähl, A. Quinn, A. Nagel, C. Gilow, C. Weitenberg, Y. Schmitt, and K. Jacobs. Protein adsorption on tailored substrates: long-range forces and conformational changes. *Journal of Physics: Condensed Matter*, 20:404226, 2008.

[21] D. Bendedouch and S. H. Chen. Structure and interparticle interactions of bovine serum albumin in solution studied by small-angle neutron scattering. *The Journal of Physical Chemistry*, 87:1473–1477, 1983.

[22] B. Bennion and V. Daggett. The molecular basis for the chemical denaturation of proteins by urea. *Proceedings of the National Academy of Sciences of the United States of America*, 100:5142–5147, 2003.

[23] A. Bentaleb, A. Abele, Y. Haikel, P. Schaaf, and J. C. Voegel. FTIR-ATR and Radiolabeling Study of the Adsorption of Ribonuclease A onto Hydrophilic Surfaces: Correlation between the Exchange Rate and the Interfacial Denaturation. *Langmuir*, 14:6493–6500, 1998.

[24] J. M. Berg, J. L. Tymoczko, and L. Stryer. *Biochemie*. Berlin, 2007.

[25] M. Berger, J. Hubbell, S. Seltzer, J. Chang, J. Coursey, R. Sukumar, D. Zucker, and K. Olsen. XCOM: Photon Cross Sections Database. http://www.nist.gov/pml/data/xcom/index.cfm, 2010.

[26] H. Betting, M. Hackel, H.-J. Hinz, and M. Stockhausen. Spectroscopic evidence for the preferential hydration of rnase a in glycerol-water mixtures: Dielectric relaxation studies. *Physical Chemistry Chemical Physics*, 3:1688–1692, 2001.

[27] C. C. F. Blake, D. F. Koenig, G. A. Mair, A. C. T. North, D. C. Phillips, and V. R. Sarma. Structure of Hen Egg-White Lysozyme: A Three-dimensional Fourier Synthesis at 2 Å Resolution. *Nature*, 206:757–761, 1965.

[28] M. Born and E. Wolf. *Principles of Optics*. Cambridge, 1999.

[29] J. Brange, L. Andersen, E. D. Laursen, G. Meyn, and E. Rasmussen. Toward understanding insulin fibrillation. *Journal of Pharmaceutical Sciences*, 86:517–525, 1997.

[30] J. L. Brash and T. A. Horbett, editors. *Proteins at interfaces*. Washington, 1987.

[31] D. N. Brems, P. L. Brown, L. A. Heckenlaible, and B. H. Frank. Equilibrium denaturation of insulin and proinsulin. *Biochemistry*, 29:9289–9293, 1990.

[32] J. B. Brzoska, I. B. Azouz, and F. Rondelez. Silanization of Solid Substrates: A Step Toward Reproducibility. *Langmuir*, 10:4367–4373, 1994.

[33] H.-J. Butt, K. Graf, and M. Kappl. *Physics and Chemistry of Interfaces*. Weinheim, 2006.

[34] D. M. Byler and H. Susi. Examination of the secondary structure of proteins by deconvolved ftir spectra. *Biopolymers*, 25:469–487, 1986.

[35] M. G. Cacace, E. M. Landau, and J. J. Ramsden. The Hofmeister series: salt and solvent effects on interfacial phenomena. *Quarterly Reviews of Biophysics*, 30:241–277, 1997.

[36] C. Calonder, Y. Tie, and P. R. Van Tassel. History dependence of protein adsorption kinetics. *Proceedings of the National Academy of Sciences of the United States*, 98:10664–10669, 2001.

[37] D. R. Canchi, D. Paschek, and A. E. Garcia. Equilibrium Study of Protein Denaturation by Urea. *Journal of the American Chemical Society*, 132:2338–2344, 2010.

[38] D. C. Carter and J. X. Ho. Structure of Serum Albumin. In F. M. R. C.B. Anfinsen, John T. Edsall and D. S. Eisenberg, editors, *Lipoproteins, Apolipoproteins, and Lipases*, volume 45 of *Advances in Protein Chemistry*, pages 153–203. Academic Press, 1994.

[39] D. Castner and B. Ratner. Biomedical surface science: Foundations to frontiers. *Surface Science*, 500:28–60, 2002.

[40] D. Chandler. Interfaces and the driving force of hydrophobic assembly. *Nature*, 437:640–647, 2005.

[41] X. Chen, L. B. Sagle, and P. S. Cremer. Urea orientation at protein surfaces. *Journal of the American Chemical Society*, 129:15104–15105, 2007.

[42] E. Y. Chi, C. Ege, A. Winans, J. Majewski, G. Wu, K. Kjaer, and K. Y. C. Lee. Lipid membrane templates the ordering and induces the fibrillogenesis of Alzheimer's disease amyloid-beta peptide. *Proteins*, 72:1–24, 2008.

[43] E. Y. Chi, S. L. Frey, A. Winans, K. L. H. Lam, K. Kjaer, J. Majewski, and K. Lee. Amyloid-beta Fibrillogenesis Seeded by Interface-Induced Peptide Misfolding and Self-Assembly. *Biophysical Journal*, 98:2299–2308, 2010.

[44] O. Cohavi, S. Corni, F. De Rienzo, R. Di Felice, K. E. Gottschalk, M. Hoefling, D. Kokh, E. Molinari, G. Schreiber, A. Vaskevich, and R. C. Wade. Protein-surface interactions: challenging experiments and computations. *Journal of Molecular Recognition*, 23:259–262, 2010.

[45] F. E. Cohen and J. W. Kelly. Therapeutic approaches to protein-misfolding diseases. *Nature*, 426:905–909, 2003.

[46] K. Collins. Charge density-dependent strength of hydration and biological structure. *Biophysical Journal*, 72:65–76, 1997.

[47] A. K. Covington, M. Paabo, R. A. Robinson, and R. G. Bates. Use of the glass electrode in deuterium oxide and the relation between the standardized pd (pad) scale and the operational ph in heavy water. *Analytical Chemistry*, 40:700–706, 1968.

[48] T. E. Creighton. *Proteins: Structures and Molecular Properties*. New York, 1992.

[49] E. P. K. Currie, A. B. Sieval, M. Avena, H. Zuilhof, E. J. R. Sudholter, and M. A. Cohen Stuart. Weak Polyacid Brushes: Preparation by LB Deposition and Optically Detected Titrations, journal = Langmuir. 15:7116–7118, 1999.

[50] C. Czeslik. Factors Ruling Protein Adsorption. *Zeitschrift für Physikalische Chemie*, 218:771–801, 2004.

[51] C. Czeslik. Proteinadsorption an festen Grenzflächen. *Chemie in unserer Zeit*, 40:238–245, 2006.

[52] C. Czeslik, G. Jackler, R. Steitz, and H.-H. von Grünberg. Protein Binding to Like-Charged Polyelectrolyte Brushes by Counterion Evaporation. *The Journal of Physical Chemistry B*, 108:13395–13402, 2004.

[53] C. Czeslik, R. Jansen, M. Ballauff, A. Wittemann, C. A. Royer, E. Gratton, and T. Hazlett. Mechanism of protein binding to spherical polyelectrolyte brushes studied in situ using two-photon excitation fluorescence fluctuation spectroscopy. *Physical Review E*, 69:021401, 2004.

[54] J. Daillant. Recent developments and applications of grazing incidence scattering. *Current Opinion in Colloid & Interface Science*, 14:396–401, 2009.

[55] J. Daillant and A. Gibaud. *X-Ray and Neutron Reflectivity: Principles and Applications*. Berlin, 1999.

[56] S. M. Daly, T. M. Przybycien, and R. D. Tilton. Coverage-Dependent Orientation of Lysozyme Adsorbed on Silica. *Langmuir*, 19:3848–3857, 2003.

[57] G. Decher. Fuzzy Nanoassemblies: Toward Layered Polymeric Multicomposites. *Science*, 277:1232–1237, 1997.

[58] R. Diamond. Real-space refinement of the structure of hen egg-white lysozyme. *Journal of Molecular Biology*, 82:371–391, 1974.

[59] E. Dickinson. *An Introduction to Food Colloids*. Oxford, 1992.

[60] E. Dickinson. Adsorbed protein layers at fluid interfaces: interactions, structure and surface rheology. *Colloids and Surfaces B: Biointerfaces*, 15:161–176, 1999.

[61] E. Dickinson. Food emulsions and foams: Stabilization by particles. *Current Opinion in Colloid and Interface Science*, 15:40–49, 2010.

[62] C. M. Dobson. Principles of protein folding, misfolding and aggregation. *Seminars in Cell & Developmental Biology*, 15:3–16, 2004.

[63] D. A. Doshi, E. B. Watkins, J. N. Israelachvili, and J. Majewski. Reduced water density at hydrophobic surfaces: Effect of dissolved gases. *Proceedings of the National Academy of Sciences of the United States*, 102:9458–9462, 2005.

[64] W. Dzwolak, S. Grudzielanek, V. Smirnovas, R. Ravindra, C. Nicolini, R. Jansen, A. Loksztejn, S. Porowski, and R. Winter. Ethanol-Perturbed Amyloidogenic Self-Assembly of Insulin: Looking for Origins of Amyloid Strains. *Biochemistry*, 44:8948–8958, 2005.

[65] W. Dzwolak, V. Smirnovas, R. Jansen, and R. Winter. Insulin forms amyloid in a strain-dependent manner: An FT-IR spectroscopic study. *Protein Science*, 13:1927–1932, 2004.

[66] C. Ege, J. Majewski, G. Wu, K. Kjaer, and K. Y. C. Lee. Templating Effect of Lipid Membranes on Alzheimer's Amyloid Beta Peptide. *ChemPhysChem*, 6:226–229, 2005.

[67] D. K. Eggers and J. S. Valentine. Molecular confinement influences protein structure and enhances thermal protein stability. *Protein Science*, 10:250–261, 2001.

[68] I. G. Elliott, D. E. Mulder, P. T. Traskelin, J. R. Ell, T. E. Patten, T. L. Kuhl, and R. Faller. Confined polymer systems: synergies between simulations and neutron scattering experiments. *Soft Matter*, 5:4612–4622, 2009.

[69] M. F. M. Engel, A. J. W. G. Visser, and C. P. M. van Mierlo. Conformation and orientation of a protein folding intermediate trapped by adsorption. *Proceedings of the National Academy of Sciences of the United States*, 101:11316–11321, 2004.

[70] S. Engemann, H. Reichert, H. Dosch, J. Bilgram, V. Honkimäki, and A. Snigirev. Interfacial Melting of Ice in Contact with SiO_2. *Phys. Rev. Lett.*, 92:205701, 2004.

[71] F. Evers. *In-situ-Hochenergie-Röntgenreflexionsexperimente zur Untersuchung der Proteinadsorption an Fest-Flüssig-Grenzflächen.* Diplomarbeit, Technische Universität Dortmund, 2008.

[72] F. Evers, A. K. Hüsecken, T. Brenner, C. Sternemann, C. Jeworrek, M. Tolan, and C. Czeslik. Effect of non-ionic cosolvents on protein adsorption studied by X-ray reflectivity. *5th DELTA User Meeting*, 2009.

[73] F. Evers, C. Jeworrek, S. Tiemeyer, K. Weise, D. Sellin, M. Paulus, B. Struth, M. Tolan, and R. Winter. Elucidating the Mechanisms of Lipid-Membrane Induced IAPP Fibrillogenesis and Its Inhibition by the Red Wine Compound Resveratrol: A Synchrotron X-ray Reflectivity Study. *Journal of the American Chemical Society*, 131:9516–9521, 2009.

[74] F. Evers, C. Jeworrek, S. Tiemeyer, K. Weise, D. Sellin, M. Paulus, B. Struth, M. Tolan, and R. Winter. Red wine and diabetes mellitus. *Photon Science 2009*, pages 40–41, 2010.

[75] F. Evers, C. Reichhart, R. Steitz, M. Tolan, and C. Czeslik. Probing adsorption and aggregation of insulin at a poly(acrylic acid) brush. *Physical Chemistry Chemical Physics*, 12:4375–4382, 2010.

[76] F. Evers, K. Shokuie, M. Paulus, C. Sternemann, C. Czeslik, and M. Tolan. Exploring the interfacial structure of protein adsorbates and the kinetics of protein adsorption: An in situ high-energy X-ray reflectivity study. *Langmuir*, 24:10216–10221, 2008.

[77] F. Evers, K. Shokuie, M. Paulus, C. Sternemann, M. Tolan, and C. Czeslik. Characterizing the Structure and Kinetics of Protein Adsorbates by X-Ray Reflectivity at DELTA beamline BL 9. *4th DELTA User Meeting*, 2008.

[78] F. Evers, K. Shokuie, M. Paulus, S. Tiemeyer, C. Sternemann, C. Czeslik, and M. Tolan. Characterizing the structure of protein layers adsorbed onto functionalized surfaces by means of in-situ X-ray reflectivity. *European Physical Journal Special Topics*, 167:185–189, 2009.

[79] F. Evers, R. Steitz, M. Tolan, and C. Czeslik. Analysis of Hofmeister Effects on the Density Profile of Protein Adsorbates: A Neutron Reflectivity Study. *The Journal of Physical Chemistry B*, 113:8462–8465, 2009.

[80] F. Evers, R. Steitz, M. Tolan, and C. Czeslik. Reduced Protein Adsorption by Osmolytes. *In Preparation*, 2010.

[81] J. Fitter, T. Gutberlet, and J. Katsaras, editors. *Neutron Scattering in Biology.* Springer-Verlag, Berlin, 2006.

[82] G. Fragneto-Cusani. Neutron reflectivity at the solid/liquid interface: examples of applications in biophysics. *Journal of Physics Condensed Matter*, 13:4973–4989, 2001.

[83] F. Gabel, M. R. Jensen, G. Zaccai, and M. Blackledge. Quantitative Modelfree Analysis of Urea Binding to Unfolded Ubiquitin Using a Combination of Small Angle X-ray and Neutron Scattering. *Journal of the American Chemical Society*, 131:8769–8771, 2009.

[84] K. Gekko and S. Timasheff. Mechanism of Protein Stabilization by Glycerol: Preferential Hydration in Glycerol-Water Mixtures. *Biochemistry*, 20:4667–4676, 1981.

[85] D. Gidalevitz, Z. Huang, and S. A. Rice. Protein folding at the air-water interface studied with x-ray reflectivity. *Proceedings of the National Academy of Sciences of the United States of America*, 96:2608–2611, 1999.

[86] J. J. Gray. The interaction of proteins with solid surfaces. *Current Opinion in Structural Biology*, 14:110–115, 2004.

[87] J. Greene, Raymond F. and C. N. Pace. Urea and Guanidine Hydrochloride Denaturation of Ribonuclease, Lysozyme, agr-Chymotrypsin, and β-Lactoglobulin. *Journal of Biological Chemistry*, 249:5388–5393, 1974.

[88] X. Guo and M. Ballauff. Spatial Dimensions of Colloidal Polyelectrolyte Brushes As Determined by Dynamic Light Scattering. *Langmuir*, 16:8719–8726, 2000.

[89] H. Hähl, F. Evers, M. Paulus, A. K. Hüsecken, T. Brenner, C. Sternemann, S. Grandthyll, M. Tolan, and K. Jacobs. The structure of protein adsorbates affected by short- and long-range forces studied by X-ray reflectivity. *5th DELTA User Meeting*, 2009.

[90] H. Hähl, F. Evers, M. Paulus, A. K. Hüsecken, T. Brenner, C. Sternemann, S. Grandthyll, M. Tolan, and K. Jacobs. Protein Adsorbates in Different Surface Potentials: A Film Structure Analysis by X-Ray Reflectivity. *6th DELTA User Meeting*, 2010.

[91] P. Harder, M. Grunze, R. Dahint, G. M. Whitesides, and P. E. Laibinis. Molecular Conformation in Oligo(ethylene glycol)-Terminated Self-Assembled Monolayers on Gold and Silver Surfaces Determines Their Ability To Resist Protein Adsorption. *The Journal of Physical Chemistry B*, 102:426–436, 1998.

[92] B. Haupt, T. Neumann, A. Wittemann, and M. Ballauff. Activity of Enzymes Immobilized in Colloidal Spherical Polyelectrolyte Brushes. *Biomacromolecules*, 6:948–955, 2005.

[93] C. Haynes and W. Norde. Globular proteins at solid/liquid interfaces. *Colloids and Surfaces B*, 2:517–566, 1994.

[94] C. Haynes and W. Norde. Structures and Stabilities of Adsorbed Proteins. *Journal of Colloid and Interface Science*, 169:313–328, 1995.

[95] K. Henzler, S. Rosenfeldt, A. Wittemann, L. Harnau, S. Finet, T. Narayanan, and M. Ballauff. Directed Motion of Proteins along Tethered Polyelectrolytes. *Physical Review Letters*, 100:158301, 2008.

[96] H. Herberhold, C. A. Royer, and R. Winter. Effects of Chaotropic and Kosmotropic Cosolvents on the Pressure-Induced Unfolding and Denaturation of Proteins: An FT-IR Study on Staphylococcal Nuclease. *Biochemistry*, 43:3336–3345, 2004.

[97] S. Herminghaus, K. Jacobs, K. Mecke, J. Bischof, A. Fery, M. Ibn-Elhaj, and S. Schlagowski. Spinodal Dewetting in Liquid Crystal and Liquid Metal Films. *Science*, 282:916–919, 1998.

[98] S. Herrwerth, W. Eck, S. Reinhardt, and M. Grunze. Factors that Determine the Protein Resistance of Oligoether Self-Assembled Monolayers - Internal Hydrophilicity, Terminal Hydrophilicity, and Lateral Packing Density. *Journal of the American Chemical Society*, 125:9359–9366, 2003.

[99] M. Heyden, E. Bründermann, U. Heugen, G. Niehues, D. M. Leitner, and M. Havenith. Long-Range Influence of Carbohydrates on the Solvation Dynamics of Water-Answers from Terahertz Absorption Measurements and Molecular Modeling Simulations. *Journal of the American Chemical Society*, 130:5773–5779, 2008.

[100] V. Hlady and J. Buijs. Protein adsorption on solid surfaces. *Current Opinion in Biotechnology*, 7:72–77, 1996.

[101] F. Hofmeister. Zur Lehre von der Wirkung der Salze. *Naunyn-Schmiedeberg's Archives of Pharmacology*, 24:247–260, 1888.

[102] O. Hollmann and C. Czeslik. Characterization of a Planar Poly(acrylic acid) Brush as a Materials Coating for Controlled Protein Immobilization. *Langmuir*, 22:3300–3305, 2006.

[103] O. Hollmann, T. Gutberlet, and C. Czeslik. Structure and Protein Binding Capacity of a Planar PAA Brush. *Langmuir*, 23:1347–1353, 2007.

[104] O. Hollmann, C. Reichhart, and C. Czeslik. Kinetics of Protein Adsorption at a Poly(Acrylic Acid) Brush Studied by Surface Plasmon Resonance Spectroscopy. *Zeitschrift für Physikalische Chemie*, 222:205–215, 2008.

[105] O. Hollmann, R. Steitz, and C. Czeslik. Structure and dynamics of alpha-lactalbumin adsorbed at a charged brush interface. *Physical Chemistry Chemical Physics*, 10:1448–1456, 2008.

[106] S. A. Holt, A. P. Le Brun, C. F. Majkrzak, D. J. McGillivray, F. Heinrich, M. Losche, and J. H. Lakey. An ion-channel-containing model membrane: structural determination by magnetic contrast neutron reflectometry. *Soft Matter*, 5:2576–2586, 2009.

[107] S. A. Holt, D. J. McGillivray, S. Poon, and J. W. White. Protein Deformation and Surfactancy at an Interface. *The Journal of Physical Chemistry B*, 104:7431–7438, 2000.

[108] D.-P. Hong and A. L. Fink. Independent Heterologous Fibrillation of Insulin and Its B-Chain Peptide. *Biochemistry*, 44:16701–16709, 2005.

[109] T. A. Horbett and J. L. Brash, editors. *Proteins at interfaces II*. Washington, 1995.

[110] J. R. Howse, E. Manzanares-Papayanopoulos, I. A. McLure, J. Bowers, R. Steitz, and G. H. Findenegg. Critical adsorption and boundary layer structure of 2-butoxyethanol + d[sub 2]o mixtures at a hydrophilic silica surface. *The Journal of Chemical Physics*, 116:7177–7188, 2002.

[111] L. Hua, R. Zhou, D. Thirumalai, and B. Berne. Urea denaturation by stronger dispersion interactions with proteins than water implies a 2-stage unfolding. *Proceedings of the National Academy of Sciences of the United States of America*, 105:16928–16933, 2008.

[112] A. K. Hüsecken. *Proteinadsorption an hydrophoben Grenzflächen*. Diplomarbeit, Technische Universität Dortmund, 2009.

[113] A. K. Hüsecken, F. Evers, C. Czeslik, and M. Tolan. Effect of Urea and Glycerol on the Adsorption of Ribonuclease A at the Air-Water Interface. *Langmuir*, 26:13429–13435, 2010.

[114] A. K. Hüsecken, F. Evers, M. Paulus, C. Sternemann, T. Brenner, K. Shokuie, S. Bieder, M. Tolan, and C. Czeslik. Protein adsorption at hydrophobic surfaces. *5th DELTA User Meeting*, 2009.

[115] J. N. Israelachvili. *Intermolecular and Surface Forces – With Applications to Colloidal and Biological Systems*. London, 1985.

[116] G. Jackler, C. Czeslik, R. Steitz, and C. A. Royer. Spatial distribution of protein molecules adsorbed at a polyelectrolyte multilayer. *Physical Review E*, 71:041912, 2005.

[117] G. Jackler, R. Steitz, and C. Czeslik. Effect of temperature on the adsorption of lysozyme at the silica/water interface studied by optical and neutron reflectometry. *Langmuir*, 18:6565–6570, 2002.

[118] K. Jacobs, S. Herminghaus, and R. Seemann. *Thin liquid films*, chapter Stability and dewetting of thin liquid films. World Scientific, 2008.

[119] D. Jacquemain, S. Wolf, F. Leveiller, M. Deutsch, K. Kjaer, J. Als-Nielsen, M. Lahav, and L. Leiserowitz. Zweidimensionale Kristallographie an amphiphilen Molekülen an der Luft-Wasser-Grenzfläche. *Angewandte Chemie*, 31:134–158, 1992.

[120] M. James. Nuclear Reactors and Neutron Optics. www.neutron.or.kr, 2010.

[121] R. James. *The Optical Principles of the Diffraction of X-Rays*. London, 1967.

[122] C. Janiak. Proteinentfernung von Kontaktlinsen: Damit der Durchblick erhalten bleibt. *Chemie in unserer Zeit*, 35:348–354, 2001.

[123] R. Jansen, W. Dzwolak, and R. Winter. Amyloidogenic Self-Assembly of Insulin Aggregates Probed by High Resolution Atomic Force Microscopy. *Biophysical Journal*, 88:1344–1353, 2005.

[124] N. Javid, K. Vogtt, C. Krywka, M. Tolan, and R. Winter. Protein-Protein Interactions in Complex Cosolvent Solutions. *ChemPhysChem*, 8:679–689, 2007.

[125] T. R. Jensen and K. Kjaer. Structural properties and interactions of thin films at the air-liquid interface explored by synchrotron x-ray scattering. In R. Möbius, D.; Miller, editor, *Novel methods to study interfacial layers, Vol. 11. Studies in Interface Science*, pages 205–254. Elsevier Science, 2001.

[126] C. Jeworrek, F. Evers, J. Höwe, K. Brandenburg, M. Tolan, and R. Winter. Effects of Specific versus Non-Specific Ionic Interactions on the Structure and Lateral Organization of Lipopolysaccharides. *In Preparation*, 2010.

[127] C. Jeworrek, O. Hollmann, R. Steitz, R. Winter, and C. Czeslik. Interaction of IAPP and Insulin with Model Interfaces Studied Using Neutron Reflectometry. *Biophysical Journal*, 96:1115–1123, 2009.

[128] J. L. Jimenez, E. J. Nettleton, M. Bouchard, C. V. Robinson, C. M. Dobson, and H. R. Saibil. The protofilament structure of insulin amyloid fibrils. *Proceedings of the National Academy of Sciences of the United States of America*, 99:9196–9201, 2002.

[129] A. Johs, L. Shi, T. Droubay, J. Ankner, and L. Liang. Characterization of the Decaheme c-Type Cytochrome OmcA in Solution and on Hematite Surfaces by Small Angle X-Ray Scattering and Neutron Reflectometry. *Biophysical Journal*, 98:3035–3043, 2010.

[130] P. Jonkheijm, D. Weinrich, H. Schöder, C. M. Niemeyer, and H. Waldmann. Chemical Strategies for Generating Protein Biochips. *Angewandte Chemie International Edition*, 47:9618–9647, 2008.

[131] T. P. Jr. Serum albumin. volume 37 of *Advances in Protein Chemistry*, pages 161–245. Academic Press, 1985.

[132] R. S. Kane, P. Deschatelets, and G. M. Whitesides. Kosmotropes Form the Basis of Protein-Resistant Surfaces. *Langmuir*, 19:2388–2391, 2003.

[133] B. Kasemo. Biological surface science. *Current Opinion in Solid State and Materials Science*, 3:451–459, 1998.

[134] B. Kasemo. Biological surface science. *Surface Science*, 500:656–677, 2002.

[135] J. Katsaras, J. Pencer, M.-P. Nieh, T. Abraham, N. Kucerka, and T. Harroun. *Structure and Dynamics of Membranous Interfaces*, chapter NEUTRON AND X-RAY SCATTERING FROM ISOTROPIC AND ALIGNED MEMBRANES, pages 107–134. John Wiley and Sons, Inc., 2008.

[136] W. Kern. The Evolution of Silicon Wafer Cleaning Technology. *J. Electrochem. Soc.*, 137:1887–1892, 1990.

[137] H. Kiessig. Untersuchungen zur Totalreflexion von Röntgenstrahlen. *Annalen der Physik*, pages 715–768, 1931.

[138] J. R. Kim, A. Muresan, K. Y. C. Lee, and R. M. Murphy. Urea modulation of beta-amyloid fibril growth: Experimental studies and kinetic models. *Protein Science*, 13:2888–2898, 2004.

[139] P. Kingshott and H. J. Griesser. Surfaces that resist bioadhesion. *Current Opinion in Solid State and Materials Science*, 4:403–412, 1999.

[140] K. Kisko, G. R. Szilvay, E. Vuorimaa, H. Lemmetyinen, M. B. Linder, M. Torkkeli, and R. Serimaa. Self-Assembled Films of Hydrophobin Proteins HFBI and HFBII Studied in Situ at the Air/Water Interface. *Langmuir*, 25:1612–1619, 2009.

[141] P. Koelsch, P. Viswanath, H. Motschmann, V. Shapovalov, G. Brezesinski, H. Möhwald, D. Horinek, R. R. Netz, K. Giewekemeyer, T. Salditt, H. Schollmeyer, R. von Klitzing, J. Daillant, and P. Guenoun. Specific ion effects in physicochemical and biological systems: Simulations, theory and experiments. *Colloids and Surfaces A: Physicochemical and Engineering Aspects*, 303:110–136, 2007.

[142] T. Koga, Y.-S. Seo, J. L. Jerome, S. Ge, M. H. Rafailovich, J. C. Sokolov, B. Chu, O. H. Seeck, M. Tolan, and R. Kolb. Low-density polymer thin film formation in supercritical carbon dioxide. *Applied Physics Letters*, 83:4309–4311, 2003.

[143] J. Koo, T. Gutberlet, and C. Czeslik. Control of protein interfacial affinity by nonionic cosolvents. *The Journal of Physical Chemistry B*, 112:6292–6295, 2008.

[144] C. Krywka, M. Paulus, C. Sternemann, M. Volmer, A. Remhof, G. Nowak, A. Nefedov, B. Pöter, M. Spiegel, and M. Tolan. The new diffractometer for surface X-ray diffraction at beamline BL9 of DELTA. *Journal of Synchrotron Radiation*, 13:8–13, 2006.

[145] C. Krywka, C. Sternemann, M. Paulus, M. Tolan, and R. Winter. Effect of Osmolytes on Pressure-Induced Unfolding of Proteins: A High-Pressure SAXS Study. *ChemPhysChem*, 9:2809–2815, 2008.

[146] W. Kunz, P. L. Nostro, and B. W. Ninham. The present state of affairs with hofmeister effects. *Current Opinion in Colloid & Interface Science*, 9:1–18, 2004.

[147] H. M. Kwaambwa, M. Hellsing, and A. R. Rennie. Adsorption of a Water Treatment Protein from Moringa oleifera Seeds to a Silicon Oxide Surface Studied by Neutron Reflection. *Langmuir*, 26:3902–3910, 2010.

[148] R. Latour. Biomaterials: Protein-Surface Interactions. *Encyclopedia of Biomaterials and Biomedical Engineering*, 2005.

[149] R. A. Latour. Molecular simulation of protein-surface interactions: Benefits, problems, solutions, and future directions (Review). *Biointerphases*, 3(3):FC2–FC12, 2008.

[150] C. S. Lee and G. Belfort. Changing activity of ribonuclease A during adsorption: a molecular explanation. *Proceedings of the National Academy of Sciences of the United States of America*, 86:8392–8396, 1989.

[151] J. C. Lee and S. N. Timasheff. The stabilization of proteins by sucrose. *Journal of Biological Chemistry*, 256:7193–7201, 1981.

[152] F. A. M. Leermakers, M. Ballauff, and O. V. Borisov. On the Mechanism of Uptake of Globular Proteins by Polyelectrolyte Brushes: A Two-Gradient Self-Consistent Field Analysis. *Langmuir*, 23:3937–3946, 2007.

[153] M. S. Lehmann and G. Zaccai. Neutron small-angle scattering studies of ribonuclease in mixed aqueous solutions and determination of the preferentially bound water. *Biochemistry*, 23:1939–1942, 1984.

[154] J. Lekner. *Theory of Reflection of Electromagnetic and Particle Waves: Of Electromagnetic and Particle Waves*. Berlin, 1987.

[155] M. Lepère, A. Muenter, C. Chevallard, P. Guenoun, and G. Brezesinski. Comparative IR and X-ray studies of natural and model amyloid peptides at the air/water interface. *Colloids and Surfaces A: Physicochemical and Engineering Aspects*, 303:73–78, 2007.

[156] I. Li, J. Bandara, and M. J. Shultz. Time Evolution Studies of the H2O/Quartz Interface Using Sum Frequency Generation, Atomic Force Microscopy, and Molecular Dynamics. *Langmuir*, 20:10474–10480, 2004.

[157] M. Li, D. J. Chaiko, and M. L. Schlossman. X-ray Reflectivity Study of a Monolayer of Ferritin Proteins at a Nanofilm Aqueous-Aqueous Interface. *The Journal of Physical Chemistry B*, 107:9079–9085, 2003.

[158] Z. Li, M. Tolan, T. Hohr, D. Kharas, S. Qu, J. Sokolov, M. H. Rafailovich, H. Lorenz, J. P. Kotthaus, J. Wang, S. K. Sinha, and A. Gibaud. Polymer Thin Films on Patterned Si Surfaces. *Macromolecules*, 31:1915–1920, 1998.

[159] T.-Y. Lin and S. N. Timasheff. Why do some organisms use a urea-methylamine mixture as osmolyte? thermodynamic compensation of urea and trimethylamine n-oxide interactions with protein. *Biochemistry*, 33:12695–12701, 1994.

[160] R. D. Lins, C. S. Pereira, and P. H. Hünenberger. Trehalose-protein interaction in aqueous solution. *Proteins: Structure, Function, and Bioinformatics*, 55:177–186, 2004.

[161] J. Lu, T. Su, and J. Penfold. Adsorption of serum albumins at the air/water interface. *Langmuir*, 15:6975–6983, 1999.

[162] J. R. Lu, T. J. Su, R. K. Thomas, J. Penfold, and J. R. P. Webster. Structural conformation of lysozyme layers at the air/water interface studied by neutron reflection. *Journal of the Chemical Society, Faraday Transactions*, 94:3279 – 3287, 1998.

[163] M. Malmsten. Formation of Adsorbed Protein Layers. *Journal of Colloid and Interface Science*, 207:186–199, 1998.

[164] M. Malmsten, editor. *Biopolymers at Interfaces*. New York, 2003.

[165] R. Maoz and J. Sagiv. On the formation and structure of self-assembling monolayers. I. A comparative ATR-wettability study of Langmuir–Blodgett and adsorbed films on flat substrates and glass microbeads. *Journal of Colloid and Interface Science*, 100:465–496, 1984.

[166] F. Meersman, D. Bowron, A. K. Soper, and M. H. Koch. Counteraction of Urea by Trimethylamine N-Oxide Is Due to Direct Interaction. *Biophysical Journal*, 97:2559–2566, 2009.

[167] F. Mezei, R. Golub, F. Klose, and H. Toews. Focussed beam reflectometer for solid and liquid surfaces. *Physica B: Condensed Matter*, 213-214:898–900, 1995.

[168] M. Mezger, H. Reichert, S. Schoder, J. Okasinski, H. Schröder, H. Dosch, D. Palms, J. Ralston, and V. Honkimäki. High-resolution in situ x-ray study of the hydrophobic gap at the water-octadecyl-trichlorosilane interface. *Proceedings of the National Academy of Sciences of the United States*, 103:18401–18404, 2006.

[169] K. E. Michael, V. N. Vernekar, B. G. Keselowsky, J. C. Meredith, R. A. Latour, and A. J. Garcia. Adsorption-Induced Conformational Changes in Fibronectin Due to Interactions with Well-Defined Surface Chemistries. *Langmuir*, 19:8033–8040, 2003.

[170] C. E. Miller, J. Majewski, T. Gog, and T. L. Kuhl. Characterization of Biological Thin Films at the Solid-Liquid Interface by X-Ray Reflectivity. *Physical Review Letters*, 94:238104, 2005.

[171] C. E. Miller, J. Majewski, E. B. Watkins, D. J. Mulder, T. Gog, and T. L. Kuhl. Probing the Local Order of Single Phospholipid Membranes Using Grazing Incidence X-Ray Diffraction. *Physical Review Letters*, 100:058103, 2008.

[172] R. Miller, V. B. Fainerman, A. V. Makievski, J. Krägel, D. O. Grigoriev, V. N. Kazakov, and O. V. Sinyachenko. Dynamics of protein and mixed protein/surfactant adsorption layers at the water/fluid interface. *Advances in Colloid and Interface Science*, 86:39–82, 2000.

[173] A. P. Minton. How can biochemical reactions within cells differ from those in test tubes? *Journal of Cell Science*, 119:2863–2869, 2006.

[174] R. Mishra, B. Bulic, D. Sellin, S. Jha, H. Waldmann, and R. Winter. Small-Molecule Inhibitors of Islet Amyloid Polypeptide Fibril Formation. *Angewandte Chemie International Edition*, 47:4679–4682, 2008.

[175] M. Mrksich and G. M. Whitesides. Using Self-Assembled Monolayers to Understand the Interactions of Man-made Surfaces with Proteins and Cells. *Annual Review of Biophysics and Biomolecular Structure*, 25:55–78, 1996.

[176] J. N. Munday, F. Capasso, and V. A. Parsegian. Measured long-range repulsive Casimir-Lifshitz forces. *Nature*, 457:170–173, 2009.

[177] K. Nakanishi, T. Sakiyama, and K. Imamura. On the Adsorption of Proteins on Solid Surfaces, a Common but Very Complicated Phenomenon. *Journal of Bioscience and Bioengineering*, 91:233–244, 2001.

[178] H. Nanda, S. A. Datta, F. Heinrich, M. Lösche, A. Rein, S. Krueger, and J. E. Curtis. Electrostatic Interactions and Binding Orientation of HIV-1 Matrix Studied by Neutron Reflectivity. *Biophysical Journal*, 99:2516–2524, 2010.

[179] L. Nielsen, R. Khurana, A. Coats, S. Frokjaer, J. Brange, S. Vyas, V. N. Uversky, and A. L. Fink. Effect of Environmental Factors on the Kinetics of Insulin Fibril Formation: Elucidation of the Molecular Mechanism. *Biochemistry*, 40:6036–6046, 2001.

[180] C. M. Niemeyer. The developments of semisynthetic DNA-protein conjugates. *Trends in Biotechnology*, 20:395–401, 2002.

[181] S. Nock and P. Wagner. Proteomics: Die post-genomische Revolution. *Chemie in unserer Zeit*, 34:348–354, 2000.

[182] W. Norde. Driving forces for protein adsorption at solid surfaces. *Macromolecular Symposia*, 103:5–18, 1996.

[183] W. Norde. *Physical Chemistry of Biological Interfaces*, chapter Proteins at Solid Surfaces, pages 115–135. New York, 2000.

[184] W. Norde. *Biopolymers at Interfaces*, chapter Driving Forces for Protein Adsorption at Solid Interfaces, pages 21–43. New York, 2003.

[185] W. Norde. My voyage of discovery to proteins in flatland ...and beyond. *Colloids and Surfaces B: Biointerfaces*, 61:1–9, 2008.

[186] W. Norde and C. A. Haynes. *Proteins at Interfaces II. Fundamentals and Applications*, chapter Reversibility and the Mechanism of Protein Adsorption, pages 26–40. 1995.

[187] R. G. Nuzzo and D. L. Allara. Adsorption of bifunctional organic disulfides on gold surfaces. *Journal of the American Chemical Society*, 105:4481–4483, 1983.

[188] O. C. Okorafor. Solubility and Density Isotherms for the Sodium Sulfate-Water-Methanol System. *Journal of Chemical & Engineering Data*, 44:488–490, 1999.

[189] S. Onclin, B. J. Ravoo, and D. N. Reinhoudt. Gestaltung der Siliciumoxidoberfläche durch selbstorganisierte Monoschichten. *Angewandte Chemie*, 117:6438–6462, 2005.

[190] C. N. Pace, D. V. Laurents, and J. A. Thomson. pH Dependence of the Urea and Guanidine Hydrochloride Denaturation of Ribonuclease A and Ribonuclease T1. *Biochemistry*, 29:2564–2572, 1990.

[191] A. Panuszko, P. Bruzdziak, J. Zielkiewicz, D. Wyrzykowski, and J. Stangret. Effects of Urea and Trimethylamine-N-oxide on the Properties of Water and the Secondary Structure of Hen Egg White Lysozyme. *The Journal of Physical Chemistry B*, 113:14797–14809, 2009.

[192] C. Park, L. W. Schultz, and R. T. Raines. Contribution of the Active Site Histidine Residues of Ribonuclease A to Nucleic Acid Binding. *Biochemistry*, 40:4949–4956, 2001.

[193] L. G. Parratt. Surface Studies of Solids by Total Reflection of X-Rays. *Physical Review*, 95:359–369, 1954.

[194] M. Paulus, D. Lietz, C. Sternemann, K. Shokuie, F. Evers, M. Tolan, C. Czeslik, and R. Winter. An access to buried interfaces: The high energy x-ray reflectivity set-up of BL9 at DELTA. *Journal of Synchrotron Radiation*, 15:600–605, 2008.

[195] L. M. Pegram and M. T. Record. Hofmeister Salt Effects on Surface Tension Arise from Partitioning of Anions and Cations between Bulk Water and the Air-Water Interface. *The Journal of Physical Chemistry B*, 111:5411–5417, 2007.

[196] L. M. Pegram and M. T. Record. Thermodynamic Origin of Hofmeister Ion Effects. *The Journal of Physical Chemistry B*, 112:9428–9436, 2008.

[197] A. W. Perriman, M. J. Henderson, C. R. Evenhuis, D. J. McGillivray, and J. W. White. Effect of the air-water interface on the structure of lysozyme in the presence of guanidinium chloride. *The Journal of Physical Chemistry B*, 112:9532–9539, 2008.

[198] A. W. Perriman, M. J. Henderson, S. A. Holt, and J. W. White. Effect of the Air-Water Interface on the Stability of β-Lactoglobulin. *The Journal of Physical Chemistry B*, 111:13527–13537, 2007.

[199] D. C. Phillips. The Hen Egg-White Lysozyme Molecule. *Proceedings of the National Academy of Sciences of the United States*, 57:483–495, 1967.

[200] U. Pietsch, V. Holý, and T. Baumbach. *High-Resolution X-Ray Scattering*. Berlin, 2001.

[201] A. Poynor, L. Hong, I. K. Robinson, S. Granick, Z. Zhang, and P. A. Fenter. How Water Meets a Hydrophobic Surface. *Physical Review Letters*, 97:266101–4, 2006.

[202] K. Prime and G. Whitesides. Self-assembled organic monolayers: model systems for studying adsorption of proteins at surfaces. *Science*, 252:1164–1167, 1991.

[203] P. L. Privalov and N. N. Khechinashvili. A thermodynamic approach to the problem of stabilization of globular protein structure: A calorimetric study. *Journal of Molecular Biology*, 86:665–684, 1974.

[204] A. Quinn, H. Mantz, K. Jacobs, M. Bellion, and L. Santen. Protein adsorption kinetics in different surface potentials. *EPL (Europhysics Letters)*, 81:56003, 2008.

[205] G. Raffaini and F. Ganazzoli. Protein Adsorption on a Hydrophobic Surface: A Molecular Dynamics Study of Lysozyme on Graphite. *Langmuir*, 26:5679–5689, 2010.

[206] R. T. Raines. Ribonuclease A. *Chemical Reviews*, 98:1045–1066, 1998.

[207] B. D. Ratner and S. J. Bryant. BIOMATERIALS: Where We Have Been and Where We are Going. *Annual Review of Biomedical Engineering*, 6:41–75, 2004.

[208] V. P. Raut, M. A. Agashe, S. J. Stuart, and R. A. Latour. Molecular Dynamics Simulations of Peptide-Surface Interactions. *Langmuir*, 21:1629–1639, 2005.

[209] C. Reich. *Structure, Fluidity and Phase Behavior of Supported Lipid Membranes: An Investigation by X-ray Reflectivity and Fluorescence Microscopy*. PhD thesis, LMU München, 2007.

[210] C. Reich, M. B. Hochrein, B. Krause, and B. Nickel. A microfluidic setup for studies of solid-liquid interfaces using x-ray reflectivity and fluorescence microscopy. *Review of Scientific Instruments*, 76:095103–7, 2005.

[211] H. Reichert, V. Honkimäki, A. Snigirev, S. Engemann, and H. Dosch. A new X-ray transmission-reflection scheme for the study of deeply buried interfaces using high-energy microbeams. *Physica B-Condensed Matter*, 336:46–55, 2003.

[212] H. Reichert, O. Klein, H. Dosch, M. Denk, V. Honkimaki, T. Lippmann, and G. Reiter. Observation of five-fold local symmetry in liquid lead. *Nature*, 408:839–841, 2000.

[213] C. Reichhart. *Untersuchung der Biokompatibilität planarer Poly(acrylsäure)-Bürsten und des Einflusses von Cosolventien auf die Proteinadsorption.* PhD thesis, Technische Universitätt Dortmund, 2010.

[214] C. Reichhart and C. Czeslik. Native-like Structure of Proteins at a Planar Poly(acrylic acid) Brush. *Langmuir*, 25:1047–1053, 2009.

[215] C. Reichhart and C. Czeslik. A quantitative study of the enzymatic activity of horseradish peroxidase at a planar poly(acrylic acid) brush. *Colloids and Surfaces B: Biointerfaces*, 75:612–616, 2010.

[216] A. Richter. In Situ X-ray Reflectivity Studies of Protein Adsorption onto Functionalized Surfaces. *APS Meeting Abstracts*, page 35003, 2007.

[217] A. G. Richter. *In situ and Interrupted Growth Studies of Self-Assembled Monolayers Using X-ray Reflectivity.* PhD thesis, Northwestern University, USA, 2000.

[218] A. G. Richter, C.-J. Yu, A. Datta, J. Kmetko, and P. Dutta. In situ and interrupted-growth studies of the self-assembly of octadecyltrichlorosilane monolayers. *Physical Review E*, 61:607–615, 2000.

[219] F. Rieutord, J. Eymery, F. Fournel, D. Buttard, R. Oeser, O. Plantevin, H. Moriceau, and B. Aspar. High-energy x-ray reflectivity of buried interfaces created by wafer bonding. *Physical Review B*, 63:125408, 2001.

[220] A. Robertson and K. Murphy. Protein Structure and the Energetics of Protein Stability. *Chemical Reviews*, 97:1251–1268, 1997.

[221] C. L. Rosa, D. Milardi, S. Fasone, and D. Grasso. A combined scanning dilatometric and differential scanning calorimetric study of the thermal unfolding of bovine serum albumin. *Thermochimica Acta*, 235:231–237, 1994.

[222] S. Rosenfeldt, A. Wittemann, M. Ballauff, E. Breininger, J. Bolze, and N. Dingenouts. Interaction of proteins with spherical polyelectrolyte brushes in solution as studied by small-angle x-ray scattering. *Physical Review E*, 70:061403, 2004.

[223] C. M. Roth and A. M. Lenhoff. *Biopolymers at Interfaces*, chapter Quantitative Modeling of Protein Adsorption, pages 71–94. New York, 2003.

[224] T. Russell. X-ray and neutron reflectivity for the investigation of polymers. *Materials Science Reports*, 5:171–271, 1990.

[225] E. Sackmann and R. Merkel. *Lehrbuch der Biophysik.* Wiley-VCH, Weinheim, 2010.

[226] J. Sagiv. Organized monolayers by adsorption. 1. Formation and structure of oleophobic mixed monolayers on solid surfaces. *Journal of the American Chemical Society*, 102:92–98, 1980.

[227] L. B. Sagle, Y. Zhang, V. A. Litosh, X. Chen, Y. Cho, and P. S. Cremer. Investigating the Hydrogen-Bonding Model of Urea Denaturation. *Journal of the American Chemical Society*, 131:9304–9310, 2009.

[228] F. Salah, B. Harzallah, and A. van der Lee. Data reduction practice in X-ray reflectometry. *Journal of Applied Crystallography*, 40:813–819, 2007.

[229] J. Santoro, C. González, M. Bruix, J. L. Neira, J. L. Nieto, J. Herranz, and M. Rico. High-resolution Three-dimensional Structure of Ribonuclease A in Solution by Nuclear Magnetic Resonance Spectroscopy. *Journal of Molecular Biology*, 229:722–734, 1993.

[230] M. K. Sanyal, J. K. Basu, A. Datta, and S. Banerjee. Determination of small fluctuations in electron density profiles of thin films: Layer formation in a polystyrene film. *EPL (Europhysics Letters)*, 36:265, 1996.

[231] M. Sch˙Self-assembled polyelectrolyte multilayers. *Current Opinion in Colloid & Interface Science*, 8:86–95, 2003.

[232] C. F. Schmidt, R. M. Zimmermann, and H. E. Gaub. Multilayer adsorption of lysozyme on a hydrophobic substrate. *Biophysical Journal*, 57:577–588, 1990.

[233] Y. Schmitt, H. Hähl, C. Gilow, H. Mantz, K. Jacobs, O. Leidinger, M. Bellion, and L. Santen. Structural evolution of protein-biofilms: Simulations and experiments. *Biomicrofluidics*, 4:032201, 2010.

[234] F. Schreiber. Structure and growth of self-assembling monolayers. *Progress in Surface Science*, 65:151–257, 2000.

[235] F. Schreiber. Self-assembled monolayers: from 'simple' model systems to biofunctionalized interfaces. *Journal of Physics: Condensed Matter*, 16:R881–R900, 2004.

[236] O. H. Seeck, I. D. Kaendler, M. Tolan, K. Shin, M. H. Rafailovich, J. Sokolov, and R. Kolb. Analysis of x-ray reflectivity data from low-contrast polymer bilayer systems using a fourier method. *Applied Physics Letters*, 76:2713–2715, 2000.

[237] R. Seemann, S. Herminghaus, and K. Jacobs. Dewetting patterns and molecular forces: A reconciliation. *Physical Review Letters*, 86:5534–5537, 2001.

[238] S. Seshadri, R. Khurana, and A. L. Fink. Fourier transform infrared spectroscopy in analysis of protein deposits. In R. Wetzel, editor, *Amyloid, Prions, and Other Protein Aggregates*, volume Volume 309, pages 559–576. Academic Press, 1999.

[239] S. Seshadri, K. A. Oberg, and A. L. Fink. Thermally Denatured Ribonuclease A Retains Secondary Structure As Shown by FTIR. *Biochemistry*, 33:1351–1355, 1994.

[240] A. Sethuraman and G. Belfort. Protein Structural Perturbation and Aggregation on Homogeneous Surfaces. *Biophysical Journal*, 88:1322–1333, 2005.

[241] W. Shang, J. H. Nuffer, J. S. Dordick, and R. W. Siegel. Unfolding of Ribonuclease A on Silica Nanoparticle Surfaces. *Nano Letters*, 7:1991–1995, 2007.

[242] O. Shekhah, H. Wang, S. Kowarik, F. Schreiber, M. Paulus, M. Tolan, C. Sternemann, F. Evers, D. Zacher, R. Fischer, and C. Woll. Step-by-Step Route for the Synthesis of Metal-Organic Frameworks. *Journal of the American Chemical Society*, 129:15118–15119, 2007.

[243] K. Shokuie. *In-situ-Untersuchung von adsorbierten Proteinfilmen an fest-flüssig-Grenzflächen mittels Röntgenreflektometrie bei hoher Energie.* PhD thesis, Technische Universität Dortmund, 2009.

[244] P. Silberzan, L. Leger, D. Ausserre, and J. J. Benattar. Silanation of silica surfaces. A new method of constructing pure or mixed monolayers. *Langmuir*, 7:1647–1651, 1991.

[245] M. W. A. Skoda, F. Schreiber, R. M. J. Jacobs, J. R. P. Webster, M. Wolff, R. Dahint, D. Schwendel, and M. Grunze. Protein Density Profile at the Interface of Water with Oligo(ethylene glycol) Self-Assembled Monolayers. *Langmuir*, 25:4056–4064, 2009.

[246] V. Sluzky, J. A. Tamada, A. M. Klibanov, and R. Langer. Kinetics of insulin aggregation in aqueous solutions upon agitation in the presence of hydrophobic surfaces. *Proceedings of the National Academy of Sciences of the United States of America*, 88:9377–9381, 1991.

[247] V. Smirnovas and R. Winter. Revealing Different Aggregation Pathways of Amyloidogenic Proteins by Ultrasound Velocimetry. *Biophysical Journal*, 94:3241–3246, 2008.

[248] V. Smirnovas, R. Winter, T. Funck, and W. Dzwolak. Protein Amyloidogenesis in the Context of Volume Fluctuations: A Case Study on Insulin. *ChemPhysChem*, 7:1046–1049, 2006.

[249] H. L. Smith, J. Hickey, M. S. Jablin, A. Trujillo, J. P. Freyer, and J. Majewski. Mouse Fibroblast Cell Adhesion Studied by Neutron Reflectometry. *Biophysical Journal*, 98:793–799, 2010.

[250] L. F. Smith. Species variation in the amino acid sequence of insulin. *The American Journal of Medicine*, 40:662–666, 1966.

[251] T. R. Sosnick and J. Trewhella. Denatured states of ribonuclease A have compact dimensions and residual secondary structure. *Biochemistry*, 31:8329–8335, 1992.

[252] L. Steinrauf. Structures of monoclinic lysozyme iodide at 1.6 Å and of triclinic lysozyme nitrate at 1.1 Å. *Acta Cryst. D*, 54:767–779, 1998.

[253] S. Streit, C. Gutt, V. Chamard, A. Robert, M. Sprung, H. Sternemann, and M. Tolan. Two-Dimensional Dynamics of Metal Nanoparticles on the Surface of Thin Polymer Films Studied with Coherent X-Rays. *Physical Review Letters*, 98:047801, 2007.

[254] T. Su, J. Lu, R. Thomas, Z. Cui, and J. Penfold. The Adsorption of Lysozyme at the Silica-Water Interface: A Neutron Reflection Study. *Journal of Colloid and Interface Science*, 203:419–429, 1998.

[255] T. J. Su, Lu, R. K. Thomas, Z. F. Cui, and J. Penfold. The Conformational Structure of Bovine Serum Albumin Layers Adsorbed at the Silica-Water Interface. *The Journal of Physical Chemistry B*, 102:8100–8108, 1998.

[256] T. J. Su, J. R. Lu, R. K. Thomas, and Z. F. Cui. Effect of pH on the Adsorption of Bovine Serum Albumin at the Silica/Water Interface Studied by Neutron Reflection. *The Journal of Physical Chemistry B*, 103:3727–3736, 1999.

[257] S. Sugio, A. Kashima, S. Mochizuki, M. Noda, and K. Kobayashi. Crystal structure of human serum albumin at 2.5 Å resolution. *Protein Engineering*, 12:439–446, 1999.

[258] C. Tanford and R. Roxby. Interpretation of protein titration curves. Application to lysozyme. *Biochemistry*, 11:2192–2198, 1972.

[259] I. M. Tidswell, B. M. Ocko, P. S. Pershan, S. R. Wasserman, G. M. Whitesides, and J. D. Axe. X-ray specular reflection studies of silicon coated by organic monolayers (alkylsiloxanes). *Physical Review B*, 41:1111–1128, 1990.

[260] I. M. Tidswell, T. A. Rabedeau, P. S. Pershan, S. D. Kosowsky, J. P. Folkers, and G. M. Whitesides. X-ray grazing incidence diffraction from alkylsiloxane monolayers on silicon wafers. *Journal of Chemical Physics*, 95:2854–2861, 1991.

[261] S. N. Timasheff. The Control of Protein Stability and Association by Weak Interactions with Water: How Do Solvents Affect These Processes? *Annual Review of Biophysics and Biomolecular Structure*, 22:67–97, 1993.

[262] S. N. Timasheff. Control of protein stability and reactions by weakly interacting cosolvents: The simplicity of the complicated. In D. S. E. Frederic M. Richards and P. S. Kim, editors, *Linkage Thermodynamics of Macromolecular Interactions*, volume 51 of *Advances in Protein Chemistry*, pages 355–432. Academic Press, 1998.

[263] S. N. Timasheff. Protein Hydration, Thermodynamic Binding, and Preferential Hydration. *Biochemistry*, 41:13473–13482, 2002.

[264] S. N. Timasheff. Protein-solvent preferential interactions, protein hydration, and the modulation of biochemical reactions by solvent components. *Proceedings of the National Academy of Sciences of the United States of America*, 99:9721–9726, 2002.

[265] S. N. Timasheff and G. Xie. Preferential interactions of urea with lysozyme and their linkage to protein denaturation. *Biophysical Chemistry*, 105:421–448, 2003.

[266] D. J. Tobias and J. C. Hemminger. CHEMISTRY: Getting Specific About Specific Ion Effects. *Science*, 319:1197–1198, 2008.

[267] M. Tolan. *X-Ray Scattering from Soft-Matter Thin Films - Materials Science and Basic Research*. Springer Tracts in Modern Physics, Berlin, 1999.

[268] M. Tolan, O. H. Seeck, J. Wang, S. K. Sinha, M. H. Rafailovich, and J. Sokolov. X-ray scattering from polymer films. *Physica B: Condensed Matter*, 283:22–26, 2000.

[269] B. C. Tripp, J. J. Magda, and J. D. Andrade. Adsorption of Globular Proteins at the Air/Water Interface as Measured via Dynamic Surface Tension: Concentration Dependence, Mass-Transfer Considerations, and Adsorption Kinetics. *Journal of Colloid and Interface Science*, 173:16–27, 1995.

[270] A. Ulman. Formation and Structure of Self-Assembled Monolayers. *Chemical Reviews*, 96:1533–1554, 1996.

[271] L. D. Unsworth, H. Sheardown, and J. L. Brash. Protein-Resistant Poly(ethylene oxide)-Grafted Surfaces: Chain Density-Dependent Multiple Mechanisms of Action. *Langmuir*, 24:1924–1929, 2008.

[272] V. Vagenende, M. G. S. Yap, and B. L. Trout. Mechanisms of Protein Stabilization and Prevention of Protein Aggregation by Glycerol. *Biochemistry*, 48:11084–11096, 2009.

[273] A. van der Lee, F. Salah, and B. Harzallah. A comparison of modern data analysis methods for X-ray and neutron specular reflectivity data. *Journal of Applied Crystallography*, 40:820–833, 2007.

[274] T. Vermonden, C. E. Giacomelli, and W. Norde. Reversibility of Structural Rearrangements in Bovine Serum Albumin during Homomolecular Exchange from AgI Particles. *Langmuir*, 17:3734–3740, 2001.

[275] D. Voet, J. G. Voet, C. W. Pratt, A. G. Beck-Sickinger, and U. Hahn. *Lehrbuch der Biochemie*. Weinheim, 2002.

[276] P. H. von Hippel and K.-Y. Wong. On the Conformational Stability of Globular Proteins. *Journal of Biological Chemistry*, 240:3909–3923, 1965.

[277] M. Wahlgren and T. Arnebrant. Protein adsorption to solid surfaces. *Trends in Biotechnology*, 9:201–208, 1991.

[278] M. Wahlgren, T. Arnebrant, and I. Lundstrom. The Adsorption of Lysozyme to Hydrophilic Silicon Oxide Surfaces: Comparison between Experimental Data and Models for Adsorption Kinetics. *Journal of Colloid and Interface Science*, 175:506–514, 1995.

[279] J. Wang, M. Tolan, O. H. Seeck, S. K. Sinha, O. Bahr, M. H. Rafailovich, and J. Sokolov. Surfaces of Strongly Confined Polymer Thin Films Studied by X-Ray Scattering. *Physical Review Letters*, 83:564–567, 1999.

[280] Y. Wang, J. Trewhella, and D. P. Goldenberg. Small-Angle X-ray Scattering of Reduced Ribonuclease A: Effects of Solution Conditions and Comparisons with a Computational Model of Unfolded Proteins. *Journal of Molecular Biology*, 377:1576–1592, 2008.

[281] S. R. Wasserman, Y. T. Tao, and G. M. Whitesides. Structure and reactivity of alkylsiloxane monolayers formed by reaction of alkyltrichlorosilanes on silicon substrates. *Langmuir*, 5:1074–1087, 1989.

[282] S. R. Wasserman, G. M. Whitesides, I. M. Tidswell, B. M. Ocko, P. S. Pershan, and J. D. Axe. The structure of self-assembled monolayers of alkylsiloxanes on silicon: a comparison of results from ellipsometry and low-angle x-ray reflectivity. *Journal of the American Chemical Society*, 111:5852–5861, 1989.

[283] D. Weinrich, P. Jonkheijm, C. M. Niemeyer, and H. Waldmann. Applications of Protein Biochips in Biomedical and Biotechnological Research. *Angewandte Chemie International Edition*, 48:7744–7751, 2009.

[284] C. Wertz and M. Santore. Effect of Surface Hydrophobicity on Adsorption and Relaxation Kinetics of Albumin and Fibrinogen: Single-Species and Competitive Behavior. *Langmuir*, 17:3006–3016, 2001.

[285] C. F. Wertz and M. M. Santore. Adsorption and Reorientation Kinetics of Lysozyme on Hydrophobic Surfaces. *Langmuir*, 18:1190–1199, 2002.

[286] P. Westermark. Aspects on human amyloid forms and their fibril polypeptides. *FEBS Journal*, 272:5942–5949, 2005.

[287] J. L. Whittingham, D. J. Scott, K. Chance, A. Wilson, J. Finch, J. Brange, and G. Guy Dodson. Insulin at pH 2: Structural Analysis of the Conditions Promoting Insulin Fibre Formation. *Journal of Molecular Biology*, 318:479–490, 2002.

[288] D. S. Wilson and S. Nock. Protein-Mikroarray-Technologie - Prinzipien und neuere Entwicklungen. *Angewandte Chemie*, 115:510–517, 2003.

[289] R. Winter and F. Noll. *Methoden der Biophysikalischen Chemie*. Berlin, 1998.

[290] O. Wintersteiner and H. A. Abramson. The isoelectric point of insulin. *Journal of Biological Chemistry*, 99:741–753, 1933.

[291] A. Wittemann and M. Ballauff. Secondary Structure Analysis of Proteins Embedded in Spherical Polyelectrolyte Brushes by FT-IR Spectroscopy. *Analytical Chemistry*, 76:2813–2819, 2004.

[292] A. Wittemann and M. Ballauff. Temperature-Induced Unfolding of Ribonuclease A Embedded in Spherical Polyelectrolyte Brushes. *Macromolecular Bioscience*, 5:13–20, 2005.

[293] A. Wittemann and M. Ballauff. Interaction of proteins with linear polyelectrolytes and spherical polyelectrolyte brushes in aqueous solution. *Physical Chemistry Chemical Physics*, 8:5269–5275, 2006.

[294] A. Wittemann, B. Haupt, and M. Ballauff. Adsorption of proteins on spherical polyelectrolyte brushes in aqueous solution. *Physical Chemistry Chemical Physics*, 5:1671–1677, 2003.

[295] A. Wlodawer, L. A. Svensson, L. Sjoelin, and G. L. Gilliland. Structure of phosphate-free ribonuclease A refined at 1.26 Å. *Biochemistry*, 27:2705–2717, 1988.

[296] G. Xie and S. N. Timasheff. The thermodynamic mechanism of protein stabilization by trehalose. *Biophysical Chemistry*, 64:25–43, 1997.

[297] P. Yancey, M. Clark, S. Hand, R. Bowlus, and G. Somero. Living with water stress: evolution of osmolyte systems. *Science*, 217:1214–1222, 1982.

[298] P. H. Yancey. Organic osmolytes as compatible, metabolic and counteracting cytoprotectants in high osmolarity and other stresses. *Journal of Experimental Biology*, 208:2819–2830, 2005.

[299] D.-S. Yang, C. M. Yip, T. H. J. Huang, A. Chakrabartty, and P. E. Fraser. Manipulating the Amyloid-β Aggregation Pathway with Chemical Chaperones. *Journal of Biological Chemistry*, 274:32970–32974, 1999.

[300] Y. F. Yano, T. Uruga, H. Tanida, H. Toyokawa, Y. Terada, M. Takagaki, and H. Yamada. Driving Force Behind Adsorption-Induced Protein Unfolding: A Time-Resolved X-ray Reflectivity Study on Lysozyme Adsorbed at an Air/Water Interface. *Langmuir*, 25:32–35, 2009.

[301] Y. Zhang and P. S. Cremer. Interactions between macromolecules and ions: the hofmeister series. *Current Opinion in Chemical Biology*, 10:658–663, 2006.

[302] H.-X. Zhou, G. Rivas, and A. P. Minton. Macromolecular Crowding and Confinement: Biochemical, Biophysical, and Potential Physiological Consequences. *Annual Review of Biophysics*, 37:375–397, 2008.

Publications

1. F. Evers, K. Shokuie, M. Paulus, C. Sternemann, C. Czeslik, M. Tolan
   Exploring the Interfacial Structure of Protein Adsorbates and the Kinetics of Protein Adsorption: An In Situ High-Energy X-ray Reflectivity Study
   Langmuir **24** (2008) 10216–10221.

2. M. Paulus, D. Lietz, C. Sternemann, K. Shokuie, F. Evers, M. Tolan, C. Czeslik, R. Winter
   An access to buried interfaces: the X-ray reflectivity set-up of BL9 at DELTA
   Journal of Synchrotron Radiation **15** (2008) 600–605.

3. F. Evers, K. Shokuie, M. Paulus, S. Tiemeyer, C. Sternemann, C. Czeslik, M. Tolan
   Characterizing the structure of protein layers adsorbed onto functionalized surfaces by means of in-situ X-ray reflectivity
   European Physical Journal Special Topics **167** (2009) 185–189.

4. F. Evers, R. Steitz, M. Tolan, C. Czeslik
   Analysis of Hofmeister Effects on the Density Profile of Protein Adsorbates: A Neutron Reflectivity Study
   Journal of Physical Chemistry B **113** (2009) 8462–8465.

5. F. Evers, C. Jeworrek, S. Tiemeyer, K. Weise, D. Sellin, M. Paulus, B. Struth, M. Tolan, R. Winter
   Elucidating the Mechanism of Lipid Membrane-Induced IAPP Fibrillogenesis and Its Inhibition by the Red Wine Compound Resveratrol: A Synchrotron X-ray Reflectivity Study
   Journal of the American Chemical Society **131** (2009) 9516–9521.

6. F. Evers, C. Jeworrek, S. Tiemeyer, K. Weise, D. Sellin, M. Paulus, B. Struth, M. Tolan, R. Winter
   Red wine and diabetes mellitus (invited article)
   Photon Science 2009 (2010) 40–41.

7. F. Evers, C. Reichhart, R. Steitz, M. Tolan, C. Czeslik
   Probing adsorption and aggregation of insulin at a poly(acrylic acid) brush
   Physical Chemistry Chemical Physics **12** (2010) 4375–4382.

8. A. K. Hüsecken, F. Evers, C. Czeslik, M. Tolan
   Effect of Urea and Glycerol on the Adsorption of Ribonuclease A at the Air–Water Interface
   Langmuir **26** (2010) 13429–13435.

9. C. Jeworrek, F. Evers, J. Höwe, K. Brandenburg, M. Tolan, R. Winter
   Effects of Specific versus Non-Specific Ionic Interactions on the Structure and Lateral Organization of Lipopolysaccharides
   In preparation.

10. F. Evers, R. Steitz, M. Tolan, C. Czeslik
    Reduced Protein Adsorption by Osmolytes
    In preparation.

11. H. Hähl, F. Evers, M. Tolan, K. Jacobs et al.
    Short- and long-range forces affect the structure of protein adsorbates – an X-ray reflectivity study
    In preparation.

Acknowledgement

This work would not have been possible without the help and support of many people. Hereby, I would like to express my gratitude towards all of them.

First of all, I would like to thank Prof. Dr. Metin Tolan for giving me the opportunity to carry out my PhD work under his supervision and to work on an intriguing and interdisciplinary research topic. Moreover, I am indebted to Prof. Tolan for his expert guidance and professional advice in the field of surface X-ray and neutron scattering as well as for his generous support of all my scientific work, including many research visits all over the world. During my diploma work in his group, I became familiar with various kinds of surface X-ray scattering. Notably, Prof. Tolan gave me the opportunity to realize and pursue quite a number of research ideas within the scope of this PhD work.

I am very much indebted to Priv.-Doz. Dr. Claus Czeslik (Physikalische Chemie I) – not only for co-supervising my PhD work, but also for introducing me to the field of neutron scattering and to the physical chemistry of protein adsorption. In particular, Claus integrated me into his research projects, and I became an associate member of his research group. Likewise, I thank him for many invaluable discussions and for scientific as well as personal advice.

Moreover, I am indebted to Prof. Dr. Roland Winter and Christoph Jeworrek (Physikalische Chemie I) not only for a close collaboration, but also for their scientific and personal support as well as for many stimulating ideas and discussions. Prof. Winter aroused my curiosity towards membrane biophysics, lipid-peptide interactions, and protein aggregation. Christoph and I performed a lot of X-ray scattering studies in these fields, and meanwhile, we became good friends. Furthermore, I thank Christoph for critical reading of parts of this work.

I would like to thank Prof. Dr. Karin Jacobs and Hendrik Hähl (Universität des Saarlandes) very much for a fruitful cooperation. We shared many inspiring discussions on protein adsorption and on the subtle interplay of short- and long-range forces in soft matter systems. Besides, I thank them for providing samples for my own research projects.

I had the pleasure to suggest topics for the diploma work of Anne K. Hüsecken and to introduce her to the intriguing field of protein adsorption. I thank her a lot for a pleasant teamwork and for in-depth discussions on protein adsorption at hydrophobic surfaces. Moreover, I thank Anne for critical reading of parts of this work.

I thank Dr. Christian Sternemann and Dr. Michael Paulus for their help with setting up high-energy X-ray scattering experiments. I thank Michael for his hints regarding the analysis of X-ray reflectivity data.

Performing scattering experiment at synchrotron radiation facilities and neutron sources is a challenging task which is only possible in a team. Therefore, I gratefully acknowledge the help of A. K. Hüsecken, Dr. K. Shokuie, Dr. M. Paulus, Dr. C. Sternemann, T. Brenner, S. Bieder, and S. Tiemeyer (Experimentelle Physik I and DELTA); Priv.-Doz. Dr. C. Czeslik, C. Jeworrek, S. Grobelny, M. Erlkamp, Dr. K. Weise, Dr. A. Gohlke, and Dr. C. Reichhart (Physikalische Chemie I); H. Hähl, S. Grandthyll, M. Lessel, and P. Loskill (Universität des Saarlandes); Dr. R. Steitz, Dr. R. Köhler, and M. Kreuzer (Helmholtz-Zentrum Berlin); Dr. B. Struth (HASYLAB); Dr. O. Konovalov and Dr. A. Vorobiev (ESRF); Dr. J. F. Ankner and C. Halbert (ORNL); Dr. J.-F. Moulin and M. Haese-Seiller (GKSS at FRMII); and Prof. Dr. P. Willmott (PSI).

I greatly appreciate the pleasant working environments at the chairs of Experimentelle Physik I (TU Dortmund), Physikalische Chemie I (TU Dortmund), and Weiche Kondensierte Materie (Universität des Saarlandes) as well as at the Helmholtz-Zentrum Berlin, at DELTA, at the European Synchrotron Radiation Facility, at HASYLAB, at the Oak Ridge National Laboratory, at the Forschungsneutronenquelle Heinz Maier-Leibnitz, and at the Paul-Scherrer-Institut. I thank the members of the mechanical workshops of the Fakultät Physik, of the Fakultät Chemie, and of DELTA for the manufacture of sample cells and the chemical workshop of the Fakultät Physik for their help in sample preparation.

The BMBF and the DFG are thanked for financial support.

Finally, my very special thanks go to my parents, to my family, and to my friends for their continuous support, endless patience, and immense encouragement throughout the last years.

Eidesstattliche Erklärung

Hiermit erkläre ich an Eides statt, dass außer den angegebenen Quellen keine weiteren Hilfsmittel zur Anfertigung dieser Arbeit verwendet wurden. Die Arbeit wurde bisher weder zu einer Promotion noch zu anderen Prüfungen verwendet.

Dortmund, November 2010

.....
(Florian Evers)